Open access • Journal Article • DOI:10.1140/EPJC/S10052-009-1055-6

Measurement of high-Q^2 neutral current deep inelastic e^- p scattering cross sections with a longitudinally polarised electron beam at HERA — Source link

Sergei Chekanov, M. Derrick, S. Magill, B. Musgrave ...+320 more authors

Institutions: Argonne National Laboratory, Andrews University, University of Bonn, University of Bristol ...+38 more institutions

Published on: 11 Jul 2009 - European Physical Journal C (Springer-Verlag)

Topics: HERA, Deep inelastic scattering and Neutral current

DESY-08-202

Measurement of high-Q^2 neutral current deep inelastic $e^- p$ scattering cross sections with a longitudinally polarised electron beam at HERA

ZEUS Collaboration

Abstract

Measurements of the neutral current cross sections for deep inelastic scattering in $e^- p$ collisions at HERA with a longitudinally polarised electron beam are presented. The single-differential cross-sections $d\sigma/dQ^2$, $d\sigma/dx$ and $d\sigma/dy$ and the double-differential cross sections in Q^2 and x are measured in the kinematic region $y < 0.9$ and $Q^2 > 185\,\mathrm{GeV}^2$ for both positively and negatively polarised electron beams and for each polarisation state separately. The measurements are based on an integrated luminosity of $169.9\,\mathrm{pb}^{-1}$ taken with the ZEUS detector in 2005 and 2006 at a centre-of-mass energy of 318 GeV. The structure functions $x\tilde{F}_3$ and $xF_3^{\gamma Z}$ are determined by combining the $e^- p$ results presented in this paper with previously measured $e^+ p$ neutral current data. The asymmetry parameter A^- is used to demonstrate the parity violating effects of electroweak interactions at large spacelike photon virtuality. The measurements agree well with the predictions of the Standard Model.

The ZEUS Collaboration

S. Chekanov, M. Derrick, S. Magill, B. Musgrave, D. Nicholass[1], J. Repond, R. Yoshida
Argonne National Laboratory, Argonne, Illinois 60439-4815, USA [n]

M.C.K. Mattingly
Andrews University, Berrien Springs, Michigan 49104-0380, USA

P. Antonioli, G. Bari, L. Bellagamba, D. Boscherini, A. Bruni, G. Bruni, F. Cindolo, M. Corradi, G. Iacobucci, A. Margotti, R. Nania, A. Polini
INFN Bologna, Bologna, Italy [e]

S. Antonelli, M. Basile, M. Bindi, L. Cifarelli, A. Contin, S. De Pasquale[2], G. Sartorelli, A. Zichichi
University and INFN Bologna, Bologna, Italy [e]

D. Bartsch, I. Brock, H. Hartmann, E. Hilger, H.-P. Jakob, M. Jüngst, A.E. Nuncio-Quiroz, E. Paul, U. Samson, V. Schönberg, R. Shehzadi, M. Wlasenko
Physikalisches Institut der Universität Bonn, Bonn, Germany [b]

N.H. Brook, G.P. Heath, J.D. Morris
H.H. Wills Physics Laboratory, University of Bristol, Bristol, United Kingdom [m]

M. Kaur, P. Kaur[3], I. Singh[3]
Panjab University, Department of Physics, Chandigarh, India

M. Capua, S. Fazio, A. Mastroberardino, M. Schioppa, G. Susinno, E. Tassi
Calabria University, Physics Department and INFN, Cosenza, Italy [e]

J.Y. Kim
Chonnam National University, Kwangju, South Korea

Z.A. Ibrahim, F. Mohamad Idris, B. Kamaluddin, W.A.T. Wan Abdullah
Jabatan Fizik, Universiti Malaya, 50603 Kuala Lumpur, Malaysia [r]

Y. Ning, Z. Ren, F. Sciulli
Nevis Laboratories, Columbia University, Irvington on Hudson, New York 10027 [o]

J. Chwastowski, A. Eskreys, J. Figiel, A. Galas, K. Olkiewicz, B. Pawlik, P. Stopa, L. Zawiejski
The Henryk Niewodniczanski Institute of Nuclear Physics, Polish Academy of Sciences, Cracow, Poland [i]

L. Adamczyk, T. Bołd, I. Grabowska-Bołd, D. Kisielewska, J. Łukasik[4], M. Przybycień, L. Suszycki
Faculty of Physics and Applied Computer Science, AGH-University of Science and Technology, Cracow, Poland [p]

A. Kotański[5], W. Słomiński[6]
Department of Physics, Jagellonian University, Cracow, Poland

O. Behnke, U. Behrens, C. Blohm, A. Bonato, K. Borras, D. Bot, R. Ciesielski, N. Coppola, S. Fang, J. Fourletova[7], A. Geiser, P. Göttlicher[8], J. Grebenyuk, I. Gregor, T. Haas, W. Hain, A. Hüttmann, F. Januschek, B. Kahle, I.I. Katkov[9], U. Klein[10], U. Kötz, H. Kowalski, M. Lisovyi, E. Lobodzinska, B. Löhr, R. Mankel[11], I.-A. Melzer-Pellmann, S. Miglioranzi[12], A. Montanari, T. Namsoo, D. Notz[11], A. Parenti, L. Rinaldi[13], P. Roloff, I. Rubinsky, U. Schneekloth, A. Spiridonov[14], D. Szuba[15], J. Szuba[16], T. Theedt, J. Ukleja[17], G. Wolf, K. Wrona, A.G. Yagües Molina, C. Youngman, W. Zeuner[11]
Deutsches Elektronen-Synchrotron DESY, Hamburg, Germany

V. Drugakov, W. Lohmann, S. Schlenstedt
Deutsches Elektronen-Synchrotron DESY, Zeuthen, Germany

G. Barbagli, E. Gallo
INFN Florence, Florence, Italy [e]

P. G. Pelfer
University and INFN Florence, Florence, Italy [e]

A. Bamberger, D. Dobur, F. Karstens, N.N. Vlasov[18]
Fakultät für Physik der Universität Freiburg i.Br., Freiburg i.Br., Germany [b]

P.J. Bussey[19], A.T. Doyle, W. Dunne, M. Forrest, M. Rosin, D.H. Saxon, I.O. Skillicorn
Department of Physics and Astronomy, University of Glasgow, Glasgow, United Kingdom [m]

I. Gialas[20], K. Papageorgiu
Department of Engineering in Management and Finance, Univ. of Aegean, Greece

U. Holm, R. Klanner, E. Lohrmann, H. Perrey, P. Schleper, T. Schörner-Sadenius, J. Sztuk, H. Stadie, M. Turcato
Hamburg University, Institute of Exp. Physics, Hamburg, Germany [b]

C. Foudas, C. Fry, K.R. Long, A.D. Tapper
Imperial College London, High Energy Nuclear Physics Group, London, United Kingdom [m]

T. Matsumoto, K. Nagano, K. Tokushuku[21], S. Yamada, Y. Yamazaki[22]
Institute of Particle and Nuclear Studies, KEK, Tsukuba, Japan [f]

A.N. Barakbaev, E.G. Boos, N.S. Pokrovskiy, B.O. Zhautykov
Institute of Physics and Technology of Ministry of Education and Science of Kazakhstan, Almaty, Kazakhstan

V. Aushev[23], O. Bachynska, M. Borodin, I. Kadenko, A. Kozulia, V. Libov, D. Lontkovskyi, I. Makarenko, Iu. Sorokin, A. Verbytskyi, O. Volynets
Institute for Nuclear Research, National Academy of Sciences, Kiev and Kiev National University, Kiev, Ukraine

D. Son
Kyungpook National University, Center for High Energy Physics, Daegu, South Korea [g]

J. de Favereau, K. Piotrzkowski
Institut de Physique Nucléaire, Université Catholique de Louvain, Louvain-la-Neuve, Belgium [q]

F. Barreiro, C. Glasman, M. Jimenez, L. Labarga, J. del Peso, E. Ron, M. Soares, J. Terrón, C. Uribe-Estrada, M. Zambrana
Departamento de Física Teórica, Universidad Autónoma de Madrid, Madrid, Spain [l]

F. Corriveau, C. Liu, J. Schwartz, R. Walsh, C. Zhou
Department of Physics, McGill University, Montréal, Québec, Canada H3A 2T8 [a]

T. Tsurugai
Meiji Gakuin University, Faculty of General Education, Yokohama, Japan [f]

A. Antonov, B.A. Dolgoshein, D. Gladkov, V. Sosnovtsev, A. Stifutkin, S. Suchkov
Moscow Engineering Physics Institute, Moscow, Russia [j]

R.K. Dementiev, P.F. Ermolov †, L.K. Gladilin, Yu.A. Golubkov, L.A. Khein, I.A. Korzhavina, V.A. Kuzmin, B.B. Levchenko[24], O.Yu. Lukina, A.S. Proskuryakov, L.M. Shcheglova, D.S. Zotkin
Moscow State University, Institute of Nuclear Physics, Moscow, Russia [k]

I. Abt, A. Caldwell, D. Kollar, B. Reisert, W.B. Schmidke
Max-Planck-Institut für Physik, München, Germany

G. Grigorescu, A. Keramidas, E. Koffeman, P. Kooijman, A. Pellegrino, H. Tiecke, M. Vázquez[12], L. Wiggers
NIKHEF and University of Amsterdam, Amsterdam, Netherlands [h]

N. Brümmer, B. Bylsma, L.S. Durkin, A. Lee, T.Y. Ling
Physics Department, Ohio State University, Columbus, Ohio 43210 [n]

P.D. Allfrey, M.A. Bell, A.M. Cooper-Sarkar, R.C.E. Devenish, J. Ferrando, B. Foster, C. Gwenlan[25], K. Horton[26], K. Oliver, A. Robertson, R. Walczak
Department of Physics, University of Oxford, Oxford United Kingdom [m]

A. Bertolin, F. Dal Corso, S. Dusini, A. Longhin, L. Stanco
INFN Padova, Padova, Italy [e]

P. Bellan, R. Brugnera, R. Carlin, A. Garfagnini, S. Limentani
Dipartimento di Fisica dell' Università and INFN, Padova, Italy [e]

B.Y. Oh, A. Raval, J.J. Whitmore[27]
Department of Physics, Pennsylvania State University, University Park, Pennsylvania 16802 [o]

Y. Iga
Polytechnic University, Sagamihara, Japan [f]

G. D'Agostini, G. Marini, A. Nigro
Dipartimento di Fisica, Università 'La Sapienza' and INFN, Rome, Italy [e]

J.E. Cole[28], J.C. Hart
Rutherford Appleton Laboratory, Chilton, Didcot, Oxon, United Kingdom [m]

H. Abramowicz[29], R. Ingbir, S. Kananov, A. Levy, A. Stern
Raymond and Beverly Sackler Faculty of Exact Sciences, School of Physics, Tel Aviv University, Tel Aviv, Israel [d]

M. Kuze, J. Maeda
Department of Physics, Tokyo Institute of Technology, Tokyo, Japan [f]

R. Hori, S. Kagawa[30], N. Okazaki, S. Shimizu, T. Tawara
Department of Physics, University of Tokyo, Tokyo, Japan [f]

R. Hamatsu, H. Kaji[31], S. Kitamura[32], O. Ota[33], Y.D. Ri
Tokyo Metropolitan University, Department of Physics, Tokyo, Japan [f]

M. Costa, M.I. Ferrero, V. Monaco, R. Sacchi, V. Sola, A. Solano
Università di Torino and INFN, Torino, Italy [e]

M. Arneodo, M. Ruspa
Università del Piemonte Orientale, Novara, and INFN, Torino, Italy [e]

S. Fourletov[7], J.F. Martin, T.P. Stewart
Department of Physics, University of Toronto, Toronto, Ontario, Canada M5S 1A7 [a]

S.K. Boutle[20], J.M. Butterworth, T.W. Jones, J.H. Loizides, M. Wing[34]
Physics and Astronomy Department, University College London, London, United Kingdom [m]

B. Brzozowska, J. Ciborowski[35], G. Grzelak, P. Kulinski, P. Łużniak[36], J. Malka[36], R.J. Nowak, J.M. Pawlak, W. Perlanski[36], T. Tymieniecka[37], A.F. Żarnecki
Warsaw University, Institute of Experimental Physics, Warsaw, Poland

M. Adamus, P. Plucinski[38], A. Ukleja
Institute for Nuclear Studies, Warsaw, Poland

Y. Eisenberg, D. Hochman, U. Karshon
Department of Particle Physics, Weizmann Institute, Rehovot, Israel [c]

E. Brownson, D.D. Reeder, A.A. Savin, W.H. Smith, H. Wolfe
Department of Physics, University of Wisconsin, Madison, Wisconsin 53706, USA [n]

S. Bhadra, C.D. Catterall, Y. Cui, G. Hartner, S. Menary, U. Noor, J. Standage, J. Whyte
Department of Physics, York University, Ontario, Canada M3J 1P3 [a]

[1] also affiliated with University College London, United Kingdom
[2] now at University of Salerno, Italy
[3] also working at Max Planck Institute, Munich, Germany
[4] now at Institute of Aviation, Warsaw, Poland
[5] supported by the research grant no. 1 P03B 04529 (2005-2008)
[6] This work was supported in part by the Marie Curie Actions Transfer of Knowledge project COCOS (contract MTKD-CT-2004-517186)
[7] now at University of Bonn, Germany
[8] now at DESY group FEB, Hamburg, Germany
[9] also at Moscow State University, Russia
[10] now at University of Liverpool, UK
[11] on leave of absence at CERN, Geneva, Switzerland
[12] now at CERN, Geneva, Switzerland
[13] now at Bologna University, Bologna, Italy
[14] also at Institut of Theoretical and Experimental Physics, Moscow, Russia
[15] also at INP, Cracow, Poland
[16] also at FPACS, AGH-UST, Cracow, Poland
[17] partially supported by Warsaw University, Poland
[18] partly supported by Moscow State University, Russia
[19] Royal Society of Edinburgh, Scottish Executive Support Research Fellow
[20] also affiliated with DESY, Germany
[21] also at University of Tokyo, Japan
[22] now at Kobe University, Japan
[23] supported by DESY, Germany
[24] partly supported by Russian Foundation for Basic Research grant no. 05-02-39028-NSFC-a
[25] STFC Advanced Fellow
[26] nee Korcsak-Gorzo
[27] This material was based on work supported by the National Science Foundation, while working at the Foundation.
[28] now at University of Kansas, Lawrence, USA
[29] also at Max Planck Institute, Munich, Germany, Alexander von Humboldt Research Award
[30] now at KEK, Tsukuba, Japan
[31] now at Nagoya University, Japan
[32] member of Department of Radiological Science, Tokyo Metropolitan University, Japan
[33] now at SunMelx Co. Ltd., Tokyo, Japan
[34] also at Hamburg University, Inst. of Exp. Physics, Alexander von Humboldt Research Award and partially supported by DESY, Hamburg, Germany

[35] also at Łódź University, Poland
[36] member of Łódź University, Poland
[37] also at University of Podlasie, Siedlce, Poland
[38] now at Lund Universtiy, Lund, Sweden
† deceased

[a] supported by the Natural Sciences and Engineering Research Council of Canada (NSERC)

[b] supported by the German Federal Ministry for Education and Research (BMBF), under contract numbers 05 HZ6PDA, 05 HZ6GUA, 05 HZ6VFA and 05 HZ4KHA

[c] supported in part by the MINERVA Gesellschaft für Forschung GmbH, the Israel Science Foundation (grant no. 293/02-11.2) and the U.S.-Israel Binational Science Foundation

[d] supported by the Israel Science Foundation

[e] supported by the Italian National Institute for Nuclear Physics (INFN)

[f] supported by the Japanese Ministry of Education, Culture, Sports, Science and Technology (MEXT) and its grants for Scientific Research

[g] supported by the Korean Ministry of Education and Korea Science and Engineering Foundation

[h] supported by the Netherlands Foundation for Research on Matter (FOM)

[i] supported by the Polish State Committee for Scientific Research, project no. DESY/256/2006 - 154/DES/2006/03

[j] partially supported by the German Federal Ministry for Education and Research (BMBF)

[k] supported by RF Presidential grant N 1456.2008.2 for the leading scientific schools and by the Russian Ministry of Education and Science through its grant for Scientific Research on High Energy Physics

[l] supported by the Spanish Ministry of Education and Science through funds provided by CICYT

[m] supported by the Science and Technology Facilities Council, UK

[n] supported by the US Department of Energy

[o] supported by the US National Science Foundation. Any opinion, findings and conclusions or recommendations expressed in this material are those of the authors and do not necessarily reflect the views of the National Science Foundation.

[p] supported by the Polish Ministry of Science and Higher Education as a scientific project (2006-2008)

[q] supported by FNRS and its associated funds (IISN and FRIA) and by an Inter-University Attraction Poles Programme subsidised by the Belgian Federal Science Policy Office

[r] supported by an FRGS grant from the Malaysian government

1 Introduction

The study of deep inelastic scattering (DIS) of leptons off nucleons has been instrumental in establishing not only the structure of nucleons but also many other aspects of the Standard Model (SM). The HERA ep collider with a centre-of-mass energy of 318 GeV has expanded the accessible kinematic region for DIS measurements allowing for direct observation of the effects of the weak interaction at high values of the negative four-momentum transfer squared, Q^2. In particular, the structure function $x\tilde{F}_3$ can be obtained from the difference of cross sections in e^+p and e^-p scattering. At HERA $x\tilde{F}_3$ is dominated by the interference of photon and Z-exchange and can be extracted from data on a pure proton target with no complications due to target mass or higher twist effects. This furnishes not only a precise test of the electroweak sector of the standard model but also provides direct information on the valence quark distributions in the nucleon.

The data samples collected from 1992–2000 by the H1 and ZEUS collaborations were used for determinations of the neutral current (NC) cross sections up to values of $Q^2 \approx 30\,000$ GeV^2 [1–5]. A first extraction of $x\tilde{F}_3$ clearly demonstrated the effect of Z-exchange. A measurement of e^+p NC DIS cross sections for a longitudinally polarised positron beam using a limited sample of data collected during 2004 has also been published by the ZEUS collaboration [6].

In this paper, measurements of the cross sections and the asymmetry parameter, representing the difference in the behaviour of negatively and positively polarised electrons, are presented. The measurement is made using data collected during 2005 and 2006 when HERA collided both positively and negatively polarised electron beams of 27.5 GeV with protons of 920 GeV. The integrated luminosity amounts to 169.9 pb^{-1} with mean luminosity-weighted polarisations of +0.29 and -0.27. This is a ten-fold increase over the previously available e^-p sample. This allows a detailed and direct probe of electro-weak effects at high Q^2 and a more precise measurement of the structure function $x\tilde{F}_3$.

2 Standard Model predictions

Inclusive deep inelastic lepton-proton scattering can be described in terms of the kinematic variables x, y, and Q^2. The variable Q^2 is defined as $Q^2 = -q^2 = -(k - k')^2$, where k and k' are the four-momenta of the incoming and scattered lepton, respectively. Bjorken x is defined as $x = Q^2/2P \cdot q$, where P is the four-momentum of the incoming proton. The fraction of the lepton energy transferred to the proton in its rest frame is given by $y = P \cdot q/P \cdot k$. The variables x, y and Q^2 are related by $Q^2 = sxy$, where s, the centre-of-mass energy is approximately given by $s = 4E_eE_p$, and E_e and E_p are the initial energies

of the electron and proton, respectively.

The electroweak Born-level cross section for the $e^{\pm}p$ NC interaction is given by [7, 8]

$$\frac{d^2\sigma(e^{\pm}p)}{dxdQ^2} = \frac{2\pi\alpha^2}{xQ^4}[Y_+\tilde{F}_2(x,Q^2) \mp Y_- x\tilde{F}_3(x,Q^2) - y^2\tilde{F}_L(x,Q^2)], \quad (1)$$

where α is the fine-structure constant, $Y_{\pm} = 1 \pm (1-y)^2$, and $\tilde{F}_2(x,Q^2)$, $\tilde{F}_3(x,Q^2)$ and $\tilde{F}_L(x,Q^2)$ are generalised structure functions. Next-to-leading order (NLO) QCD calculations predict that the contribution of the longitudinal structure function $\tilde{F}_L$ to $d^2\sigma/dxdQ^2$ is approximately 1.5%, averaged over the kinematic range considered, and therefore neglected in the discussion in this section. However, this term is included in SM calculations which are compared to the measurements presented in this paper.

The generalised structure functions depend on the longitudinal polarisation of the lepton beam which is defined as

$$P_e = \frac{N_R - N_L}{N_R + N_L} \ ,$$

where N_R and N_L are the numbers of right- and left-handed leptons in the beam[1].

Photon exchange dominates the cross section at low Q^2 and is described by $\tilde{F}_2$. It is only at Q^2 values comparable to M_Z^2 that the γ/Z interference and pure Z exchange terms become important and the $\tilde{F}_3$ term contributes significantly to the cross section. The sign of the $\tilde{F}_3$ term in Eq. (1) shows that electroweak effects increase (decrease) the e^-p (e^+p) cross sections.

Reduced cross sections, $\tilde{\sigma}$, for e^-p and e^+p scattering are defined as

$$\tilde{\sigma}^{e^{\pm}p} = \frac{xQ^4}{2\pi\alpha^2}\frac{1}{Y_+}\frac{d^2\sigma(e^{\pm}p)}{dxdQ^2} = \tilde{F}_2(x,Q^2) \mp \frac{Y_-}{Y_+}x\tilde{F}_3(x,Q^2). \quad (2)$$

The difference in the e^-p and e^+p reduced cross sections yields

$$x\tilde{F}_3 = \frac{Y_+}{2Y_-}(\tilde{\sigma}^{e^-p} - \tilde{\sigma}^{e^+p}). \quad (3)$$

The generalised structure functions can be split into terms depending on γ exchange (F_2^{γ}), Z exchange (F_2^Z, xF_3^Z) and γ/Z interference ($F_2^{\gamma Z}$, $xF_3^{\gamma Z}$) as

$$\tilde{F}_2 = F_2^{\gamma} - (v_e - P_e a_e)\chi_Z F_2^{\gamma Z} + (v_e^2 + a_e^2 - 2P_e v_e a_e)\chi_Z^2 F_2^Z, \quad (4)$$

[1] At HERA beam energies the mass of the incoming leptons may be neglected, and therefore the difference between handedness and helicity may also be neglected.

$$x\tilde{F}_3 = -(a_e - P_e v_e)\chi_Z x F_3^{\gamma Z} + (2 v_e a_e - P_e(v_e^2 + a_e^2))\chi_Z^2 x F_3^Z. \quad (5)$$

In these equations, the respective vector and axial couplings of the electron to the Z boson in the SM are given by $v_e = -1/2 + 2\sin^2\theta_W$ and $a_e = -1/2$, where θ_W is the Weinberg angle. The relative contribution of Z and γ exchange is given by $\chi_Z = \frac{1}{\sin^2 2\theta_W}\frac{Q^2}{M_Z^2+Q^2}$ and varies between 0.2 and 1.1 over the range $1\,500 < Q^2 < 30\,000$ GeV^2. For the unpolarised case ($P_e = 0$), the interference structure function $xF_3^{\gamma Z}$ is the dominant term in $x\tilde{F}_3$ as v_e is small (≈ -0.04) and thus terms containing v_e in Eq. (5) can be ignored, so that

$$x\tilde{F}_3 \simeq -a_e \chi_Z x F_3^{\gamma Z}. \quad (6)$$

In this paper, measurements of $x\tilde{F}_3$ and $xF_3^{\gamma Z}$ are presented using the full e^-p dataset collected during 2005 and 2006.

The structure functions can be written in terms of the sums and differences of the quark and anti-quark momentum distributions. In leading order (LO) QCD

$$[F_2^\gamma, F_2^{\gamma Z}, F_2^Z] = \sum_q [e_q^2, 2e_q v_q, v_q^2 + a_q^2] x(q + \bar{q}), \quad (7)$$

$$[xF_3^{\gamma Z}, xF_3^Z] = \sum_q [e_q a_q, v_q a_q] 2x(q - \bar{q}), \quad (8)$$

where v_q and a_q are the vector and axial couplings of the quark q to the Z boson, and e_q is the electric charge of the quark. The densities of the quarks and anti-quarks are given by parton distribution functions (PDFs) q and $\bar{q}$, respectively. The sums run over all quark flavours except the top quark.

The sensitivity of $xF_3^{\gamma Z}$ to u_v and d_v, the valence quark momentum distributions, is demonstrated in LO QCD through

$$xF_3^{\gamma Z} = 2x[e_u a_u u_v + e_d a_d d_v] = \frac{x}{3}(2u_v + d_v). \quad (9)$$

In addition, the integral of $xF_3^{\gamma Z}$ should obey the sum rule [9] :

$$\int_0^1 xF_3^{\gamma Z}\frac{dx}{x} = \frac{1}{3}\int_0^1 (2u_v + d_v)dx = \frac{5}{3}\ . \quad (10)$$

The charge-dependent polarisation asymmetry, A^-, is defined in terms of pure right-handed ($P_e = +1$) and left-handed ($P_e =$ -1) electron beams as

$$A^- \equiv \frac{\sigma^-(P_e = +1) - \sigma^-(P_e = -1)}{\sigma^-(P_e = +1) + \sigma^-(P_e = -1)} \ , \tag{11}$$

where $\sigma^-(P_e = +1)$ and $\sigma^-(P_e = -1)$ are the cross sections at P_e values of $+1$ and -1, respectively. When the beam polarisation is not unity A^- is given by

$$A^- = \frac{\sigma^-(P_{e,+}) - \sigma^-(P_{e,-})}{P_{e,+}\sigma^-(P_{e,-}) - P_{e,-}\sigma^-(P_{e,+})} \ , \tag{12}$$

where $\sigma^-(P_{e,+})$ and $\sigma^-(P_{e,-})$ are the cross sections evaluated at positive and negative electron polarisation values. To a good approximation the asymmetry is the ratio of the $F_2^{\gamma Z}$ and F_2^{γ} structure functions, and is proportional to the combination $a_e v_q$:

$$A^- \simeq \chi_Z a_e \frac{F_2^{\gamma Z}}{F_2^{\gamma}} = \chi_Z \sum_q [2 a_e v_q e_q (q + \bar{q})] / \sum_q [e_q^2 (q + \bar{q})]. \tag{13}$$

Thus a measurement of A^- can give direct evidence of parity violation with minimal sensitivity to the proton PDFs, and a comparison to SM predictions provides a test of the electroweak sector of the SM.

3 Experimental apparatus

A detailed description of the ZEUS detector can be found elsewhere [10]. A brief outline of the components most relevant for this analysis is given below.

Charged particles were tracked in the central tracking detector (CTD) [11], which operated in a magnetic field of 1.43 T provided by a thin superconducting solenoid. The CTD consisted of 72 cylindrical drift chamber layers, organised in nine superlayers covering the polar-angle[2] region $15^\circ < \theta < 164^\circ$. A silicon microvertex detector (MVD) [12] was installed between the beampipe and the inner radius of the CTD. The MVD was organised into a barrel with 3 cylindrical layers and a forward section with four planar layers perpendicular to the HERA beam direction. Charged-particle tracks were reconstructed using information from the CTD and MVD.

The high-resolution uranium–scintillator calorimeter (CAL) [13] consisted of three parts: the forward (FCAL), the barrel (BCAL) and the rear (RCAL) calorimeters, covering

[2] The ZEUS coordinate system is a right-handed Cartesian system, with the Z axis pointing in the proton beam direction, referred to as the "forward direction", and the X axis pointing left towards the centre of HERA. The coordinate origin is at the nominal interaction point.

99.7% of the solid angle around the nominal interaction point. Each part was subdivided transversely into towers and longitudinally into one electromagnetic section (EMC) and either one (RCAL) or two (BCAL and FCAL) hadronic sections (HAC). The smallest subdivision of the calorimeter was called a cell. The CAL relative energy resolutions, as measured under test-beam conditions, were $\sigma(E)/E = 0.18/\sqrt{E}$ for electrons and $\sigma(E)/E = 0.35/\sqrt{E}$ for hadrons, with E in GeV. The timing resolution of the CAL was better than 1 ns for energy deposits exceeding 4.5 GeV.

An iron structure that surrounded the CAL was instrumented as a backing calorimeter (BAC) [14] to measure energy leakage from the CAL. Muon chambers in the forward, barrel and rear [15] regions were used in this analysis to veto background events induced by cosmic-ray or beam-halo muons.

The luminosity was measured using the Bethe-Heitler reaction $ep \to e\gamma p$ with the luminosity detector which consisted of two independent systems, a photon calorimeter and a magnetic spectrometer.

The lepton beam in HERA became naturally transversely polarised through the Sokolov-Ternov effect [16]. The characteristic build-up time in HERA was approximately 40 minutes. Spin rotators on either side of the ZEUS detector changed the transverse polarisation of the beam into longitudinal polarisation. The electron beam polarisation was measured using two independent polarimeters, the transverse polarimeter (TPOL) [17,18] and the longitudinal polarimeter (LPOL) [19]. Both devices exploited the spin-dependent cross section for Compton scattering of circularly polarised photons off electrons to measure the beam polarisation. The luminosity and polarisation measurements were made over times that were much shorter than the polarisation build-up time.

4 Monte Carlo simulation

Monte Carlo (MC) simulated events were used to determine the efficiency for selecting events, the accuracy of kinematic reconstruction, to estimate the background rate and to correct for detector acceptance.

NC DIS events were simulated including radiative effects, using the HERACLES [20] program with the DJANGOH 1.6 [21] interface to the hadronisation programs and using CTEQ5D [22] PDFs. The hadronic final state was simulated using the colour-dipole model in ARIADNE 4.10 [23]. To investigate systematic uncertainties, the MEPS model of LEPTO6.5 [24] was also used. The Lund string model of JETSET7.4 [25] was used for the hadronisation. Diffractive NC events were generated using the RAPGAP 2.08/06 [26] program and mixed with the non-diffractive MC events to simulate the observed hadronic final states. Background from photoproduction events was simulated using HERWIG 5.9 [27].

The simulated samples were at least five times larger than the corresponding data samples. They were normalised to the integrated luminosity of the data.

The ZEUS detector response was simulated using a program based on GEANT 3.21 [28]. The generated events were passed through the detector simulation, subjected to the same trigger requirements as the data and processed by the same reconstruction programs.

5 Event reconstruction

Neutral Current events at high Q^2 are characterised by the presence of an isolated high-energy electron in the final state. The transverse momentum of the scattered electron balances that of the hadronic final state, and therefore the measured net transverse momentum, p_T, should be small. The measured p_T and the net transverse energy, E_T, are defined as

$$\begin{aligned} p_T^2 = \; & p_X^2 + p_Y^2 = \left(\sum_i E_i \sin\theta_i \cos\phi_i\right)^2 + \left(\sum_i E_i \sin\theta_i \sin\phi_i\right)^2, \\ E_T = & \sum_i E_i \sin\theta_i, \end{aligned} \tag{14}$$

where the sum runs over all calorimeter energy deposits, E_i. The polar and azimuthal angles, θ_i and ϕ_i, of the calorimeter energy deposits are measured in a coordinate system with the event vertex as origin. The variable δ, also used in the event selection, is defined as

$$\delta \equiv \sum_i (E - p_Z)_i = \sum_i (E_i - E_i \cos\theta_i). \tag{15}$$

Conservation of energy and longitudinal momentum requires $\delta = 2E_e = 55\,\text{GeV}$ if all final-state particles are detected and perfectly measured. Undetected particles that escape through the forward beam-pipe have a negligible effect on δ. However, particles lost through the rear beam-pipe can lead to a substantial reduction in δ.

Backsplash of low energy particles originating from secondary interactions and deposited at large angles were suppressed by removing low energy deposits with a polar angle greater than γ_{max}, which was calculated on an event-by-event basis. The specific value of γ_{max} was tuned using both data and MC samples containing a reduced amount of backsplash. Studies [29] have shown that this procedure depends on the Q^2 threshold of the sample. This effect is accounted for in the study of systematic effects.

Furthermore, CAL energy deposits are separated into those associated with the scattered electron, and all other energy deposits. The sum of the latter is called the hadronic energy. In the naive quark-parton model, the hadronic polar angle, γ_h, defined as

$$\cos\gamma_h = \frac{p_{T,h}^2 - \delta_h^2}{p_{T,h}^2 + \delta_h^2} \ , \tag{16}$$

is the scattering angle of the struck quark, where the quantities $p_{T,h}$ and δ_h are derived from Eqs. (14−15) using only the hadronic energy.

The double-angle (DA) method [30] is used for reconstructing the kinematic variables. It makes use of the polar angle of the scattered electron, θ_e, and γ_h to reconstruct the kinematic variables $x_{\rm DA}$, $y_{\rm DA}$, and $Q^2_{\rm DA}$. The DA method is insensitive to uncertainties in the overall energy scale of the calorimeter. However, it is sensitive to initial-state QED radiation and an accurate simulation of the detector response is necessary. The variable y is also reconstructed using the electron method, y_e, and the Jacquet-Blondel method, $y_{\rm JB}$ [31]. These estimators for y are used only for the event selection.

6 Neutral Current event selection

ZEUS operated a three-level trigger system [10, 32, 33]. At the first level, only coarse calorimeter and tracking information were available. Events were selected using criteria based on an energy deposit in the CAL consistent with an isolated electron. In addition, events with high E_T in coincidence with a CTD track were accepted. At the second level, a requirement on δ was used to select NC DIS events. Timing information from the calorimeter was used to reject events inconsistent with the bunch-crossing time. At the third level, events were fully reconstructed. The requirements were similar to, but looser than, the offline cuts described below.

Scattered electrons were identified using an algorithm that combined information from the energy deposits in the calorimeter with tracks measured in the central tracking detectors [1]. To ensure high electron finding efficiency and to reject backgrounds, the identified electron was required to have an energy of at least 10 GeV. A track matched to the energy deposit in the calorimeter was required for events in which an electron was found within the acceptance of the tracking detectors. This was done by requiring the distance of closest approach (DCA) between the track extrapolated to the calorimeter surface and the energy cluster position to be less than 10 cm and the electron track momentum, $p_e^{\rm trk}$, to be larger than 3 GeV. A matched track was not required if the electron emerged at a polar angle outside the acceptance of the tracking detector. If the electron emerged in FCAL with a polar angle outside the acceptance of the tracking detector, it was required

to have energy greater than 30 GeV. An isolation requirement was imposed such that the energy not associated with the electron in an $\eta - \phi$ cone of radius 0.8 centred on the electron was less than 5 GeV.

In photoproduction events where the electron emerges at very small scattering angles, δ is substantially smaller than 55 GeV, and in beam-gas events overlaid on NC events, δ is substantially larger than 55 GeV. A requirement $38 < \delta < 65$ GeV was imposed to remove these backgrounds. To further reduce background from photoproduction events, y_e was required to be less than 0.95. The net transverse momentum was expected to be small for balanced NC events, so to remove cosmic-ray events and beam-related background events the quantity $p_T/\sqrt{E_T}$ was required to be less than $4\sqrt{\text{GeV}}$ and the quantity p_T/E_T was required to be less than 0.7.

In order to reject events where most of the hadronic final state was lost in the forward beam-pipe, the projection of γ_h onto the face of FCAL was required to be outside a radius of 20 cm centred on the beam-pipe axis. The Z coordinate of the ep interaction vertex, reconstructed using tracks in the CTD and the MVD, was required to satisfy $|Z_{\text{vtx}}| < 50$ cm. The final event sample was defined by requiring $Q^2_{\text{DA}} > 185\,\text{GeV}^2$ and $y_{\text{DA}} < 0.9$.

A total of 360 437 candidate events passed the selection criteria. The background is dominated by photoproduction which was estimated to contribute, on average, about 0.3% to the event sample but tend to populate mainly in smaller Q^2 and larger y regions. Other backgrounds were negligible.

A comparison between data and MC distributions is shown in Fig. 1 for the variables Q^2_{DA}, x_{DA}, y_{DA}, energy E'_e and θ_e of the scattered electron, γ_h and $p_{T,h}$ of the final hadronic system, and Z_{vtx} for the event. The distributions from the data and MC (NC + photoproduction) agree well.

7 Cross section determination

The single-differential cross-sections $d\sigma/dQ^2$, $d\sigma/dx$ and $d\sigma/dy$ for $Q^2 > 185\,\text{GeV}^2$ and $y < 0.9$, and $d\sigma/dx$ and $d\sigma/dy$ for $Q^2 > 3\,000\,\text{GeV}^2$ and $y < 0.9$, and the double-differential cross-section $d^2\sigma/dxdQ^2$ were measured. The cross sections in a particular bin ($d^2\sigma/dxdQ^2$ is shown as an example) was determined according to

$$\frac{d^2\sigma}{dxdQ^2} = \frac{N_{\text{data}} - N_{\text{bg}}}{N_{\text{MC}}} \cdot \frac{d^2\sigma^{\text{SM}}_{\text{Born}}}{dxdQ^2} \ ,$$

where N_{data} is the number of data events in the bin, N_{bg} is the number of background events predicted from the photoproduction MC, and N_{MC} is the number of signal MC

events normalised to the luminosity of the data. The SM prediction for the Born-level cross section, $d^2\sigma^{\rm SM}_{\rm Born}/dxdQ^2$, was evaluated using CTEQ5D PDFs [22] as in the MC simulation and using the PDG [34] values for the fine-structure constant, the mass of the Z boson, and the weak mixing angle. This procedure implicitly takes into account the acceptance, bin-centering, and radiative corrections from the MC simulation. The bin sizes used for the determination of the single- and double-differential cross sections were chosen to be commensurate with the detector resolutions. The statistical uncertainties on the cross sections were calculated from the numbers of events observed in the bins, taking into account the statistical uncertainty of the MC simulation (signal and background). Poisson statistics were used for all bins.

8 Systematic uncertainties

Systematic uncertainties were estimated by re-calculating the cross sections after modifying the analysis to account for known uncertainties. The positive and negative deviations from the nominal cross-section values were added in quadrature separately to obtain the total positive and negative systematic uncertainty. The total systematic uncertainties for the bins used in the reduced cross section measurements are shown in Fig. 2. The description of each systematic uncertainty follows.

The following systematic uncertainties were treated as correlated between bins :

- $\{\delta_1\}$ to estimate the systematic uncertainty associated with the electron finder, an alternative electron-finding algorithm [35] was used and the results were compared to those using the nominal algorithm. In addition, to evaluate the systematic uncertainty of electron finding in an environment of densely packed energy deposits, the electron isolation requirement was varied by $\pm 2\,\text{GeV}$. These two checks were combined to give the systematic uncertainty from electron finding which was less than 1% for the bulk of the phase space. In the double-differential cross-section bins at high Q^2 and high y, the uncertainty was about 4%, and increased to 18% in the high-y bins of $d\sigma/dy$ for $Q^2 > 3\,000\,\text{GeV}^2$;
- $\{\delta_2\}$ the variation of the electron energy scale by $\pm 2\%$ in the MC resulted in changes less than 1% in the cross sections over most of the kinematic region due to the use of the DA reconstruction method. The effect was at most 5% at high y in $d\sigma/dy$;
- $\{\delta_3\}$ the nominal procedure to calculate $\gamma_{\rm max}$ used MC sample with a similar Q^2 cut as in the NC event selection. To account for the Q^2 dependence of $\gamma_{\rm max}$ in the backsplash removal procedure, it was also derived with higher Q^2 thresholds and the results were compared. The effect on the cross sections was generally less than 1%, but increased to typically 5% in the high-x bins;

- $\{\delta_4\}$ the systematic uncertainty in the parton-shower scheme was evaluated by using the MEPS model of LEPTO to calculate the acceptance instead of ARIADNE [3]. The uncertainty was typically within $\pm 2\%$ but reached 5% in some bins of the double-differential cross sections;
- $\{\delta_5\}$ the cut of 20 cm on the projected radius of the hadronic angle onto the FCAL was varied by ± 3 cm. The cross sections typically changed less than $\pm 1\%$. The effect increased up to $\pm 6\%$ for the highest x bins of both $d\sigma/dx$ and the double-differential cross section;
- $\{\delta_6\}$ the uncertainty due to "overlay" events, in which a normal DIS event coincided with additional energy deposits in the RCAL from some other interaction, and photoproduction contamination was estimated by narrowing or widening the $38 < \delta < 65$ GeV interval symmetrically by ± 4 GeV. The effect on the cross sections was typically below 2%. In a few high-Q^2 bins the uncertainty was as large as 4%;
- $\{\delta_7\}$ systematic uncertainties arising from the normalisation of the photoproduction background were estimated by changing the background normalisation by $\pm 40\%$. In addition, systematic uncertainties arising from the estimation of the photoproduction background were also estimated by reducing the cut on y_e to $y_e < 0.9$. The resulting changes in the cross sections were typically below $\pm 1\%$, and at most 2% in the high-Q^2 bins of the double-differential cross-section.

The following systematic uncertainties are either small or not correlated between bins :

- $\{\delta_8\}$ the energy resolution used in the MC for the scattered electron was varied by $\pm 1\%$, and the effect was less than 0.5% over the full kinematic range;
- $\{\delta_9\}$ to reflect uncertainties in the alignment of the CAL with respect to the CTD, the electron scattering angle was varied by ± 1 mrad. Typically, the deviations were within $\pm 1\%$ over the full kinematic range;
- $\{\delta_{10}\}$ to account for differences in the description of the $p_e^{\rm trk}$ distribution between data and MC, the $p_e^{\rm trk}$ requirement was varied by ± 1 GeV, resulting in a variation of the cross section by $\pm 1\%$ over most of the kinematic range, and up to 2% in a few double-differential cross-section bins;
- $\{\delta_{11}\}$ the uncertainty resulting from the hadronic energy scale was evaluated by varying the hadronic energy in the MC by $\pm 1\%$. This caused changes of less than $\pm 1\%$ over the full kinematic range in the MC;

[3] Since the simulation of parton-shower scheme also changes the description of the electron isolation, the comparison was made without the electron isolation requirement to prevent double counting of systematic errors.

- $\{\delta_{12}\}$ the DCA requirement was changed to 8 cm to estimate the uncertainty in the background contamination due to falsely identified electrons. The uncertainties in the cross sections associated with this variation were below $\pm 1\%$ over the full kinematic range;
- $\{\delta_{13}\}$ the systematic uncertainty associated with cosmic-ray rejection was evaluated by varying the $p_T/\sqrt{E_T}$ cut by $\pm 1\sqrt{\text{GeV}}$. The cross-section uncertainties were below $\pm 1\%$ over the full kinematic range.

The relative uncertainty in the measured polarisation was 3.6% using the LPOL and 4.2% using the TPOL. The choice of polarimeter was made run-by-run to maximise the available luminosity and minimise the uncertainty in the measured polarisation. The measured luminosity was assigned a relative uncertainty of 2.6%. The uncertainties in the luminosity and polarisation measurements were not included in the total systematic uncertainty shown in the final results.

9 Results

9.1 Unpolarised cross sections

The single-differential cross-sections with respect to Q^2, x and y, tabulated in Tables 1, 2, 3, 4, 5 and 6, are shown in Fig. 3 for $Q^2 > 185\,\text{GeV}^2$ and $y < 0.9$ for the combined positive and negative polarisation samples having a residual polarisation of -0.03. The cross-sections $d\sigma/dx$ and $d\sigma/dy$ for $Q^2 > 3\,000\,\text{GeV}^2$ and $y < 0.9$ are also presented in Fig. 3. The measured cross sections demonstrate the precision of this measurement. The measured cross sections are well described by the SM prediction evaluated using the ZEUS-JETS PDFs [36]. The measurement of $d\sigma/dQ^2$ spans two orders of magnitude in Q^2, and at $Q^2 \sim 40\,000\,\text{GeV}^2$, the spatial resolution reaches $\sim 10^{-18}$ m.

The reduced cross sections of unpolarised e^-p NC DIS, tabulated in Tables 7 and 8, are presented in Fig. 4 with the residual polarisation of -0.03 corrected using theoretical predictions. The correction factors were at most 2% in the highest-Q^2 bins. The SM predictions are in good agreement with the measurements over the full kinematic range. Also shown are unpolarised e^+p NC DIS measurements with an integrated luminosity of $63.2\,\text{pb}^{-1}$ collected in 1999 and 2000 [4]. As discussed earlier, a significant difference between the e^-p and e^+p unpolarised reduced cross sections is seen at high-Q^2 values due to the contribution of $x\tilde{F}_3$.

Figure 5 shows the structure function $x\tilde{F}_3$ obtained from the unpolarised e^-p and e^+p reduced cross sections in the high-Q^2 region, according to Eq. (3). The systematic uncertainties between the measurements were treated as uncorrelated. The results are also

given in Table 9. The reduced cross sections visibly differ and are well described by the SM predictions.

The structure function $xF_3^{\gamma Z}$ has little dependence on Q^2 and so the measurements from $1\,500 < Q^2 < 30\,000\,\mathrm{GeV}^2$ have been extrapolated to $5\,000\,\mathrm{GeV}^2$, and then averaged, to obtain a higher statistical significance. The structure function $xF_3^{\gamma Z}$ measured at $Q^2 = 5\,000\,\mathrm{GeV}^2$, tabulated in Table 10, is shown in Fig. 6. It is well described by the SM predictions. The integral of $xF_3^{\gamma Z}$ in the region of $0.032 < x < 0.65$ is

$$\int_{0.032}^{0.65} \frac{dx}{x} xF_3^{\gamma Z} = 0.80 \pm 0.08(\mathrm{stat.}) \pm 0.03(\mathrm{syst.}). \tag{17}$$

This value is consistent with the SM prediction of 0.94 ± 0.02 as evaluated with the ZEUS-JETS PDFs, where the error is from the PDF uncertainty. Figure 6 also shows the measurement of $xF_3^{\gamma Z}$ obtained by the BCDMS collaboration from NC muon-carbon scattering at lower energies, which was extracted over the kinematic range $40 < Q^2 < 180\,\mathrm{GeV}^2$ and $0.2 < x < 0.7$ [37]. The BCDMS measurements were corrected for the difference of the u-valence and d-valence quark PDFs so as to be directly comparable to the $xF_3^{\gamma Z}$ obtained from NC $e^- p$ scattering [4]. The measurements presented in this paper extend the x range for $xF_3^{\gamma Z}$ data down to $x \sim 0.03$, well below the range of the BCDMS measurements. Furthermore, they are extracted at higher Q^2 values where perturbative QCD calculations are more reliable. Moreover, this measurement is also free from heavy-target corrections and isospin-symmetry assumptions which are inherent in previous fixed-target measurements. Therefore, at Bjorken x values from $\sim 10^{-2}$ to 0.65, this measurement adds valuable information to the global fits [38] for parton distribution functions.

9.2 Polarised cross sections

At HERA during 2005 and 2006 longitudinal polarisation effects in ep DIS become significant at the electroweak scale, where the contributions of both γ and Z exchange to the cross section are comparable. The reduced cross sections for positive and negative longitudinal polarisations, tabulated in Tables 11, 12, 13 and 14, are shown separately in Fig. 7 and are well described by the SM evaluated using the ZEUS-JETS PDFs.

At high Q^2, a difference between the positively and negatively polarised cross sections is predicted. To demonstrate this effect, the single-differential cross-section $d\sigma/dQ^2$ for

[4] In ep scattering, $xF_3^{\gamma Z} = (2u_v + d_v)/3$, while in eN scattering, $xF_3^{\gamma Z} = (u_v + d_v)/2$. The correction was evaluated by using the ZEUS-JETS PDFs and was typically about 15%.

$y < 0.9$, tabulated in Tables 15 and 16, was measured for positive and negative beam polarisations separately and is shown in Fig. 8. Both measurements are well described by the SM prediction.

The ratio of measured cross sections for the two different polarisation states are shown in Fig. 9 (a). The difference between the two polarisation states is clearly visible at higher Q^2. The asymmetry A^- (see Eq. 12) extracted from these measurements is tabulated in Table 19 and is shown in Fig. 9 (b), where only statistical uncertainties are considered. The uncertainty in A^- arising from the relative normalization between data sets was evaluated to be 1.4 %. The other systematic uncertainties are assumed to be cancelled. The results compare well to the SM prediction. The deviation of A^- from zero, particularly at high Q^2, shows the difference in the behaviour of the two polarisation states and is clear evidence of parity violation.

The effect of γ/Z interference is quantified by calculating the χ^2 per degree of freedom of A^- with respect both to zero and the SM prediction using the ZEUS-JETS PDFs. The χ^2/d.o.f. with respect to zero is determined to be 5.5, whereas the χ^2/d.o.f. with respect to the SM prediction is 1.5. Thus parity violation in ep NC DIS at very small distances is demonstrated at scales down to $\sim 10^{-18}$ m. At large Q^2 where the u quark dominates the PDF it is expected that $A^- \simeq 2a_e v_u e_u/e_u^2 \simeq 0.3$. The cross sections obtained from NC DIS measurements can be used to constrain the NC quark couplings within PDF fits [39], and the polarised electron beam data provide sensitivity to quark vector couplings. Therefore, this measurement is a stringent test of the electroweak sector of the Standard Model.

10 Summary

The cross sections for neutral current deep inelastic scattering in e^-p collisions with a longitudinally polarised electron beam have been measured. The measurements are based on a data sample with an integrated luminosity of 169.9 pb^{-1} collected with the ZEUS detector at HERA from 2005 to 2006 at a centre-of-mass energy of 318 GeV. The accessible range in Q^2 extended to $Q^2 = 50\,000$ GeV^2 and has allowed a stringent test of electroweak effects in the Standard Model.

The single-differential cross-sections with respect to Q^2, x and y are presented for $Q^2 > 185$ GeV^2 and $y < 0.9$, where the data obtained with negatively and positively polarised beams are combined. The cross sections $d\sigma/dx$ and $d\sigma/dy$ are also measured for $Q^2 > 3\,000$ GeV^2 and $y < 0.9$. The reduced cross sections are measured in the kinematic range $200 < Q^2 < 30\,000$ GeV^2 and $0.005 < x < 0.65$ at zero polarisation by correcting the residual polarisation of the combined data sample. These measurements are combined with previously measured e^+p neutral current cross sections to extract $x\tilde{F}_3$.

In addition, the interference structure function $xF_3^{\gamma Z}$ is extracted at an average value of $Q^2 = 5\,000\,\mathrm{GeV}^2$.

The reduced cross-sections and the single-differential cross-section $d\sigma/dQ^2$ have also been measured separately for positive and negative values of the longitudinal polarisation of the electron beam. Parity violation is observed through the polarisation asymmetry A^-. The measured cross sections confirm the predictions of the Standard Model and provide strong constraints at the electroweak scale.

Acknowledgements

We appreciate the contributions to the construction and maintenance of the ZEUS detector of many people who are not listed as authors. The HERA machine group and the DESY computing staff are especially acknowledged for their success in providing excellent operation of the collider and the data-analysis environment. We thank the DESY directorate for their strong support and encouragement.

References

[1] ZEUS Collab., J. Breitweg et al., Eur. Phys. J. **C 11**, 427 (1999).

[2] ZEUS Collab., S. Chekanov et al., Eur. Phys. J. **C 21**, 443 (2001).

[3] ZEUS Collab., S. Chekanov et al., Eur. Phys. J. **C 28**, 175 (2003).

[4] ZEUS Collab.; S. Chekanov et al., Phys. Rev. **D 70**, 052001 (2004).

[5] H1 Collab., S. Aid et al., Nucl. Phys. **B 470**, 3 (1996);
H1 Collab., C. Adloff et al., Nucl. Phys. **B 497**, 3 (1997);
H1 Collab., C. Adloff et al., Eur. Phys. J. **C 13**, 609 (2000);
H1 Collab., C. Adloff et al., Eur. Phys. J. **C 21**, 33 (2001);
H1 Collab., C. Adloff et al., Eur. Phys. J. **C 19**, 269 (2001);
H1 Collab., C. Adloff et al., Eur. Phys. J. **C 30**, 1 (2003).

[6] ZEUS Collab., S. Chekanov et al., Phys. Lett. **B 637**, 210 (2006).

[7] R. Devenish and A. Cooper-Sarkar, *Deep Inelastic Scattering*. Oxford University Press, 2003.

[8] M. Klein and T. Riemann, Z. Phys. **C 24**, 151 (1984).

[9] E. Rizvi and T. Sloan, EPJdirect **CN2**, 1 (2001). DOI 10.1007/s1010501c00N2.

[10] ZEUS Collab., U. Holm (ed.), *The ZEUS Detector*. Status Report (unpublished), DESY (1993), available on `http://www-zeus.desy.de/bluebook/bluebook.html`.

[11] N. Harnew et al., Nucl. Instr. and Meth. **A 279**, 290 (1989);
B. Foster et al., Nucl. Phys. Proc. Suppl. **B 32**, 181 (1993);
B. Foster et al., Nucl. Instr. and Meth. **A 338**, 254 (1994).

[12] A. Polini et al., Nucl. Instr. and Meth. **A 581**, 656 (2007).

[13] M. Derrick et al., Nucl. Instr. and Meth. **A 309**, 77 (1991);
A. Andresen et al., Nucl. Instr. and Meth. **A 309**, 101 (1991);
A. Caldwell et al., Nucl. Instr. and Meth. **A 321**, 356 (1992);
A. Bernstein et al., Nucl. Instr. and Meth. **A 336**, 23 (1993).

[14] H. Abramowicz et al., Nucl. Instr. and Meth. **A 313**, 126 (1992).

[15] G. Abbiendi et al., Nucl. Instr. and Meth. **A 333**, 342 (1993).

[16] A.A. Sokolov and I.M. Ternov, Sov. Phys. Dokl. **8**, 1203 (1964).

[17] V.N. Baier and V.A. Khoze, Sov. J. Nucl. Phys. **238** (1969).

[18] D.P. Barber et al., Nucl. Instr. and Meth. **A 329**, 79 (1993).

[19] M. Beckmann et al., Nucl. Instr. and Meth. **A 479**, 334 (2002).

[20] A. Kwiatkowski, H. Spiesberger and H.-J. Möhring, Comp. Phys. Comm. **69**, 155 (1992). Also in *Proc. Workshop Physics at HERA*, eds. W. Buchmüller and G.Ingelman, (DESY, Hamburg, 1991).

[21] G.A. Schuler and H. Spiesberger, *Proc. Workshop on Physics at HERA*, W. Buchmüller and G. Ingelman (eds.), Vol. 3, p. 1419. Hamburg, Germany, DESY (1991);
H. Spiesberger, HERACLES *and* DJANGOH*: Event Generation of ep Interactions at HERA Including Radiative Processes*, 2005, available on `http://wwwthep.physik.uni-mainz.de/~hspiesb/djangoh/djangoh.html`.

[22] CTEQ Collab., H.L. Lai et al., Eur. Phys. J. **C 12**, 375 (2000).

[23] L. Lönnblad, Comp. Phys. Comm. **71**, 15 (1992).

[24] G. Ingelman, A. Edin and J. Rathsman, Comp. Phys. Comm. **101**, 108 (1997).

[25] T. Sjöstrand, Comp. Phys. Comm. **39**, 347 (1986);
T. Sjöstrand and M. Bengtsson, Comp. Phys. Comm. **43**, 367 (1987);
T. Sjöstrand, Comp. Phys. Comm. **82**, 74 (1994).

[26] H. Jung, Comp. Phys. Comm. **86**, 147 (1995).

[27] G. Marchesini et al., Comp. Phys. Comm. **67**, 465 (1992).

[28] R. Brun et al., GEANT3, Technical Report CERN-DD/EE/84-1, CERN, 1987.

[29] S.U. Noor, *Measurement of Neutral Current Electron-Proton Cross Sections with Longitudinally Polarised Electrons using the ZEUS Detector.* Ph.D. Thesis, York University, 2007, available on `http://www-zeus.desy.de/physics/exo/ZEUS_PUBLIC/theses.php`.

[30] S. Bentvelsen, J. Engelen and P. Kooijman, *Proc. Workshop on Physics at HERA*, W. Buchmüller and G. Ingelman (eds.), Vol. 1, p. 23. Hamburg, Germany, DESY (1992);
K.C. Höger, *Proc. Workshop on Physics at HERA*, W. Buchmüller and G. Ingelman (eds.), Vol. 1, p. 43. Hamburg, Germany, DESY (1992).

[31] F. Jacquet and A. Blondel, *Proceedings of the Study for an ep Facility for Europe*, U. Amaldi (ed.), p. 391. Hamburg, Germany (1979). Also in preprint DESY 79/48.

[32] W. H. Smith, K. Tokushuku and L. W. Wiggers, *Proc. Computing in High-Energy Physics (CHEP), Annecy, France, Sept. 1992*, C. Verkerk and W. Wojcik (eds.), p. 222. CERN, Geneva, Switzerland (1992). Also in preprint DESY 92-150B.

[33] P. Allfrey et al., Nucl. Instr. and Meth. **A 580**, 1257 (2007).

[34] Particle Data Group, D.E. Groom et al., Eur. Phys. J. **C 15**, 1 (2000).

[35] H. Abramowicz, A. Caldwell and R. Sinkus, Nucl. Instr. and Meth. **A 365**, 508 (1995).

[36] ZEUS Collab., S. Chekanov et al., Eur. Phys. J. **C 42**, 1 (2005).

[37] BCDMS Collab., A. Argento et al., Phys. Lett. **B 140**, 142 (1984).

[38] P.M. Nadolsky et al., Phys. Rev. **D 78**, 013004 (2008); A.D. Martin et al., Preprint hep-ph/090100002.

[39] S. Shimizu, *Proc.* 14^{th} *Int. Workshop on Deep Inelastic Scattering (DIS2006), Tsukuba, Japan, April 2006*, M. Kuze, K. Nagano and K. Tokushuku (eds.), pp. 145–148. World Scientific, Singapore (2006).

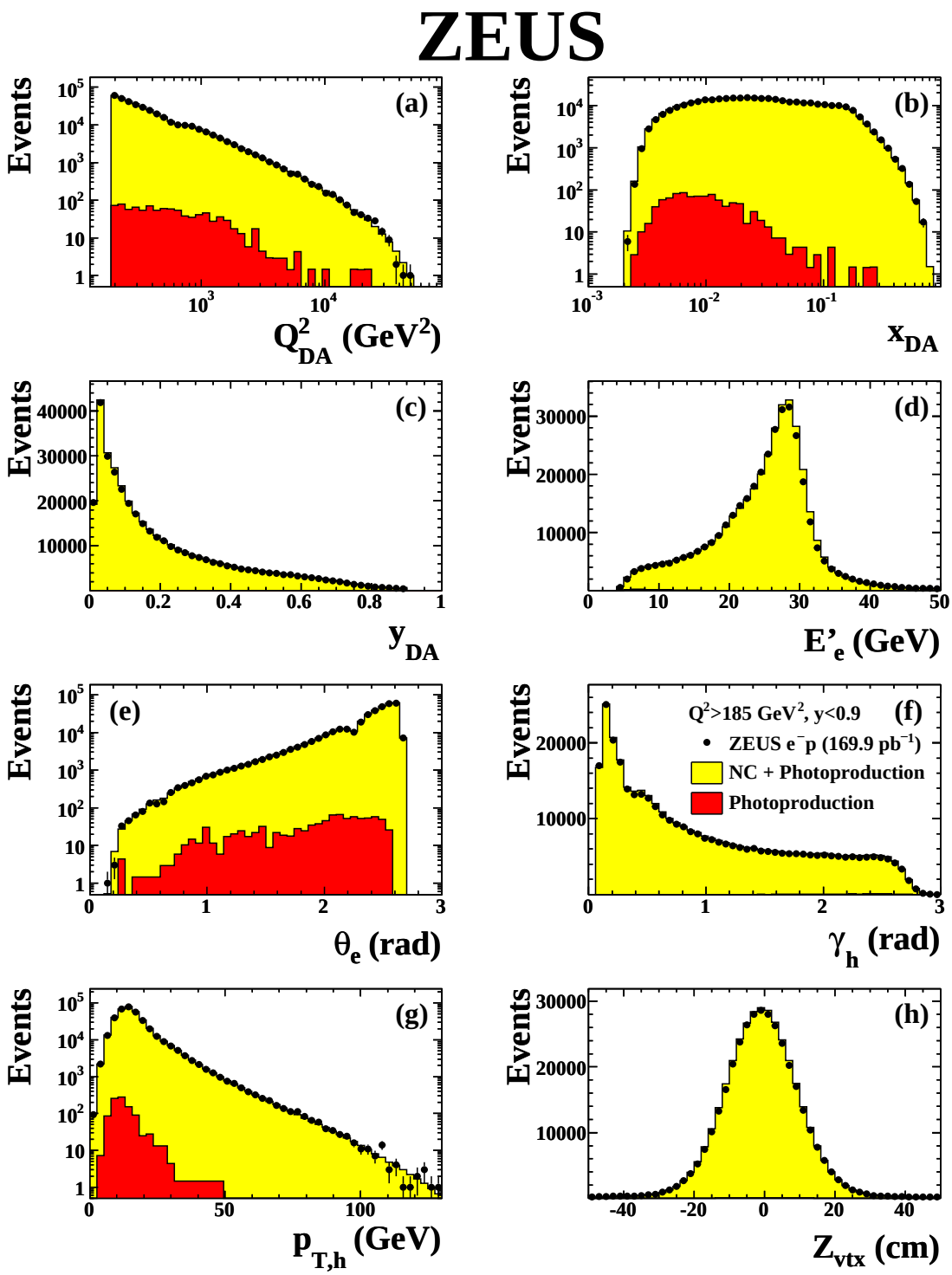

Figure 1: *Comparison of the final e^-p NC data sample with the expectations of the MC simulation described in the text. The MCs are normalised to the data luminosity. The distributions of (a) $Q^2_{\rm DA}$, (b) $x_{\rm DA}$, (c) $y_{\rm DA}$, (d) the energy of the scattered electron, $E'_{\rm e}$, (e) the angle of the scattered electron, $\theta_{\rm e}$, (f) the hadronic angle, γ_h, (g) the transverse momentum of the hadronic system, $p_{T,h}$, and (h) the Z coordinate of the event vertex, $Z_{\rm vtx}$, are shown.*

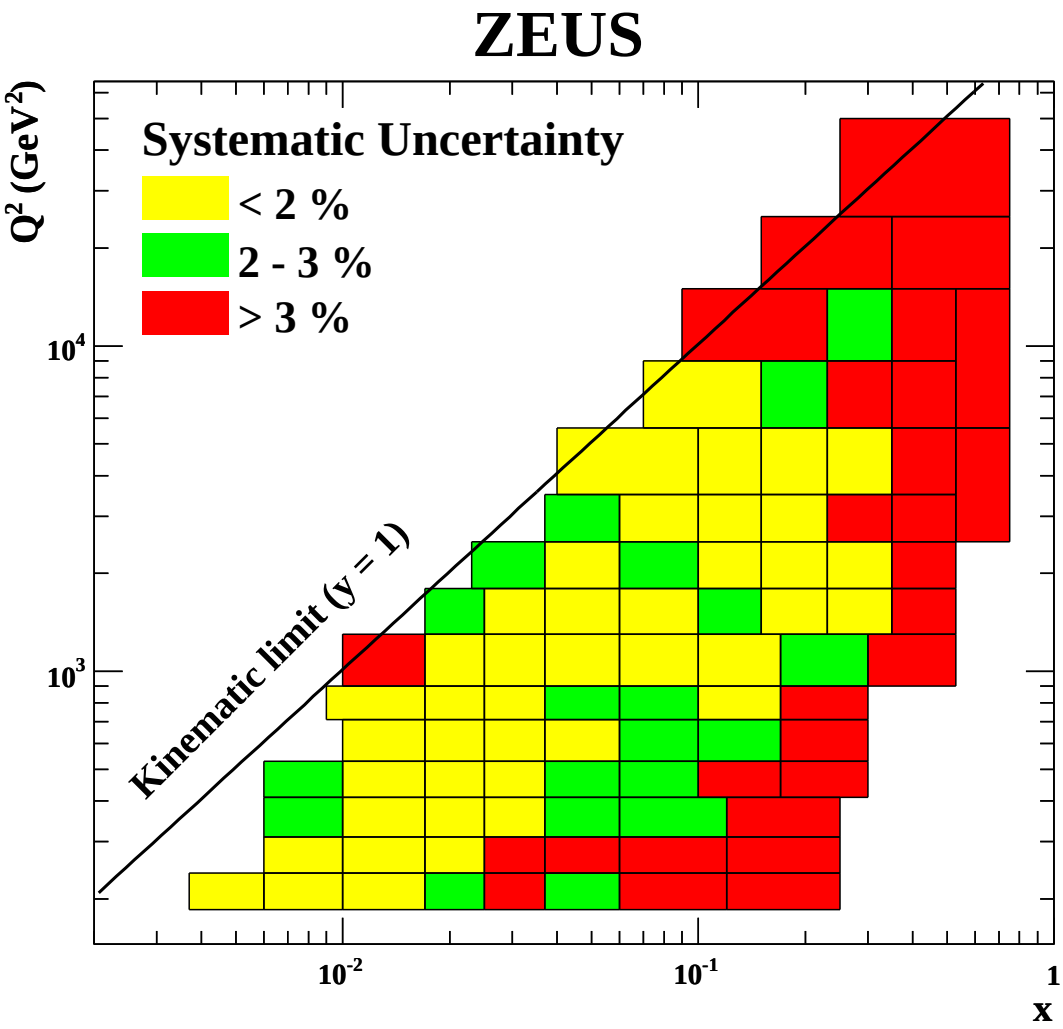

Figure 2: *The total systematic uncertainty for the bins used in the reduced cross section measurements.*

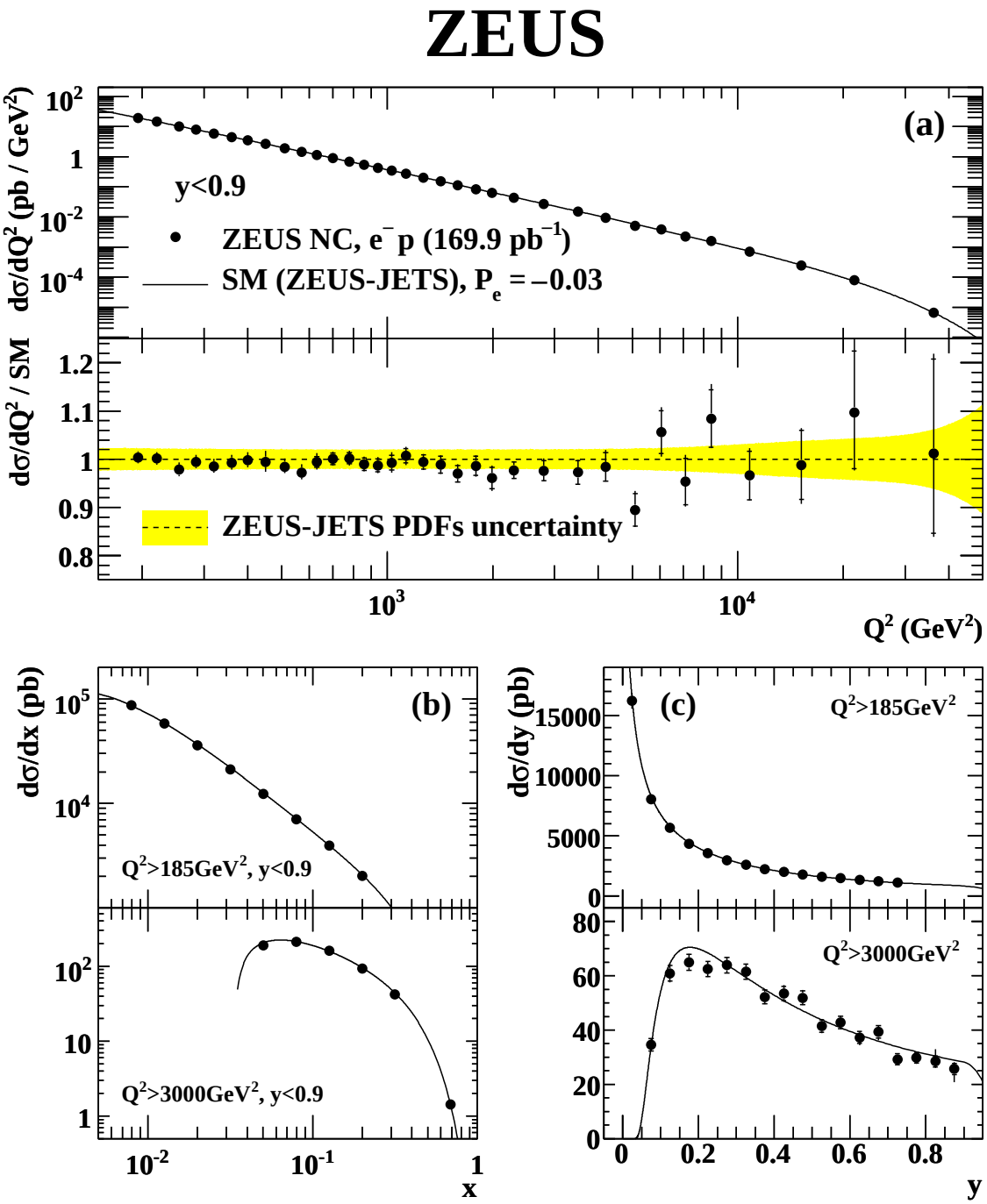

Figure 3: *The e^-p NC DIS cross sections: (a) $d\sigma/dQ^2$ for $y < 0.9$ and the ratio to the SM prediction, (b) $d\sigma/dx$ for $Q^2 > 185\ GeV^2$ and $Q^2 > 3000\ GeV^2$ for $y < 0.9$ and (c) $d\sigma/dy$ for $Q^2 > 185\ GeV^2$ and $Q^2 > 3000\ GeV^2$. The closed circles represent data points in which the inner error bars show the statistical uncertainty while the outer bars show the statistical and systematic uncertainties added in quadrature. The curves show the predictions of the SM evaluated using the ZEUS-JETS PDFs at a polarisation corresponding to the residual polarisation in the data and the shaded band shows the uncertainties from the ZEUS-JETS PDFs.*

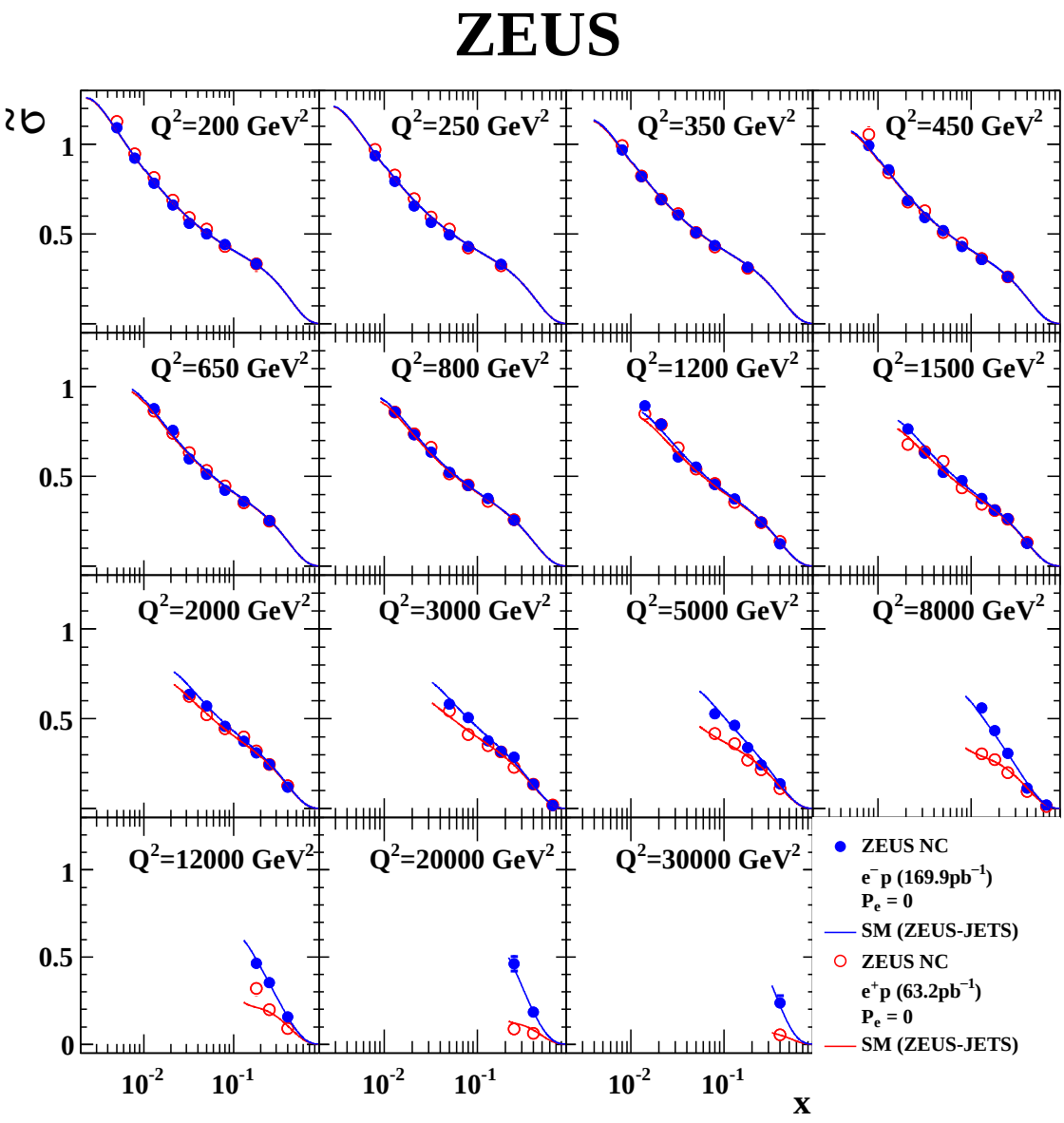

Figure 4: *The $e^{\pm}p$ unpolarised NC DIS reduced cross section $\tilde{\sigma}$ plotted as a function of x at fixed Q^2. The closed (open) circles represent data points for e^-p (e^+p) collisions in which the inner error bars show the statistical uncertainty while the outer bars show the statistical and systematic uncertainties added in quadrature, although errors are too small to be seen in most cases. The curves show the predictions of the SM evaluated using the ZEUS-JETS PDFs.*

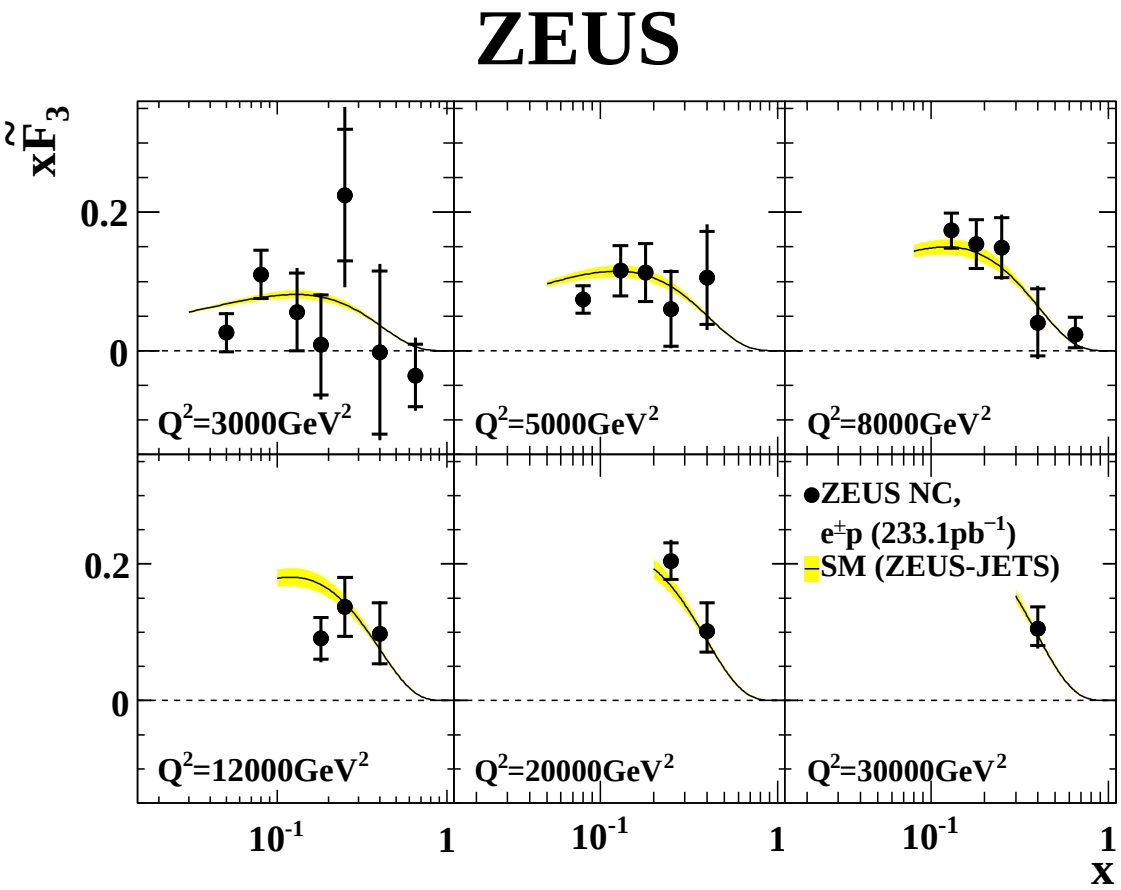

Figure 5: *The structure function $x\tilde{F}_3$ plotted as a function of x at fixed-Q^2. The closed circles represent the ZEUS data. The inner error bars show the statistical uncertainty while the outer ones show the statistical and systematic uncertainties added in quadrature. The curves show the predictions of the SM evaluated using the ZEUS-JETS PDFs with the shaded band indicating the uncertainties.*

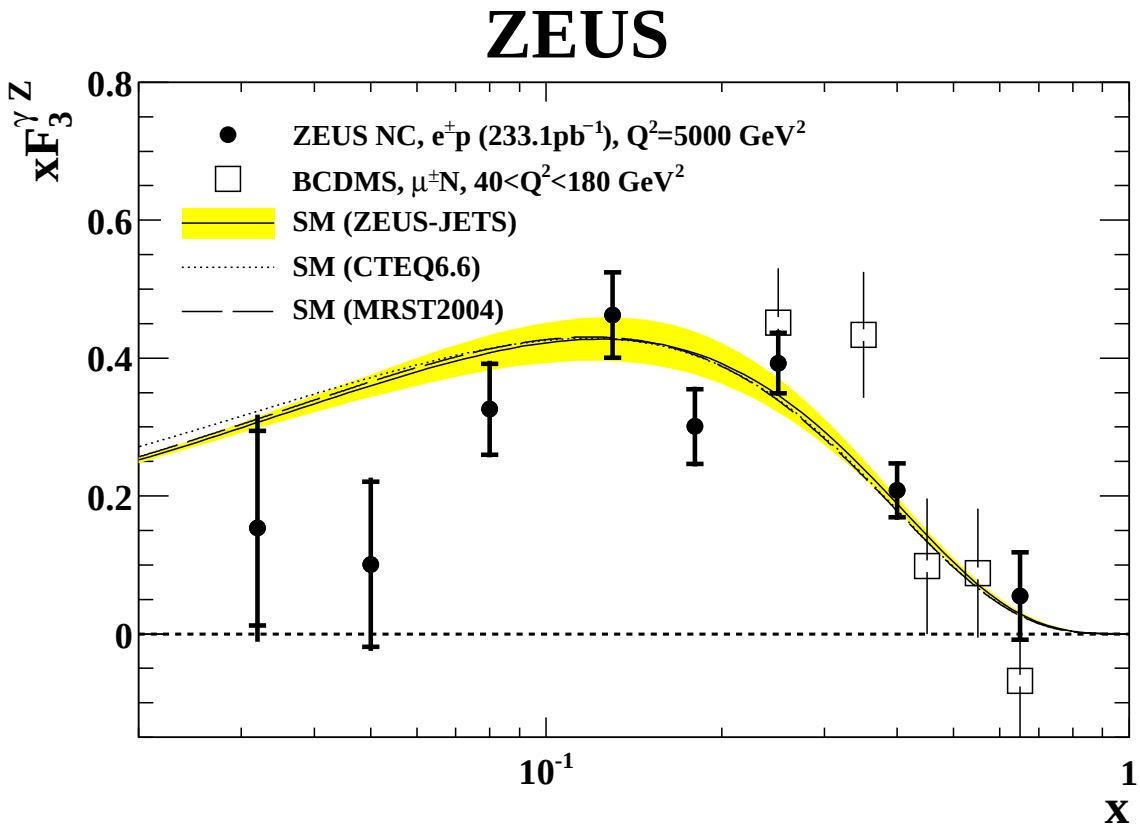

Figure 6: *The structure function $xF_3^{\gamma Z}$ extrapolated to a single Q^2 value of $5\,000\ GeV^2$ and plotted as a function of x. The closed circles represent data points in which the inner error bars show the statistical uncertainty while the outer bars show the statistical and systematic uncertainties added in quadrature. The curves show the predictions of the SM evaluated using several PDFs : ZEUS-JETS (shaded band shows the uncertainties), CTEQ6.6 and MRST2004. The measurements by the BCDMS collaboration are shown as open squares.*

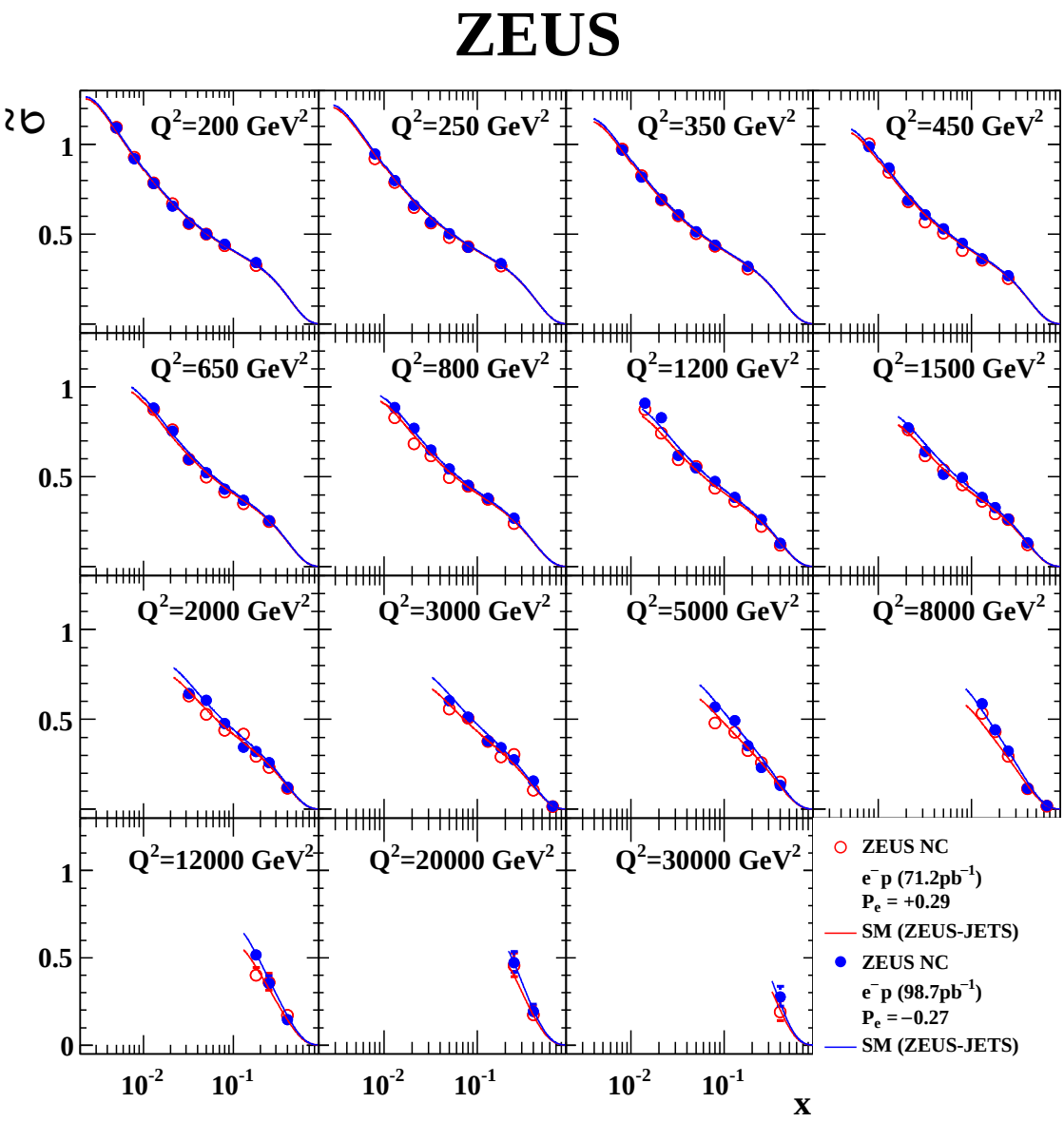

Figure 7: *The e^-p NC DIS reduced cross section $\tilde{\sigma}$ for positively and negatively polarised beams plotted as a function of x at fixed Q^2. The closed (open) circles represent the ZEUS data for negative (positive) polarisation. The inner error bars show the statistical uncertainty while the outer bars show the statistical and systematic uncertainties added in quadrature. The curves show the predictions of the SM evaluated using the ZEUS-JETS PDFs.*

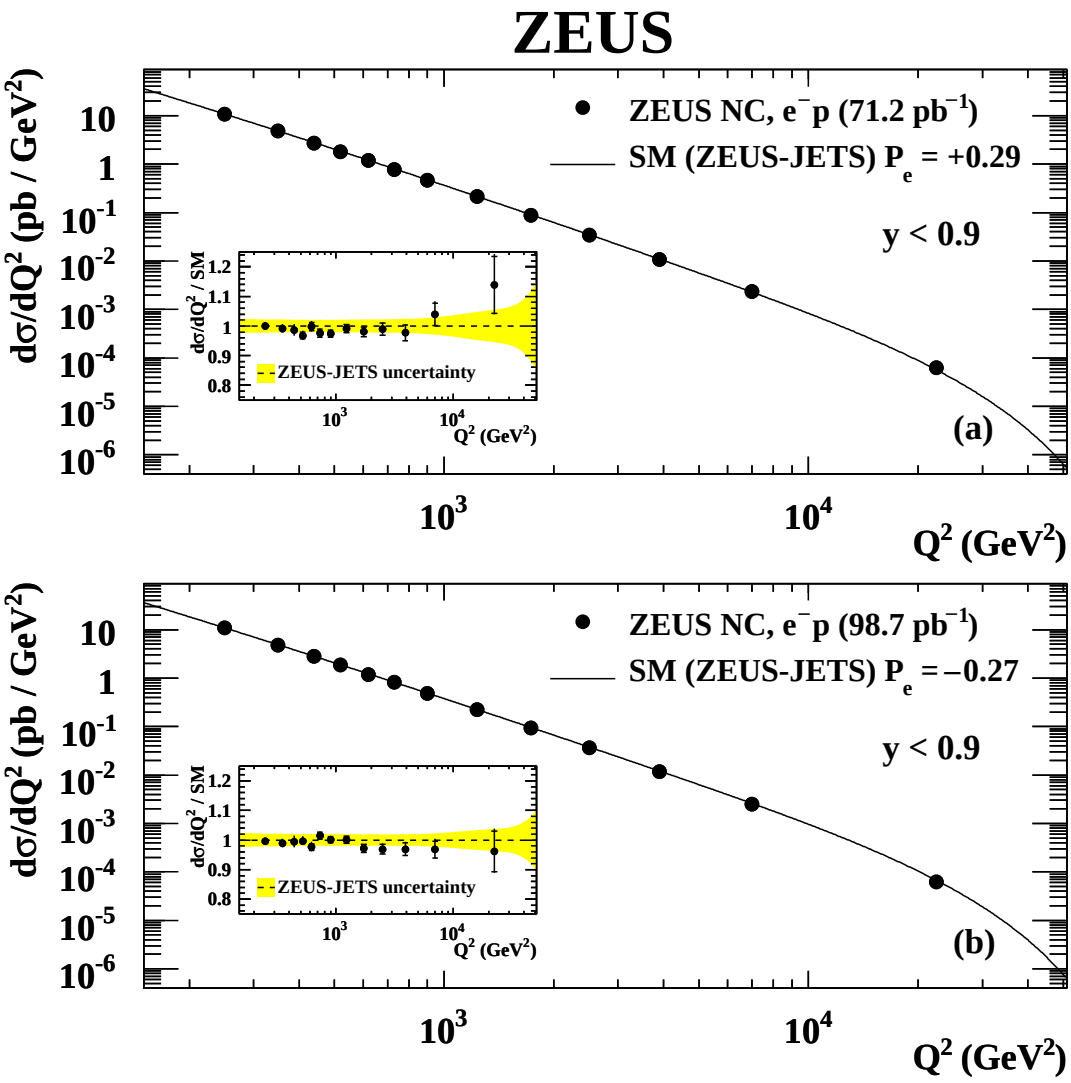

Figure 8: *The e^-p NC DIS cross section $d\sigma/dQ^2$ for (a) positive and (b) negative polarisation. The inset shows the ratio to the SM prediction. The closed circles represent the ZEUS data. The inner error bars show the statistical uncertainty while the outer bars show the statistical and systematic uncertainties added in quadrature. The curves show the predictions of the SM evaluated using the ZEUS-JETS PDFs.*

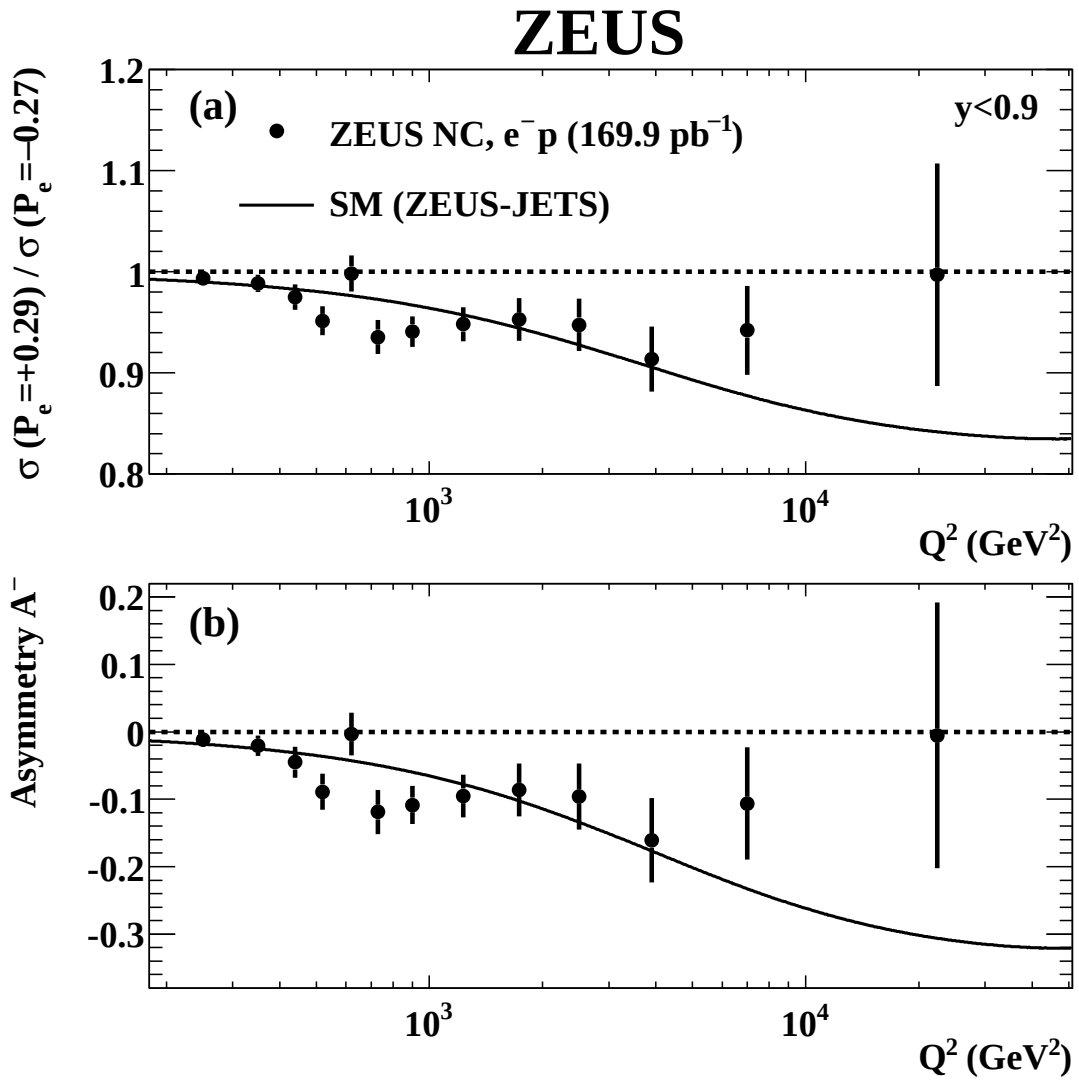

Figure 9: *The ratio of $d\sigma/dQ^2$ using positive and negative polarisation in (a), and the polarisation asymmetry A^- as a function of Q^2 in (b). The closed circles represent ZEUS data. Only statistical uncertainties are considered as the systematic uncertainties are assumed to cancel. The curves show the predictions of the SM evaluated using the ZEUS-JETS PDFs.*

Q^2 range (GeV^2)			Q_c^2 (GeV^2)	$d\sigma/dQ^2$ (pb/ GeV^2)	$N_{\rm data}$	$N_{\rm bg}^{\rm MC}$
185	–	210	195	$(1.96 \pm 0.01\ ^{+0.02}_{-0.02})\cdot 10^{1}$	58678	65.4
210	–	240	220	$(1.47 \pm 0.01\ ^{+0.02}_{-0.02})\cdot 10^{1}$	51660	83.5
240	–	270	255	$(1.01 \pm 0.01\ ^{+0.01}_{-0.01})\cdot 10^{1}$	37659	52.4
270	–	300	285	$7.89 \pm 0.05\ ^{+0.11}_{-0.09}$	29355	51.1
300	–	340	320	$5.93 \pm 0.04\ ^{+0.08}_{-0.07}$	29377	53.3
340	–	380	360	$4.51 \pm 0.03\ ^{+0.06}_{-0.05}$	22298	55.0
380	–	430	400	$3.52 \pm 0.03\ ^{+0.05}_{-0.04}$	21008	59.4
430	–	480	450	$2.63 \pm 0.02\ ^{+0.06}_{-0.05}$	15502	54.9
480	–	540	510	$1.92 \pm 0.02\ ^{+0.03}_{-0.02}$	13332	45.5
540	–	600	570	$1.45 \pm 0.02\ ^{+0.02}_{-0.01}$	9290	49.4
600	–	670	630	$1.16 \pm 0.01\ ^{+0.02}_{-0.01}$	8405	48.6
670	–	740	700	$(8.98 \pm 0.11\ ^{+0.07}_{-0.07})\cdot 10^{-1}$	7483	20.6
740	–	820	780	$(6.88 \pm 0.08\ ^{+0.06}_{-0.06})\cdot 10^{-1}$	7608	26.3
820	–	900	860	$(5.33 \pm 0.07\ ^{+0.04}_{-0.04})\cdot 10^{-1}$	6287	33.5
900	–	990	940	$(4.27 \pm 0.06\ ^{+0.05}_{-0.04})\cdot 10^{-1}$	5690	32.1
990	–	1080	1030	$(3.41 \pm 0.05\ ^{+0.05}_{-0.05})\cdot 10^{-1}$	4644	29.4
1080	–	1200	1130	$(2.75 \pm 0.04\ ^{+0.03}_{-0.03})\cdot 10^{-1}$	4907	30.5
1200	–	1350	1270	$(2.02 \pm 0.03\ ^{+0.01}_{-0.01})\cdot 10^{-1}$	4645	24.4
1350	–	1500	1420	$(1.52 \pm 0.03\ ^{+0.02}_{-0.01})\cdot 10^{-1}$	3499	31.8
1500	–	1700	1590	$(1.12 \pm 0.02\ ^{+0.01}_{-0.01})\cdot 10^{-1}$	3452	27.6
1700	–	1900	1790	$(8.40 \pm 0.17\ ^{+0.09}_{-0.09})\cdot 10^{-2}$	2611	18.8
1900	–	2100	1990	$(6.25 \pm 0.14\ ^{+0.09}_{-0.10})\cdot 10^{-2}$	1957	7.2
2100	–	2600	2300	$(4.39 \pm 0.08\ ^{+0.03}_{-0.03})\cdot 10^{-2}$	3315	13.3
2600	–	3200	2800	$(2.65 \pm 0.06\ ^{+0.04}_{-0.02})\cdot 10^{-2}$	2345	21.9
3200	–	3900	3500	$(1.48 \pm 0.04\ ^{+0.01}_{-0.01})\cdot 10^{-2}$	1597	4.5
3900	–	4700	4200	$(9.32 \pm 0.28\ ^{+0.18}_{-0.08})\cdot 10^{-3}$	1111	2.9
4700	–	5600	5100	$(5.08 \pm 0.19\ ^{+0.11}_{-0.06})\cdot 10^{-3}$	708	2.8
5600	–	6600	6050	$(3.81 \pm 0.16\ ^{+0.10}_{-0.09})\cdot 10^{-3}$	586	4.4
6600	–	7800	7100	$(2.23 \pm 0.11\ ^{+0.07}_{-0.04})\cdot 10^{-3}$	401	1.5
7800	–	9200	8400	$(1.59 \pm 0.09\ ^{+0.06}_{-0.02})\cdot 10^{-3}$	331	0.0
9200	–	12800	10800	$(6.90 \pm 0.36\ ^{+0.19}_{-0.05})\cdot 10^{-4}$	369	1.4
12800	–	18100	15200	$(2.45 \pm 0.18\ ^{+0.07}_{-0.09})\cdot 10^{-4}$	193	1.4
18100	–	25600	21500	$(7.99\ ^{+0.93}_{-0.85}\ ^{+0.65}_{-0.24})\cdot 10^{-5}$	97	3.0
25600	–	51200	36200	$(6.62\ ^{+1.28}_{-1.08}\ ^{+0.45}_{-0.33})\cdot 10^{-6}$	37	0.0

Table 1: *The single differential cross section $d\sigma/dQ^2$ ($y < 0.9$) for the reaction $e^- p \to e^- X$ ($\mathcal{L} = 169.9\,pb^{-1}, P_e = -0.03$). The bin range, bin centre (Q_c^2) and measured cross section corrected to the electroweak Born level are shown. The first (second) error on the cross section corresponds to the statistical (systematic) uncertainties. The number of observed data events (N_{data}) and simulated background events (N_{bg}^{MC}) are also shown.*

Q_c^2 (GeV^2)	$d\sigma/dQ^2$ (pb/ GeV^2)	stat. (%)	sys. (%)	δ_1 (%)	δ_2 (%)	δ_3 (%)	δ_4 (%)	δ_5 (%)	δ_6 (%)	δ_7 (%)	$\delta_8 - \delta_{13}$ (%)
195	1.96 $\cdot 10^1$	$\pm$ 0.4	$^{+1.2}_{-1.1}$	$^{+0.0}_{-0.1}$	$^{-0.5}_{+0.6}$	$^{+0.4}_{-0.4}$	$^{+0.1}_{-0.1}$	$^{-0.1}_{+0.1}$	$^{+0.1}_{+0.2}$	$^{+0.0}_{-0.0}$	$^{+0.9}_{-0.9}$
220	1.47 $\cdot 10^1$	$\pm$ 0.5	$^{+1.3}_{-1.2}$	$^{+0.4}_{-0.0}$	$^{-0.5}_{+0.6}$	$^{+0.4}_{-0.4}$	$^{+0.6}_{-0.6}$	$^{-0.0}_{+0.1}$	$^{-0.0}_{+0.2}$	$^{+0.1}_{-0.1}$	$^{+0.6}_{-0.8}$
255	1.01 $\cdot 10^1$	$\pm$ 0.6	$^{+1.5}_{-1.3}$	$^{+0.6}_{-0.0}$	$^{-0.5}_{+0.6}$	$^{+0.8}_{-0.8}$	$^{+0.6}_{-0.6}$	$^{-0.1}_{+0.2}$	$^{-0.1}_{+0.2}$	$^{+0.1}_{-0.1}$	$^{+0.7}_{-0.7}$
285	7.89	$\pm$ 0.6	$^{+1.4}_{-1.1}$	$^{+0.7}_{-0.0}$	$^{-0.5}_{+0.7}$	$^{+0.2}_{-0.2}$	$^{+0.7}_{-0.7}$	$^{-0.1}_{+0.2}$	$^{-0.1}_{+0.1}$	$^{+0.1}_{-0.1}$	$^{+0.6}_{-0.6}$
320	5.93	$\pm$ 0.6	$^{+1.4}_{-1.2}$	$^{+0.5}_{+0.0}$	$^{-0.5}_{+0.7}$	$^{+0.6}_{-0.6}$	$^{+0.5}_{-0.5}$	$^{-0.1}_{+0.3}$	$^{-0.2}_{+0.2}$	$^{+0.1}_{-0.1}$	$^{+0.7}_{-0.7}$
360	4.51	$\pm$ 0.7	$^{+1.4}_{-1.2}$	$^{+0.8}_{-0.1}$	$^{-0.5}_{+0.6}$	$^{+0.4}_{-0.4}$	$^{+0.7}_{-0.7}$	$^{+0.1}_{+0.1}$	$^{-0.2}_{+0.1}$	$^{+0.1}_{-0.1}$	$^{+0.6}_{-0.7}$
400	3.52	$\pm$ 0.7	$^{+1.5}_{-1.2}$	$^{+0.5}_{-0.0}$	$^{-0.5}_{+0.6}$	$^{-0.1}_{+0.1}$	$^{+0.9}_{-0.9}$	$^{-0.0}_{+0.0}$	$^{-0.4}_{+0.5}$	$^{+0.1}_{-0.1}$	$^{+0.6}_{-0.5}$
450	2.63	$\pm$ 0.8	$^{+2.1}_{-1.9}$	$^{+0.5}_{-0.0}$	$^{-0.5}_{+0.6}$	$^{+0.9}_{-0.9}$	$^{+1.4}_{-1.4}$	$^{-0.2}_{+0.5}$	$^{-0.3}_{+0.7}$	$^{+0.1}_{-0.1}$	$^{+0.6}_{-0.7}$
510	1.92	$\pm$ 0.9	$^{+1.5}_{-1.0}$	$^{+1.0}_{-0.0}$	$^{-0.6}_{+0.7}$	$^{+0.3}_{-0.3}$	$^{+0.2}_{-0.2}$	$^{-0.1}_{+0.1}$	$^{-0.3}_{+0.4}$	$^{+0.1}_{-0.1}$	$^{+0.7}_{-0.6}$
570	1.45	$\pm$ 1.1	$^{+1.4}_{-0.9}$	$^{+0.8}_{-0.1}$	$^{-0.5}_{+0.7}$	$^{+0.3}_{-0.3}$	$^{+0.1}_{-0.1}$	$^{-0.2}_{+0.4}$	$^{+0.1}_{+0.2}$	$^{+0.2}_{-0.2}$	$^{+0.7}_{-0.6}$
630	1.16	$\pm$ 1.1	$^{+1.5}_{-1.1}$	$^{+1.0}_{-0.2}$	$^{-0.7}_{+0.7}$	$^{+0.0}_{-0.0}$	$^{-0.7}_{+0.7}$	$^{+0.1}_{-0.1}$	$^{+0.1}_{+0.2}$	$^{+0.2}_{-0.2}$	$^{+0.2}_{-0.3}$
700	8.98 $\cdot 10^{-1}$	$\pm$ 1.2	$^{+0.8}_{-0.7}$	$^{+0.1}_{-0.2}$	$^{-0.6}_{+0.7}$	$^{+0.1}_{-0.1}$	$^{+0.1}_{-0.1}$	$^{+0.1}_{+0.2}$	$^{+0.3}_{-0.1}$	$^{+0.1}_{-0.1}$	$^{+0.3}_{-0.4}$
780	6.88 $\cdot 10^{-1}$	$\pm$ 1.2	$^{+0.9}_{-0.9}$	$^{+0.0}_{-0.4}$	$^{-0.5}_{+0.6}$	$^{+0.5}_{-0.5}$	$^{+0.5}_{-0.5}$	$^{+0.1}_{+0.0}$	$^{+0.1}_{+0.0}$	$^{+0.1}_{-0.1}$	$^{+0.2}_{-0.3}$
860	5.33 $\cdot 10^{-1}$	$\pm$ 1.3	$^{+0.8}_{-0.8}$	$^{+0.4}_{+0.0}$	$^{-0.4}_{+0.5}$	$^{-0.4}_{+0.4}$	$^{-0.1}_{+0.1}$	$^{-0.3}_{-0.3}$	$^{-0.1}_{-0.1}$	$^{+0.2}_{-0.2}$	$^{+0.3}_{-0.4}$
940	4.27 $\cdot 10^{-1}$	$\pm$ 1.4	$^{+1.1}_{-0.9}$	$^{+0.0}_{-0.2}$	$^{-0.4}_{+0.5}$	$^{-0.4}_{+0.4}$	$^{+0.6}_{-0.6}$	$^{+0.4}_{-0.1}$	$^{-0.0}_{-0.1}$	$^{+0.2}_{-0.2}$	$^{+0.4}_{-0.2}$
1030	3.41 $\cdot 10^{-1}$	$\pm$ 1.5	$^{+1.5}_{-1.4}$	$^{+0.4}_{-0.1}$	$^{-0.3}_{+0.5}$	$^{+0.7}_{-0.7}$	$^{+1.1}_{-1.1}$	$^{+0.1}_{+0.2}$	$^{-0.1}_{-0.4}$	$^{+0.3}_{-0.3}$	$^{+0.4}_{-0.4}$
1130	2.75 $\cdot 10^{-1}$	$\pm$ 1.5	$^{+1.2}_{-1.2}$	$^{+0.2}_{-0.3}$	$^{-0.4}_{+0.4}$	$^{+0.9}_{-0.9}$	$^{-0.1}_{+0.1}$	$^{-0.1}_{+0.4}$	$^{+0.1}_{-0.4}$	$^{+0.2}_{-0.3}$	$^{+0.3}_{-0.4}$
1270	2.02 $\cdot 10^{-1}$	$\pm$ 1.5	$^{+0.7}_{-0.7}$	$^{+0.0}_{-0.1}$	$^{-0.3}_{+0.4}$	$^{-0.4}_{+0.4}$	$^{-0.1}_{+0.1}$	$^{+0.1}_{-0.1}$	$^{-0.1}_{-0.2}$	$^{+0.3}_{-0.2}$	$^{+0.3}_{-0.4}$
1420	1.52 $\cdot 10^{-1}$	$\pm$ 1.7	$^{+1.0}_{-0.9}$	$^{+0.5}_{+0.0}$	$^{-0.3}_{+0.4}$	$^{+0.1}_{-0.1}$	$^{-0.6}_{+0.6}$	$^{+0.1}_{-0.2}$	$^{-0.1}_{-0.0}$	$^{+0.4}_{-0.4}$	$^{+0.4}_{-0.4}$
1590	1.12 $\cdot 10^{-1}$	$\pm$ 1.7	$^{+1.0}_{-0.6}$	$^{+0.6}_{-0.1}$	$^{-0.3}_{+0.3}$	$^{+0.1}_{-0.1}$	$^{-0.2}_{+0.2}$	$^{+0.3}_{+0.0}$	$^{+0.0}_{+0.3}$	$^{+0.4}_{-0.3}$	$^{+0.3}_{-0.3}$
1790	8.40 $\cdot 10^{-2}$	$\pm$ 2.0	$^{+1.0}_{-1.1}$	$^{+0.5}_{-0.1}$	$^{-0.3}_{+0.3}$	$^{+0.6}_{-0.6}$	$^{-0.5}_{+0.5}$	$^{+0.2}_{-0.1}$	$^{-0.5}_{-0.4}$	$^{+0.3}_{-0.3}$	$^{+0.3}_{-0.4}$
1990	6.25 $\cdot 10^{-2}$	$\pm$ 2.3	$^{+1.5}_{-1.6}$	$^{+0.1}_{-0.7}$	$^{-0.3}_{+0.4}$	$^{-0.5}_{+0.5}$	$^{+1.3}_{-1.3}$	$^{+0.1}_{+0.0}$	$^{+0.1}_{-0.2}$	$^{+0.1}_{-0.2}$	$^{+0.3}_{-0.3}$
2300	4.39 $\cdot 10^{-2}$	$\pm$ 1.8	$^{+0.7}_{-0.6}$	$^{+0.2}_{+0.0}$	$^{-0.2}_{+0.3}$	$^{+0.2}_{-0.2}$	$^{+0.1}_{-0.1}$	$^{-0.2}_{-0.0}$	$^{+0.3}_{+0.1}$	$^{+0.3}_{-0.2}$	$^{+0.3}_{-0.4}$
2800	2.65 $\cdot 10^{-2}$	$\pm$ 2.1	$^{+1.6}_{-0.7}$	$^{+1.4}_{-0.3}$	$^{-0.2}_{+0.3}$	$^{-0.2}_{+0.2}$	$^{+0.4}_{-0.4}$	$^{+0.1}_{+0.0}$	$^{+0.3}_{+0.1}$	$^{+0.4}_{-0.4}$	$^{+0.4}_{-0.2}$
3500	1.48 $\cdot 10^{-2}$	$\pm$ 2.5	$^{+0.8}_{-0.8}$	$^{+0.2}_{+0.0}$	$^{-0.2}_{+0.3}$	$^{-0.5}_{+0.5}$	$^{-0.2}_{+0.2}$	$^{-0.1}_{-0.0}$	$^{+0.0}_{-0.4}$	$^{+0.3}_{-0.1}$	$^{+0.4}_{-0.4}$
4200	9.32 $\cdot 10^{-3}$	$\pm$ 3.0	$^{+1.9}_{-0.8}$	$^{+1.8}_{-0.3}$	$^{-0.2}_{+0.3}$	$^{+0.4}_{-0.4}$	$^{-0.0}_{+0.0}$	$^{+0.1}_{-0.0}$	$^{-0.4}_{+0.0}$	$^{+0.1}_{-0.2}$	$^{+0.2}_{-0.4}$
5100	5.08 $\cdot 10^{-3}$	$\pm$ 3.8	$^{+2.2}_{-1.1}$	$^{+1.9}_{-0.3}$	$^{-0.2}_{+0.2}$	$^{+0.9}_{-0.9}$	$^{-0.0}_{+0.0}$	$^{+0.0}_{+0.0}$	$^{+0.1}_{+0.2}$	$^{+0.2}_{-0.2}$	$^{+0.5}_{-0.5}$
6050	3.81 $\cdot 10^{-3}$	$\pm$ 4.2	$^{+2.5}_{-2.4}$	$^{+1.0}_{+0.0}$	$^{-0.2}_{+0.3}$	$^{-2.1}_{+2.1}$	$^{-0.4}_{+0.4}$	$^{+0.0}_{+0.0}$	$^{-0.8}_{-0.1}$	$^{+0.8}_{-0.3}$	$^{+0.4}_{-0.4}$
7100	2.23 $\cdot 10^{-3}$	$\pm$ 5.0	$^{+3.0}_{-1.9}$	$^{+2.4}_{-0.1}$	$^{-0.3}_{+0.3}$	$^{+1.4}_{-1.4}$	$^{+0.9}_{-0.9}$	$^{+0.0}_{+0.0}$	$^{-0.8}_{+0.5}$	$^{+0.2}_{-0.1}$	$^{+0.4}_{-0.5}$
8400	1.59 $\cdot 10^{-3}$	$\pm$ 5.5	$^{+3.7}_{-1.2}$	$^{+3.7}_{-0.9}$	$^{-0.3}_{+0.4}$	$^{-0.2}_{+0.2}$	$^{+0.1}_{-0.1}$	$^{+0.0}_{+0.0}$	$^{-0.0}_{-0.0}$	$^{+0.2}_{+0.0}$	$^{+0.3}_{-0.8}$
10800	6.90 $\cdot 10^{-4}$	$\pm$ 5.2	$^{+2.8}_{-0.7}$	$^{+2.7}_{+0.0}$	$^{-0.3}_{+0.4}$	$^{-0.2}_{+0.2}$	$^{+0.1}_{-0.1}$	$^{+0.0}_{+0.0}$	$^{-0.2}_{-0.1}$	$^{+0.3}_{-0.2}$	$^{+0.4}_{-0.5}$
15200	2.45 $\cdot 10^{-4}$	$\pm$ 7.2	$^{+2.8}_{-3.7}$	$^{+1.4}_{-0.7}$	$^{-1.1}_{+0.3}$	$^{-2.1}_{+2.1}$	$^{+0.7}_{-0.7}$	$^{+0.0}_{+0.0}$	$^{-0.9}_{-2.6}$	$^{+0.6}_{-0.3}$	$^{+0.5}_{-0.6}$
21500	7.99 $\cdot 10^{-5}$	$^{+11.7}_{-10.6}$	$^{+8.1}_{-2.9}$	$^{+7.8}_{-1.4}$	$^{-0.2}_{+0.2}$	$^{+0.1}_{-0.1}$	$^{+1.1}_{-1.1}$	$^{+0.0}_{+0.0}$	$^{-1.7}_{+0.4}$	$^{+1.5}_{-1.3}$	$^{+1.0}_{-1.0}$
36200	6.62 $\cdot 10^{-6}$	$^{+19.3}_{-16.4}$	$^{+6.7}_{-4.9}$	$^{+6.5}_{+0.0}$	$^{-0.3}_{+0.3}$	$^{-0.9}_{+0.9}$	$^{+0.8}_{-0.8}$	$^{+0.0}_{+0.0}$	$^{+0.1}_{-3.0}$	$^{+0.0}_{-3.5}$	$^{+1.4}_{-1.4}$

Table 2: *Systematic uncertainties with bin-to-bin correlations for $d\sigma/dQ^2$ ($y < 0.9$) for the reaction $e^-p \to e^-X$ ($\mathcal{L} = 169.9\,pb^{-1}, P_e = -0.03$). The left four columns of the table contain the bin centre (Q_c^2), the measured cross section, the statistical uncertainty and the total systematic uncertainty. The right eight columns of the table list the bin-to-bin correlated systematic uncertainties for $\delta_1 - \delta_7$, and the systematic uncertainties summed in quadrature for $\delta_8 - \delta_{13}$, as defined in the section 8. The upper and lower correlated uncertainties correspond to a positive or negative variation of a cut value for example. However, if this is not possible for a particular systematic, the uncertainty is symmetrised.*

$Q^2 >$ (GeV^2)	x range	x_c	$d\sigma/dx$ (pb)	$N_{\rm data}$	$N_{\rm bg}^{\rm MC}$
185	$(0.63 - 1.00)\cdot10^{-2}$	$0.794\cdot10^{-2}$	$(8.66 \pm 0.05\ ^{+0.15}_{-0.13})\cdot10^{4}$	39875	243.8
	$(0.10 - 0.16)\cdot10^{-1}$	$0.126\cdot10^{-1}$	$(5.80 \pm 0.03\ ^{+0.08}_{-0.07})\cdot10^{4}$	48561	202.6
	$(0.16 - 0.25)\cdot10^{-1}$	$0.200\cdot10^{-1}$	$(3.60 \pm 0.02\ ^{+0.04}_{-0.03})\cdot10^{4}$	49042	122.0
	$(0.25 - 0.40)\cdot10^{-1}$	$0.316\cdot10^{-1}$	$(2.11 \pm 0.01\ ^{+0.05}_{-0.04})\cdot10^{4}$	49989	58.2
	$(0.40 - 0.63)\cdot10^{-1}$	$0.501\cdot10^{-1}$	$(1.24 \pm 0.01\ ^{+0.03}_{-0.03})\cdot10^{4}$	41427	14.5
	$(0.63 - 1.00)\cdot10^{-1}$	$0.794\cdot10^{-1}$	$(7.05 \pm 0.04\ ^{+0.18}_{-0.18})\cdot10^{3}$	37564	8.6
	$0.10 - 0.16$	0.126	$(3.96 \pm 0.02\ ^{+0.14}_{-0.14})\cdot10^{3}$	34201	4.3
	$0.16 - 0.25$	0.200	$(2.03 \pm 0.02\ ^{+0.09}_{-0.09})\cdot10^{3}$	19029	2.9
3000	$(0.40 - 0.63)\cdot10^{-1}$	$0.501\cdot10^{-1}$	$(1.89 \pm 0.08\ ^{+0.08}_{-0.04})\cdot10^{2}$	640	7.4
	$(0.63 - 1.00)\cdot10^{-1}$	$0.794\cdot10^{-1}$	$(2.11 \pm 0.06\ ^{+0.03}_{-0.02})\cdot10^{2}$	1211	5.8
	$0.10 - 0.16$	0.126	$(1.62 \pm 0.04\ ^{+0.02}_{-0.01})\cdot10^{2}$	1522	4.3
	$0.16 - 0.25$	0.200	$(9.37 \pm 0.26\ ^{+0.17}_{-0.15})\cdot10^{1}$	1306	2.9
	$0.25 - 0.40$	0.316	$(4.21 \pm 0.14\ ^{+0.04}_{-0.04})\cdot10^{1}$	941	1.5
	$0.40 - 0.75$	0.687	$1.42 \pm 0.07\ ^{+0.06}_{-0.05}$	381	0.0

Table 3: *The single differential cross section $d\sigma/dx$ ($y < 0.9$) for $Q^2 > 185\ GeV^2$ and $Q^2 > 3\,000\ GeV^2$ for the reaction $e^-p \to e^-X$ ($\mathcal{L} = 169.9\,pb^{-1}, P_e = -0.03$). The Q^2 and bin range, bin centre (x_c) and measured cross section corrected to the electroweak Born level are shown. The first (second) error on the cross section corresponds to the statistical (systematic) uncertainties. The number of observed data events (N_{data}) and simulated background events (N_{bg}^{MC}) are also shown.*

Q^2 > (GeV^2)	x_c	$d\sigma/dx$ (pb)	stat. (%)	sys. (%)	δ_1 (%)	δ_2 (%)	δ_3 (%)	δ_4 (%)	δ_5 (%)	δ_6 (%)	δ_7 (%)	$\delta_8 - \delta_{13}$ (%)
185	0.794 $\cdot 10^{-2}$	8.66 $\cdot 10^{4}$	$\pm$ 0.5	$^{+1.7}_{-1.5}$	$^{+0.6}_{-0.1}$	$^{-0.7}_{+0.8}$	$^{+0.4}_{-0.4}$	$^{-1.0}_{+1.0}$	$^{+0.0}_{+0.0}$	$^{-0.1}_{+0.4}$	$^{+0.2}_{-0.2}$	$^{+0.7}_{-0.7}$
	0.126 $\cdot 10^{-1}$	5.80 $\cdot 10^{4}$	$\pm$ 0.5	$^{+1.4}_{-1.3}$	$^{+0.4}_{-0.0}$	$^{-0.5}_{+0.6}$	$^{-0.0}_{+0.0}$	$^{-1.0}_{+1.0}$	$^{+0.0}_{+0.0}$	$^{-0.2}_{+0.3}$	$^{+0.2}_{-0.2}$	$^{+0.6}_{-0.6}$
	0.200 $\cdot 10^{-1}$	3.60 $\cdot 10^{4}$	$\pm$ 0.5	$^{+1.1}_{-0.9}$	$^{+0.5}_{-0.0}$	$^{-0.4}_{+0.5}$	$^{-0.4}_{+0.4}$	$^{+0.4}_{-0.4}$	$^{+0.0}_{+0.0}$	$^{-0.2}_{+0.2}$	$^{+0.1}_{-0.1}$	$^{+0.6}_{-0.6}$
	0.316 $\cdot 10^{-1}$	2.11 $\cdot 10^{4}$	$\pm$ 0.5	$^{+2.2}_{-2.1}$	$^{+0.4}_{-0.0}$	$^{-0.3}_{+0.4}$	$^{-1.0}_{+1.0}$	$^{+1.7}_{-1.7}$	$^{+0.0}_{+0.0}$	$^{-0.1}_{+0.2}$	$^{+0.1}_{-0.0}$	$^{+0.6}_{-0.7}$
	0.501 $\cdot 10^{-1}$	1.24 $\cdot 10^{4}$	$\pm$ 0.5	$^{+2.3}_{-2.2}$	$^{+0.3}_{-0.0}$	$^{-0.2}_{+0.3}$	$^{-1.3}_{+1.3}$	$^{+1.7}_{-1.7}$	$^{+0.0}_{+0.0}$	$^{-0.0}_{+0.2}$	$^{+0.0}_{-0.0}$	$^{+0.6}_{-0.6}$
	0.794 $\cdot 10^{-1}$	7.05 $\cdot 10^{3}$	$\pm$ 0.5	$^{+2.5}_{-2.5}$	$^{+0.3}_{-0.0}$	$^{-0.1}_{+0.3}$	$^{+1.8}_{-1.8}$	$^{+1.5}_{-1.5}$	$^{+0.0}_{+0.0}$	$^{+0.0}_{+0.0}$	$^{+0.0}_{-0.0}$	$^{+0.6}_{-0.7}$
	0.126	3.96 $\cdot 10^{3}$	$\pm$ 0.6	$^{+3.6}_{-3.6}$	$^{+0.3}_{+0.0}$	$^{-0.1}_{+0.2}$	$^{+3.1}_{-3.1}$	$^{+1.6}_{-1.6}$	$^{-0.1}_{+0.0}$	$^{-0.1}_{+0.1}$	$^{+0.0}_{-0.0}$	$^{+0.6}_{-0.6}$
	0.200	2.03 $\cdot 10^{3}$	$\pm$ 0.8	$^{+4.7}_{-4.5}$	$^{+0.3}_{-0.0}$	$^{-0.1}_{+0.2}$	$^{+4.4}_{-4.4}$	$^{+0.5}_{-0.5}$	$^{-0.3}_{+1.3}$	$^{-0.0}_{+0.1}$	$^{+0.0}_{-0.0}$	$^{+0.6}_{-0.6}$
3000	0.501 $\cdot 10^{-1}$	1.89 $\cdot 10^{2}$	$\pm$ 4.0	$^{+4.2}_{-2.1}$	$^{+3.8}_{+0.0}$	$^{-0.2}_{+0.1}$	$^{-1.7}_{+1.7}$	$^{-0.1}_{+0.1}$	$^{+0.0}_{+0.0}$	$^{-0.4}_{-0.9}$	$^{+0.6}_{-0.5}$	$^{+0.7}_{-0.5}$
	0.794 $\cdot 10^{-1}$	2.11 $\cdot 10^{2}$	$\pm$ 2.9	$^{+1.4}_{-1.1}$	$^{+1.0}_{-0.3}$	$^{-0.2}_{+0.3}$	$^{+0.5}_{-0.5}$	$^{+0.6}_{-0.6}$	$^{+0.0}_{+0.0}$	$^{-0.5}_{-0.3}$	$^{+0.5}_{-0.2}$	$^{+0.3}_{-0.4}$
	0.126	1.62 $\cdot 10^{2}$	$\pm$ 2.6	$^{+1.1}_{-0.5}$	$^{+1.0}_{-0.0}$	$^{-0.2}_{+0.3}$	$^{+0.0}_{-0.0}$	$^{-0.1}_{+0.1}$	$^{+0.0}_{+0.0}$	$^{-0.4}_{-0.1}$	$^{+0.1}_{-0.1}$	$^{+0.2}_{-0.2}$
	0.200	9.37 $\cdot 10^{1}$	$\pm$ 2.8	$^{+1.8}_{-1.6}$	$^{+1.0}_{-0.1}$	$^{-0.3}_{+0.2}$	$^{-1.5}_{+1.5}$	$^{+0.1}_{-0.1}$	$^{+0.0}_{+0.0}$	$^{+0.1}_{-0.3}$	$^{+0.2}_{-0.1}$	$^{+0.3}_{-0.3}$
	0.316	4.21 $\cdot 10^{1}$	$\pm$ 3.3	$^{+0.9}_{-1.0}$	$^{+0.6}_{-0.5}$	$^{-0.2}_{+0.2}$	$^{-0.2}_{+0.2}$	$^{-0.3}_{+0.3}$	$^{+0.0}_{+0.0}$	$^{+0.1}_{-0.5}$	$^{+0.1}_{-0.1}$	$^{+0.4}_{-0.5}$
	0.687	1.42	$\pm$ 5.1	$^{+4.3}_{-3.9}$	$^{+1.9}_{+0.0}$	$^{-0.4}_{+0.6}$	$^{+3.6}_{-3.6}$	$^{-0.3}_{+0.3}$	$^{+0.3}_{+0.1}$	$^{-1.1}_{+1.1}$	$^{+0.0}_{-0.2}$	$^{+0.8}_{-0.9}$

Table 4: *Systematic uncertainties with bin-to-bin correlations for $d\sigma/dx$ ($y < 0.9$) for $Q^2 > 185\,GeV^2$ and $Q^2 > 3\,000\,GeV^2$ for the reaction $e^-p \to e^-X$ ($\mathcal{L} = 169.9\,pb^{-1}, P_e = -0.03$). The left five columns of the table contain the Q^2 range, bin centre (x_c), the measured cross section, the statistical uncertainty and the total systematic uncertainty. The right eight columns of the table list the bin-to-bin correlated systematic uncertainties for $\delta_1 - \delta_7$, and the systematic uncertainties summed in quadrature for $\delta_8 - \delta_{13}$, as defined in the section 8. The upper and lower correlated uncertainties correspond to a positive or negative variation of a cut value for example. However, if this is not possible for a particular systematic, the uncertainty is symmetrised.*

$Q^2 >$ (GeV^2)	y range	y_c	$d\sigma/dy$ (pb)	N_{data}	$N_{\mathrm{bg}}^{\mathrm{MC}}$
185	0.00 – 0.05	0.025	$(1.62 \pm 0.01 \,^{+0.07}_{-0.07})\cdot 10^4$	77160	0.0
	0.05 – 0.10	0.075	$(8.04 \pm 0.03 \,^{+0.20}_{-0.20})\cdot 10^3$	63212	0.0
	0.10 – 0.15	0.125	$(5.65 \pm 0.03 \,^{+0.07}_{-0.06})\cdot 10^3$	44182	0.0
	0.15 – 0.20	0.175	$(4.33 \pm 0.03 \,^{+0.05}_{-0.04})\cdot 10^3$	32450	2.9
	0.20 – 0.25	0.225	$(3.54 \pm 0.02 \,^{+0.03}_{-0.03})\cdot 10^3$	25546	18.8
	0.25 – 0.30	0.275	$(2.97 \pm 0.02 \,^{+0.04}_{-0.04})\cdot 10^3$	20660	11.4
	0.30 – 0.35	0.325	$(2.59 \pm 0.02 \,^{+0.04}_{-0.03})\cdot 10^3$	17536	34.0
	0.35 – 0.40	0.375	$(2.23 \pm 0.02 \,^{+0.03}_{-0.02})\cdot 10^3$	14668	53.5
	0.40 – 0.45	0.425	$(1.98 \pm 0.02 \,^{+0.03}_{-0.02})\cdot 10^3$	12363	69.7
	0.45 – 0.50	0.475	$(1.76 \pm 0.02 \,^{+0.03}_{-0.02})\cdot 10^3$	10889	101.1
	0.50 – 0.55	0.525	$(1.60 \pm 0.02 \,^{+0.03}_{-0.02})\cdot 10^3$	9651	108.2
	0.55 – 0.60	0.575	$(1.47 \pm 0.02 \,^{+0.03}_{-0.03})\cdot 10^3$	8568	81.8
	0.60 – 0.65	0.625	$(1.33 \pm 0.02 \,^{+0.04}_{-0.04})\cdot 10^3$	7248	99.8
	0.65 – 0.70	0.675	$(1.21 \pm 0.02 \,^{+0.04}_{-0.04})\cdot 10^3$	5936	95.1
	0.70 – 0.75	0.725	$(1.12 \pm 0.02 \,^{+0.06}_{-0.05})\cdot 10^3$	4376	83.4
3000	0.05 – 0.10	0.075	$(3.46 \pm 0.22 \,^{+0.07}_{-0.06})\cdot 10^1$	242	0.0
	0.10 – 0.15	0.125	$(6.09 \pm 0.29 \,^{+0.21}_{-0.18})\cdot 10^1$	452	0.0
	0.15 – 0.20	0.175	$(6.49 \pm 0.29 \,^{+0.10}_{-0.10})\cdot 10^1$	493	0.0
	0.20 – 0.25	0.225	$(6.25 \pm 0.28 \,^{+0.05}_{-0.07})\cdot 10^1$	505	0.0
	0.25 – 0.30	0.275	$(6.39 \pm 0.28 \,^{+0.11}_{-0.07})\cdot 10^1$	525	0.0
	0.30 – 0.35	0.325	$(6.15 \pm 0.28 \,^{+0.12}_{-0.07})\cdot 10^1$	501	1.4
	0.35 – 0.40	0.375	$(5.22 \pm 0.25 \,^{+0.13}_{-0.07})\cdot 10^1$	425	0.0
	0.40 – 0.45	0.425	$(5.34 \pm 0.26 \,^{+0.18}_{-0.17})\cdot 10^1$	439	0.0
	0.45 – 0.50	0.475	$(5.19 \pm 0.25 \,^{+0.14}_{-0.11})\cdot 10^1$	421	0.0
	0.50 – 0.55	0.525	$(4.14 \pm 0.23 \,^{+0.12}_{-0.13})\cdot 10^1$	332	2.9
	0.55 – 0.60	0.575	$(4.28 \pm 0.23 \,^{+0.05}_{-0.07})\cdot 10^1$	335	0.0
	0.60 – 0.65	0.625	$(3.72 \pm 0.22 \,^{+0.08}_{-0.18})\cdot 10^1$	286	0.0
	0.65 – 0.70	0.675	$(3.93 \pm 0.23 \,^{+0.09}_{-0.20})\cdot 10^1$	301	3.0
	0.70 – 0.75	0.725	$(2.92 \pm 0.20 \,^{+0.08}_{-0.08})\cdot 10^1$	218	1.5
	0.75 – 0.80	0.775	$(2.98 \pm 0.20 \,^{+0.10}_{-0.10})\cdot 10^1$	219	1.5
	0.80 – 0.85	0.825	$(2.85 \pm 0.20 \,^{+0.39}_{-0.12})\cdot 10^1$	201	4.4
	0.85 – 0.90	0.875	$(2.57 \pm 0.21 \,^{+0.14}_{-0.43})\cdot 10^1$	173	8.7

Table 5: *The single differential cross section $d\sigma/dy$ for $Q^2 > 185\,GeV^2$ and $Q^2 > 3\,000\,GeV^2$ for the reaction $e^-p \to e^-X$ ($\mathcal{L} = 169.9\,pb^{-1}, P_e = -0.03$). The Q^2 and bin range, bin centre (y_c) and measured cross section corrected to the electroweak Born level are shown. The first (second) error on the cross section corresponds to the statistical (systematic) uncertainties. The number of observed data events (N_{data}) and simulated background events (N_{bg}^{MC}) are also shown.*

$Q^2 >$ (GeV^2)	y_c	$d\sigma/dy$ (pb)	stat. (%)	sys. (%)	δ_1 (%)	δ_2 (%)	δ_3 (%)	δ_4 (%)	δ_5 (%)	δ_6 (%)	δ_7 (%)	$\delta_8 - \delta_{13}$ (%)
185	0.025	$1.62 \cdot 10^4$	$\pm$ 0.4	$^{+4.1}_{-4.1}$	$^{+0.1}_{-0.0}$	$^{-0.1}_{+0.2}$	$^{+3.6}_{-3.6}$	$^{+1.7}_{-1.7}$	$^{-0.1}_{+0.5}$	$^{-0.0}_{+0.2}$	$^{+0.0}_{+0.0}$	$^{+0.7}_{-0.8}$
	0.075	$8.04 \cdot 10^3$	$\pm$ 0.4	$^{+2.5}_{-2.5}$	$^{+0.4}_{-0.0}$	$^{-0.2}_{+0.3}$	$^{-1.5}_{+1.5}$	$^{+1.9}_{-1.9}$	$^{+0.0}_{-0.0}$	$^{+0.0}_{+0.2}$	$^{+0.0}_{+0.0}$	$^{+0.7}_{-0.7}$
	0.125	$5.65 \cdot 10^3$	$\pm$ 0.5	$^{+1.2}_{-1.1}$	$^{+0.5}_{-0.0}$	$^{-0.3}_{+0.4}$	$^{-0.5}_{+0.5}$	$^{+0.7}_{-0.7}$	$^{+0.0}_{+0.0}$	$^{-0.1}_{+0.2}$	$^{+0.0}_{+0.0}$	$^{+0.6}_{-0.6}$
	0.175	$4.33 \cdot 10^3$	$\pm$ 0.6	$^{+1.1}_{-1.0}$	$^{+0.4}_{-0.0}$	$^{-0.4}_{+0.5}$	$^{-0.2}_{+0.2}$	$^{-0.6}_{+0.6}$	$^{+0.0}_{+0.0}$	$^{+0.0}_{+0.2}$	$^{+0.0}_{-0.0}$	$^{+0.5}_{-0.7}$
	0.225	$3.54 \cdot 10^3$	$\pm$ 0.7	$^{+1.0}_{-0.8}$	$^{+0.4}_{+0.0}$	$^{-0.4}_{+0.5}$	$^{+0.1}_{-0.1}$	$^{-0.4}_{+0.4}$	$^{+0.0}_{+0.0}$	$^{-0.1}_{+0.2}$	$^{+0.0}_{-0.0}$	$^{+0.6}_{-0.5}$
	0.275	$2.97 \cdot 10^3$	$\pm$ 0.7	$^{+1.2}_{-1.2}$	$^{+0.4}_{-0.0}$	$^{-0.4}_{+0.5}$	$^{-0.2}_{+0.2}$	$^{-0.8}_{+0.8}$	$^{+0.0}_{+0.0}$	$^{-0.2}_{+0.2}$	$^{+0.0}_{-0.0}$	$^{+0.6}_{-0.7}$
	0.325	$2.59 \cdot 10^3$	$\pm$ 0.8	$^{+1.4}_{-1.2}$	$^{+0.7}_{-0.1}$	$^{-0.4}_{+0.4}$	$^{+0.2}_{-0.2}$	$^{-1.0}_{+1.0}$	$^{+0.0}_{+0.0}$	$^{-0.1}_{+0.4}$	$^{+0.1}_{-0.1}$	$^{+0.5}_{-0.6}$
	0.375	$2.23 \cdot 10^3$	$\pm$ 0.9	$^{+1.1}_{-0.8}$	$^{+0.7}_{-0.0}$	$^{-0.3}_{+0.5}$	$^{-0.0}_{+0.0}$	$^{+0.1}_{-0.1}$	$^{+0.0}_{+0.0}$	$^{-0.2}_{+0.3}$	$^{+0.1}_{-0.1}$	$^{+0.6}_{-0.7}$
	0.425	$1.98 \cdot 10^3$	$\pm$ 1.0	$^{+1.4}_{-1.0}$	$^{+0.9}_{-0.0}$	$^{-0.3}_{+0.5}$	$^{+0.8}_{-0.8}$	$^{-0.1}_{+0.1}$	$^{+0.0}_{+0.0}$	$^{-0.1}_{-0.0}$	$^{+0.2}_{-0.2}$	$^{+0.5}_{-0.5}$
	0.475	$1.76 \cdot 10^3$	$\pm$ 1.0	$^{+1.9}_{-1.0}$	$^{+1.7}_{-0.2}$	$^{-0.3}_{+0.5}$	$^{-0.3}_{+0.3}$	$^{+0.1}_{-0.1}$	$^{+0.0}_{+0.0}$	$^{+0.1}_{+0.2}$	$^{+0.4}_{-0.4}$	$^{+0.6}_{-0.7}$
	0.525	$1.60 \cdot 10^3$	$\pm$ 1.1	$^{+1.6}_{-1.3}$	$^{+0.9}_{-0.0}$	$^{-0.5}_{+0.6}$	$^{+0.6}_{-0.6}$	$^{-0.8}_{+0.8}$	$^{+0.0}_{+0.0}$	$^{-0.3}_{+0.2}$	$^{+0.5}_{-0.5}$	$^{+0.5}_{-0.4}$
	0.575	$1.47 \cdot 10^3$	$\pm$ 1.2	$^{+2.3}_{-2.3}$	$^{+0.1}_{-0.3}$	$^{-0.7}_{+0.9}$	$^{+0.8}_{-0.8}$	$^{-1.8}_{+1.8}$	$^{+0.0}_{+0.0}$	$^{-0.1}_{+0.1}$	$^{+0.4}_{-0.4}$	$^{+0.4}_{-0.5}$
	0.625	$1.33 \cdot 10^3$	$\pm$ 1.3	$^{+3.3}_{-3.2}$	$^{+0.5}_{-0.1}$	$^{-1.5}_{+1.6}$	$^{-1.8}_{+1.8}$	$^{-2.1}_{+2.1}$	$^{+0.0}_{+0.0}$	$^{-0.3}_{+0.1}$	$^{+0.6}_{-0.6}$	$^{+0.4}_{-0.4}$
	0.675	$1.21 \cdot 10^3$	$\pm$ 1.4	$^{+3.5}_{-3.2}$	$^{+0.4}_{-0.9}$	$^{-2.7}_{+3.2}$	$^{+0.6}_{-0.6}$	$^{-0.8}_{+0.8}$	$^{+0.0}_{+0.0}$	$^{-0.1}_{+0.4}$	$^{+0.7}_{-0.7}$	$^{+0.4}_{-0.5}$
	0.725	$1.12 \cdot 10^3$	$\pm$ 1.6	$^{+5.7}_{-4.7}$	$^{+0.2}_{-0.1}$	$^{-4.3}_{+5.3}$	$^{+0.1}_{-0.1}$	$^{-1.6}_{+1.6}$	$^{+0.0}_{+0.0}$	$^{-0.1}_{+0.2}$	$^{+0.8}_{-0.8}$	$^{+0.8}_{-0.8}$
3000	0.075	$3.46 \cdot 10^1$	$\pm$ 6.5	$^{+1.9}_{-1.7}$	$^{+0.1}_{-0.0}$	$^{-0.4}_{+0.5}$	$^{-0.2}_{+0.2}$	$^{-0.3}_{+0.3}$	$^{+1.3}_{-0.1}$	$^{-1.0}_{+0.5}$	$^{+0.0}_{+0.0}$	$^{+1.2}_{-1.3}$
	0.125	$6.09 \cdot 10^1$	$\pm$ 4.7	$^{+3.4}_{-2.9}$	$^{+1.4}_{-0.0}$	$^{-0.2}_{+0.3}$	$^{+2.5}_{-2.5}$	$^{-1.3}_{+1.3}$	$^{+0.0}_{+0.0}$	$^{+1.0}_{-0.1}$	$^{+0.0}_{+0.0}$	$^{+0.4}_{-0.6}$
	0.175	$6.49 \cdot 10^1$	$\pm$ 4.5	$^{+1.5}_{-1.5}$	$^{+0.1}_{-0.4}$	$^{-0.3}_{+0.3}$	$^{-1.3}_{+1.3}$	$^{-0.5}_{+0.5}$	$^{+0.0}_{+0.0}$	$^{+0.1}_{-0.2}$	$^{+0.0}_{+0.0}$	$^{+0.5}_{-0.3}$
	0.225	$6.25 \cdot 10^1$	$\pm$ 4.5	$^{+0.8}_{-1.2}$	$^{+0.2}_{-0.5}$	$^{-0.2}_{+0.3}$	$^{+0.5}_{-0.5}$	$^{+0.2}_{-0.2}$	$^{+0.0}_{+0.0}$	$^{-0.9}_{-0.1}$	$^{+0.0}_{+0.0}$	$^{+0.5}_{-0.3}$
	0.275	$6.39 \cdot 10^1$	$\pm$ 4.4	$^{+1.8}_{-1.1}$	$^{+1.5}_{-0.1}$	$^{-0.2}_{+0.2}$	$^{-0.9}_{+0.9}$	$^{-0.1}_{+0.1}$	$^{+0.0}_{+0.0}$	$^{-0.6}_{-0.4}$	$^{+0.0}_{+0.0}$	$^{+0.4}_{-0.3}$
	0.325	$6.15 \cdot 10^1$	$\pm$ 4.5	$^{+2.0}_{-1.2}$	$^{+1.6}_{-0.1}$	$^{-0.2}_{+0.3}$	$^{+0.5}_{-0.5}$	$^{+0.8}_{-0.8}$	$^{+0.0}_{+0.0}$	$^{+0.5}_{+0.2}$	$^{+0.1}_{-0.1}$	$^{+0.4}_{-0.6}$
	0.375	$5.22 \cdot 10^1$	$\pm$ 4.9	$^{+2.5}_{-1.3}$	$^{+2.3}_{-0.2}$	$^{-0.2}_{+0.3}$	$^{+0.6}_{-0.6}$	$^{+0.8}_{-0.8}$	$^{+0.0}_{+0.0}$	$^{+0.1}_{+0.0}$	$^{+0.0}_{+0.0}$	$^{+0.4}_{-0.7}$
	0.425	$5.34 \cdot 10^1$	$\pm$ 4.8	$^{+3.3}_{-3.1}$	$^{+1.0}_{-0.3}$	$^{-0.2}_{+0.3}$	$^{-3.0}_{+3.0}$	$^{+0.9}_{-0.9}$	$^{+0.0}_{+0.0}$	$^{-0.3}_{-0.3}$	$^{+0.0}_{+0.0}$	$^{+0.4}_{-0.4}$
	0.475	$5.19 \cdot 10^1$	$\pm$ 4.9	$^{+2.7}_{-2.1}$	$^{+2.1}_{+0.0}$	$^{-0.2}_{+0.3}$	$^{+1.5}_{-1.5}$	$^{+0.9}_{-0.9}$	$^{+0.0}_{+0.0}$	$^{-0.0}_{-0.9}$	$^{+0.0}_{+0.0}$	$^{+0.3}_{-0.7}$
	0.525	$4.14 \cdot 10^1$	$\pm$ 5.5	$^{+3.0}_{-3.2}$	$^{+0.2}_{-0.8}$	$^{-0.3}_{+0.3}$	$^{-2.8}_{+2.8}$	$^{+0.0}_{-0.0}$	$^{+0.0}_{+0.0}$	$^{-0.5}_{+0.4}$	$^{+0.4}_{-0.4}$	$^{+0.9}_{-1.0}$
	0.575	$4.28 \cdot 10^1$	$\pm$ 5.5	$^{+1.2}_{-1.5}$	$^{+0.4}_{-0.6}$	$^{-0.2}_{+0.2}$	$^{+1.1}_{-1.1}$	$^{+0.0}_{-0.0}$	$^{+0.0}_{+0.0}$	$^{-0.8}_{-0.2}$	$^{+0.0}_{+0.0}$	$^{+0.3}_{-0.4}$
	0.625	$3.72 \cdot 10^1$	$\pm$ 5.9	$^{+2.1}_{-4.9}$	$^{+0.9}_{-4.5}$	$^{-0.2}_{+0.3}$	$^{-1.8}_{+1.8}$	$^{-0.6}_{+0.6}$	$^{+0.0}_{+0.0}$	$^{-0.6}_{+0.0}$	$^{+0.0}_{+0.0}$	$^{+0.5}_{-0.3}$
	0.675	$3.93 \cdot 10^1$	$\pm$ 5.9	$^{+2.2}_{-5.0}$	$^{+1.8}_{-4.9}$	$^{-0.2}_{+0.2}$	$^{+0.9}_{-0.9}$	$^{+0.5}_{-0.5}$	$^{+0.0}_{+0.0}$	$^{-0.6}_{+0.2}$	$^{+0.4}_{-0.4}$	$^{+0.7}_{-0.6}$
	0.725	$2.92 \cdot 10^1$	$\pm$ 6.8	$^{+2.8}_{-2.8}$	$^{+0.1}_{-2.0}$	$^{-0.2}_{+0.2}$	$^{-1.5}_{+1.5}$	$^{-1.0}_{+1.0}$	$^{+0.0}_{+0.0}$	$^{-0.7}_{+1.8}$	$^{+0.3}_{-0.3}$	$^{+1.2}_{-0.7}$
	0.775	$2.98 \cdot 10^1$	$\pm$ 6.8	$^{+3.4}_{-3.4}$	$^{+3.1}_{+0.0}$	$^{-0.2}_{+0.2}$	$^{+0.9}_{-0.9}$	$^{+0.5}_{-0.5}$	$^{+0.0}_{+0.0}$	$^{-0.6}_{-3.1}$	$^{+0.3}_{-0.3}$	$^{+0.7}_{-0.7}$
	0.825	$2.85 \cdot 10^1$	$\pm$ 7.2	$^{+13.8}_{-4.1}$	$^{+13.7}_{-0.5}$	$^{-0.1}_{+0.2}$	$^{+0.2}_{-0.2}$	$^{-0.0}_{+0.0}$	$^{+0.0}_{+0.0}$	$^{+1.6}_{-3.9}$	$^{+1.1}_{-0.9}$	$^{+0.6}_{-0.5}$
	0.875	$2.57 \cdot 10^1$	$\pm$ 8.2	$^{+5.3}_{-16.8}$	$^{+2.1}_{-16.1}$	$^{-1.5}_{+0.5}$	$^{+0.6}_{-0.6}$	$^{+0.2}_{-0.2}$	$^{+0.0}_{+0.0}$	$^{-3.9}_{-0.1}$	$^{+4.6}_{-2.1}$	$^{+1.4}_{-2.0}$

Table 6: *Systematic uncertainties with bin-to-bin correlations for $d\sigma/dy$ for $Q^2 > 185\,GeV^2$ and $Q^2 > 3\,000\,GeV^2$ for the reaction $e^- p \to e^- X$ ($\mathcal{L} = 169.9\,pb^{-1}, P_e = -0.03$). The left five columns of the table contain the Q^2 range, bin centre (y_c), the measured cross section, the statistical uncertainty and the total systematic uncertainty. The right eight columns of the table list the bin-to-bin correlated systematic uncertainties for $\delta_1 - \delta_7$, and the systematic uncertainties summed in quadrature for $\delta_8 - \delta_{13}$, as defined in the section 8. The upper and lower correlated uncertainties correspond to a positive or negative variation of a cut value for example. However, if this is not possible for a particular systematic, the uncertainty is symmetrised.*

Q^2 range (GeV^2)	Q_c^2 (GeV^2)	x range	x_c	$\tilde{\sigma}$	N_{data}	$N_{\mathrm{bg}}^{\mathrm{MC}}$
185 – 240	200	0.0037 – 0.006	0.005	$1.092 \pm 0.010\ ^{+0.014}_{-0.011}$	14079	88.0
		0.006 – 0.01	0.008	$0.922 \pm 0.008\ ^{+0.018}_{-0.018}$	16389	23.3
		0.01 – 0.017	0.013	$0.783 \pm 0.006\ ^{+0.013}_{-0.013}$	17628	2.9
		0.017 – 0.025	0.021	$0.662 \pm 0.006\ ^{+0.014}_{-0.014}$	12598	0.0
		0.025 – 0.037	0.032	$0.561 \pm 0.006\ ^{+0.023}_{-0.022}$	11904	0.0
		0.037 – 0.06	0.05	$0.500 \pm 0.005\ ^{+0.012}_{-0.012}$	11002	0.0
		0.06 – 0.12	0.08	$0.441 \pm 0.004\ ^{+0.024}_{-0.024}$	14235	0.0
		0.12 – 0.25	0.18	$0.334 \pm 0.004\ ^{+0.018}_{-0.018}$	7372	0.0
240 – 310	250	0.006 – 0.01	0.008	$0.936 \pm 0.010\ ^{+0.014}_{-0.012}$	11341	26.1
		0.01 – 0.017	0.013	$0.793 \pm 0.008\ ^{+0.013}_{-0.012}$	12602	6.0
		0.017 – 0.025	0.021	$0.656 \pm 0.008\ ^{+0.011}_{-0.009}$	8935	1.5
		0.025 – 0.037	0.032	$0.565 \pm 0.007\ ^{+0.019}_{-0.019}$	8745	0.0
		0.037 – 0.06	0.05	$0.494 \pm 0.006\ ^{+0.017}_{-0.016}$	8494	0.0
		0.06 – 0.12	0.08	$0.429 \pm 0.005\ ^{+0.022}_{-0.022}$	10350	0.0
		0.12 – 0.25	0.18	$0.331 \pm 0.004\ ^{+0.016}_{-0.015}$	6985	0.0
310 – 410	350	0.006 – 0.01	0.008	$0.969 \pm 0.013\ ^{+0.021}_{-0.015}$	6903	71.5
		0.01 – 0.017	0.013	$0.821 \pm 0.009\ ^{+0.016}_{-0.010}$	9505	8.8
		0.017 – 0.025	0.021	$0.693 \pm 0.009\ ^{+0.006}_{-0.004}$	7274	0.0
		0.025 – 0.037	0.032	$0.605 \pm 0.008\ ^{+0.012}_{-0.011}$	7071	0.0
		0.037 – 0.06	0.05	$0.509 \pm 0.006\ ^{+0.014}_{-0.013}$	7509	0.0
		0.06 – 0.12	0.08	$0.435 \pm 0.005\ ^{+0.009}_{-0.009}$	8417	0.0
		0.12 – 0.25	0.18	$0.314 \pm 0.004\ ^{+0.020}_{-0.020}$	6571	0.0
410 – 530	450	0.006 – 0.01	0.008	$0.993 \pm 0.014\ ^{+0.023}_{-0.021}$	5334	84.2
		0.01 – 0.017	0.013	$0.857 \pm 0.013\ ^{+0.010}_{-0.009}$	4719	16.1
		0.017 – 0.025	0.021	$0.685 \pm 0.012\ ^{+0.013}_{-0.012}$	3668	1.3
		0.025 – 0.037	0.032	$0.591 \pm 0.009\ ^{+0.011}_{-0.010}$	4173	0.0
		0.037 – 0.06	0.05	$0.519 \pm 0.007\ ^{+0.013}_{-0.012}$	5225	0.0
		0.06 – 0.1	0.08	$0.432 \pm 0.007\ ^{+0.009}_{-0.008}$	4249	0.0
		0.1 – 0.17	0.13	$0.359 \pm 0.006\ ^{+0.018}_{-0.018}$	3727	0.0
		0.17 – 0.3	0.25	$0.262 \pm 0.005\ ^{+0.015}_{-0.014}$	2819	0.0

Table 7: *The reduced cross section $\tilde{\sigma}$ for the reaction $e^- p \to e^- X$ ($\mathcal{L} = 169.9\,pb^{-1}, P_e = 0$). The bin range, bin centre (Q_c^2 and x_c) and measured cross section corrected to the electroweak Born level are shown. The first (second) error on the cross section corresponds to the statistical (systematic) uncertainties. The number of observed data events (N_{data}) and simulated background events (N_{bg}^{MC}) are also shown. This table has two continuations.*

Q^2 range (GeV^2)	Q_c^2 (GeV^2)	x range	x_c	$\tilde{\sigma}$	N_{data}	$N_{\mathrm{bg}}^{\mathrm{MC}}$
530 – 710	650	0.01 – 0.017	0.013	$0.878 \pm 0.013\ ^{+0.013}_{-0.007}$	5347	59.5
		0.017 – 0.025	0.021	$0.755 \pm 0.013\ ^{+0.009}_{-0.008}$	3568	5.7
		0.025 – 0.037	0.032	$0.597 \pm 0.012\ ^{+0.007}_{-0.006}$	2740	1.3
		0.037 – 0.06	0.05	$0.512 \pm 0.010\ ^{+0.005}_{-0.005}$	2908	0.0
		0.06 – 0.1	0.08	$0.424 \pm 0.009\ ^{+0.010}_{-0.010}$	2418	0.0
		0.1 – 0.17	0.13	$0.361 \pm 0.008\ ^{+0.010}_{-0.009}$	2201	0.0
		0.17 – 0.3	0.25	$0.253 \pm 0.006\ ^{+0.017}_{-0.017}$	1887	0.0
710 – 900	800	0.009 – 0.017	0.013	$0.860 \pm 0.016\ ^{+0.015}_{-0.016}$	3339	49.4
		0.017 – 0.025	0.021	$0.733 \pm 0.016\ ^{+0.008}_{-0.006}$	2360	3.1
		0.025 – 0.037	0.032	$0.634 \pm 0.013\ ^{+0.009}_{-0.009}$	2453	7.4
		0.037 – 0.06	0.05	$0.522 \pm 0.010\ ^{+0.011}_{-0.011}$	2719	0.0
		0.06 – 0.1	0.08	$0.448 \pm 0.010\ ^{+0.012}_{-0.012}$	2332	0.0
		0.1 – 0.17	0.13	$0.377 \pm 0.009\ ^{+0.004}_{-0.004}$	1903	0.0
		0.17 – 0.3	0.25	$0.257 \pm 0.007\ ^{+0.009}_{-0.009}$	1405	0.0
900 – 1300	1200	0.01 – 0.017	0.014	$0.892 \pm 0.020\ ^{+0.022}_{-0.029}$	2217	75.7
		0.017 – 0.025	0.021	$0.791 \pm 0.016\ ^{+0.015}_{-0.013}$	2553	23.2
		0.025 – 0.037	0.032	$0.608 \pm 0.013\ ^{+0.007}_{-0.007}$	2478	11.7
		0.037 – 0.06	0.05	$0.551 \pm 0.010\ ^{+0.007}_{-0.008}$	3197	1.3
		0.06 – 0.1	0.08	$0.456 \pm 0.009\ ^{+0.006}_{-0.006}$	3039	0.0
		0.1 – 0.17	0.13	$0.375 \pm 0.008\ ^{+0.004}_{-0.004}$	2451	0.0
		0.17 – 0.3	0.25	$0.247 \pm 0.006\ ^{+0.006}_{-0.006}$	1872	0.0
		0.3 – 0.53	0.4	$0.125 \pm 0.005\ ^{+0.010}_{-0.007}$	641	0.0
1300 – 1800	1500	0.017 – 0.025	0.021	$0.765 \pm 0.023\ ^{+0.020}_{-0.018}$	1273	58.3
		0.025 – 0.037	0.032	$0.629 \pm 0.017\ ^{+0.005}_{-0.004}$	1402	7.1
		0.037 – 0.06	0.05	$0.522 \pm 0.013\ ^{+0.005}_{-0.004}$	1756	1.4
		0.06 – 0.1	0.08	$0.477 \pm 0.011\ ^{+0.005}_{-0.005}$	1887	0.0
		0.1 – 0.15	0.13	$0.376 \pm 0.011\ ^{+0.008}_{-0.007}$	1201	0.0
		0.15 – 0.23	0.18	$0.312 \pm 0.010\ ^{+0.006}_{-0.005}$	1028	0.0
		0.23 – 0.35	0.25	$0.264 \pm 0.010\ ^{+0.005}_{-0.005}$	729	0.0
		0.35 – 0.53	0.4	$0.128 \pm 0.007\ ^{+0.011}_{-0.006}$	318	0.0
1800 – 2500	2000	0.023 – 0.037	0.032	$0.636 \pm 0.021\ ^{+0.016}_{-0.009}$	977	19.1
		0.037 – 0.06	0.05	$0.571 \pm 0.016\ ^{+0.005}_{-0.005}$	1229	0.0
		0.06 – 0.1	0.08	$0.459 \pm 0.013\ ^{+0.009}_{-0.009}$	1246	1.3
		0.1 – 0.15	0.13	$0.374 \pm 0.013\ ^{+0.003}_{-0.004}$	883	0.0
		0.15 – 0.23	0.18	$0.309 \pm 0.012\ ^{+0.002}_{-0.006}$	723	0.0
		0.23 – 0.35	0.25	$0.247 \pm 0.011\ ^{+0.004}_{-0.004}$	502	0.0
		0.35 – 0.53	0.4	$0.120 \pm 0.008\ ^{+0.004}_{-0.005}$	239	0.0

Table 7: *Continuation 1.*

Q^2 range (GeV^2)	Q_c^2 (GeV^2)	x range	x_c	$\tilde{\sigma}$	N_{data}	$N_{\mathrm{bg}}^{\mathrm{MC}}$
2500 – 3500	3000	0.037 – 0.06	0.05	$0.581 \pm 0.021\ ^{+0.012}_{-0.006}$	777	9.0
		0.06 – 0.1	0.08	$0.507 \pm 0.017\ ^{+0.006}_{-0.006}$	902	1.5
		0.1 – 0.15	0.13	$0.378 \pm 0.015\ ^{+0.004}_{-0.003}$	623	0.0
		0.15 – 0.23	0.18	$0.320 \pm 0.014\ ^{+0.004}_{-0.004}$	528	0.0
		0.23 – 0.35	0.25	$0.286 \pm 0.014\ ^{+0.021}_{-0.021}$	427	0.0
		0.35 – 0.53	0.4	$0.135 \pm 0.010\ ^{+0.005}_{-0.005}$	185	0.0
		0.53 – 0.75	0.65	$0.017\ ^{+0.002}_{-0.002}\ ^{+0.002}_{-0.002}$	62	0.0
3500 – 5600	5000	0.04 – 0.1	0.08	$0.527 \pm 0.017\ ^{+0.009}_{-0.005}$	1001	7.3
		0.1 – 0.15	0.13	$0.463 \pm 0.019\ ^{+0.005}_{-0.004}$	610	1.4
		0.15 – 0.23	0.18	$0.340 \pm 0.015\ ^{+0.003}_{-0.002}$	499	0.0
		0.23 – 0.35	0.25	$0.243 \pm 0.014\ ^{+0.004}_{-0.003}$	318	0.0
		0.35 – 0.53	0.4	$0.140 \pm 0.011\ ^{+0.009}_{-0.009}$	176	0.0
5600 – 9000	8000	0.07 – 0.15	0.13	$0.560 \pm 0.024\ ^{+0.006}_{-0.010}$	582	4.4
		0.15 – 0.23	0.18	$0.433 \pm 0.023\ ^{+0.011}_{-0.012}$	346	0.0
		0.23 – 0.35	0.25	$0.309 \pm 0.020\ ^{+0.012}_{-0.012}$	232	0.0
		0.35 – 0.53	0.4	$0.114\ ^{+0.014}_{-0.012}\ ^{+0.008}_{-0.008}$	87	0.0
		0.53 – 0.75	0.65	$0.019\ ^{+0.004}_{-0.003}\ ^{+0.001}_{-0.001}$	35	0.0
9000 – 15000	12000	0.09 – 0.23	0.18	$0.464 \pm 0.028\ ^{+0.006}_{-0.018}$	275	1.4
		0.23 – 0.35	0.25	$0.353 \pm 0.029\ ^{+0.010}_{-0.008}$	149	0.0
		0.35 – 0.53	0.4	$0.156\ ^{+0.021}_{-0.018}\ ^{+0.007}_{-0.006}$	72	0.0
15000 – 25000	20000	0.15 – 0.35	0.25	$0.461 \pm 0.043\ ^{+0.028}_{-0.017}$	129	4.4
		0.35 – 0.75	0.4	$0.183\ ^{+0.030}_{-0.026}\ ^{+0.009}_{-0.007}$	48	0.0
25000 – 50000	30000	0.25 – 0.75	0.4	$0.237\ ^{+0.042}_{-0.036}\ ^{+0.016}_{-0.014}$	42	0.0

Table 7: *Continuation 2.*

Q_c^2 (GeV^2)	x_c	$\tilde{\sigma}$	stat. (%)	sys. (%)	δ_1 (%)	δ_2 (%)	δ_3 (%)	δ_4 (%)	δ_5 (%)	δ_6 (%)	δ_7 (%)	$\delta_8 - \delta_{13}$ (%)
200	0.005	1.092	± 0.9	$^{+1.3}_{-1.0}$	$^{+0.7}_{-0.0}$	$^{-0.4}_{+0.6}$	$^{+0.4}_{-0.4}$	$^{-0.4}_{+0.4}$	$^{+0.0}_{+0.0}$	$^{+0.1}_{-0.1}$	$^{+0.3}_{-0.3}$	$^{+0.7}_{-0.7}$
	0.008	0.922	± 0.8	$^{+1.9}_{-1.9}$	$^{+0.3}_{-0.0}$	$^{-0.4}_{+0.5}$	$^{+0.2}_{-0.2}$	$^{-1.6}_{+1.6}$	$^{+0.0}_{+0.0}$	$^{+0.1}_{+0.4}$	$^{+0.1}_{-0.1}$	$^{+0.8}_{-1.0}$
	0.013	0.783	± 0.8	$^{+1.7}_{-1.6}$	$^{+0.2}_{+0.0}$	$^{-0.5}_{+0.5}$	$^{-0.2}_{+0.2}$	$^{-1.3}_{+1.3}$	$^{+0.0}_{+0.0}$	$^{+0.0}_{+0.4}$	$^{+0.0}_{-0.0}$	$^{+0.8}_{-0.9}$
	0.021	0.662	± 1.0	$^{+2.1}_{-2.1}$	$^{+0.4}_{+0.0}$	$^{-0.3}_{+0.5}$	$^{-1.6}_{+1.6}$	$^{+0.9}_{-0.9}$	$^{+0.0}_{+0.0}$	$^{-0.1}_{+0.1}$	$^{+0.0}_{+0.0}$	$^{+0.8}_{-0.9}$
	0.032	0.561	± 1.0	$^{+4.0}_{-4.0}$	$^{+0.1}_{-0.0}$	$^{-0.3}_{+0.4}$	$^{-1.5}_{+1.5}$	$^{+3.6}_{-3.6}$	$^{+0.0}_{+0.0}$	$^{+0.2}_{+0.4}$	$^{+0.0}_{+0.0}$	$^{+0.8}_{-0.8}$
	0.05	0.500	± 1.0	$^{+2.5}_{-2.4}$	$^{+0.0}_{-0.3}$	$^{-0.2}_{+0.3}$	$^{-0.5}_{+0.5}$	$^{+2.2}_{-2.2}$	$^{+0.0}_{+0.0}$	$^{+0.0}_{+0.3}$	$^{+0.0}_{+0.0}$	$^{+1.0}_{-0.9}$
	0.08	0.441	± 0.9	$^{+5.5}_{-5.5}$	$^{+0.0}_{-0.1}$	$^{-0.2}_{+0.2}$	$^{+5.0}_{-5.0}$	$^{+2.0}_{-2.0}$	$^{-0.0}_{+0.0}$	$^{-0.0}_{+0.1}$	$^{+0.0}_{+0.0}$	$^{+0.8}_{-1.0}$
	0.18	0.334	± 1.3	$^{+5.4}_{-5.4}$	$^{+0.1}_{+0.0}$	$^{-0.1}_{+0.2}$	$^{+5.3}_{-5.3}$	$^{+0.5}_{-0.5}$	$^{+0.7}_{+0.2}$	$^{-0.1}_{+0.1}$	$^{+0.0}_{+0.0}$	$^{+0.7}_{-0.9}$
250	0.008	0.936	± 1.0	$^{+1.5}_{-1.3}$	$^{+0.6}_{-0.0}$	$^{-0.3}_{+0.4}$	$^{+0.5}_{-0.5}$	$^{-0.9}_{+0.9}$	$^{+0.0}_{+0.0}$	$^{-0.2}_{+0.3}$	$^{+0.1}_{-0.1}$	$^{+0.7}_{-0.7}$
	0.013	0.793	± 1.0	$^{+1.7}_{-1.5}$	$^{+0.7}_{+0.0}$	$^{-0.5}_{+0.6}$	$^{+0.0}_{-0.0}$	$^{-1.3}_{+1.3}$	$^{+0.0}_{+0.0}$	$^{-0.1}_{+0.2}$	$^{+0.0}_{-0.0}$	$^{+0.5}_{-0.7}$
	0.021	0.656	± 1.1	$^{+1.6}_{-1.4}$	$^{+0.7}_{-0.0}$	$^{-0.3}_{+0.5}$	$^{-0.1}_{+0.1}$	$^{+1.1}_{-1.1}$	$^{+0.0}_{+0.0}$	$^{-0.2}_{+0.2}$	$^{+0.0}_{-0.0}$	$^{+0.8}_{-0.7}$
	0.032	0.565	± 1.2	$^{+3.3}_{-3.3}$	$^{+0.6}_{-0.0}$	$^{-0.3}_{+0.4}$	$^{-0.8}_{+0.8}$	$^{+3.0}_{-3.0}$	$^{+0.0}_{+0.0}$	$^{+0.0}_{+0.1}$	$^{+0.0}_{+0.0}$	$^{+0.7}_{-0.9}$
	0.05	0.494	± 1.2	$^{+3.4}_{-3.3}$	$^{+0.4}_{+0.0}$	$^{-0.1}_{+0.3}$	$^{-2.4}_{+2.4}$	$^{+2.2}_{-2.2}$	$^{+0.0}_{+0.0}$	$^{-0.0}_{-0.1}$	$^{+0.0}_{+0.0}$	$^{+0.7}_{-0.6}$
	0.08	0.429	± 1.1	$^{+5.2}_{-5.1}$	$^{+0.7}_{-0.0}$	$^{-0.1}_{+0.3}$	$^{+4.6}_{-4.6}$	$^{+2.2}_{-2.2}$	$^{+0.0}_{+0.0}$	$^{-0.0}_{+0.1}$	$^{+0.0}_{+0.0}$	$^{+0.7}_{-0.7}$
	0.18	0.331	± 1.3	$^{+4.8}_{-4.7}$	$^{+0.2}_{+0.0}$	$^{+0.0}_{+0.2}$	$^{+4.1}_{-4.1}$	$^{+2.0}_{-2.0}$	$^{+0.3}_{+1.0}$	$^{+0.0}_{+0.2}$	$^{+0.0}_{+0.0}$	$^{+0.8}_{-0.8}$
350	0.008	0.969	± 1.3	$^{+2.1}_{-1.5}$	$^{+1.6}_{-0.1}$	$^{-0.5}_{+0.6}$	$^{+0.9}_{-0.9}$	$^{-0.4}_{+0.4}$	$^{+0.0}_{+0.0}$	$^{-0.6}_{+0.4}$	$^{+0.4}_{-0.4}$	$^{+0.6}_{-0.8}$
	0.013	0.821	± 1.1	$^{+1.9}_{-1.2}$	$^{+1.4}_{-0.0}$	$^{-0.2}_{+0.5}$	$^{-0.2}_{+0.2}$	$^{-1.0}_{+1.0}$	$^{+0.0}_{+0.0}$	$^{-0.2}_{+0.5}$	$^{+0.0}_{-0.0}$	$^{+0.7}_{-0.6}$
	0.021	0.693	± 1.3	$^{+0.9}_{-0.6}$	$^{+0.4}_{-0.1}$	$^{-0.3}_{+0.4}$	$^{+0.3}_{-0.3}$	$^{+0.0}_{-0.0}$	$^{+0.0}_{+0.0}$	$^{-0.2}_{-0.0}$	$^{+0.0}_{+0.0}$	$^{+0.6}_{-0.5}$
	0.032	0.605	± 1.3	$^{+1.9}_{-1.8}$	$^{+0.8}_{-0.0}$	$^{-0.2}_{+0.4}$	$^{-1.6}_{+1.6}$	$^{+0.2}_{-0.2}$	$^{+0.0}_{+0.0}$	$^{-0.3}_{+0.1}$	$^{+0.0}_{+0.0}$	$^{+0.6}_{-0.7}$
	0.05	0.509	± 1.2	$^{+2.7}_{-2.6}$	$^{+0.6}_{-0.0}$	$^{-0.1}_{+0.2}$	$^{-1.9}_{+1.9}$	$^{+1.6}_{-1.6}$	$^{+0.0}_{+0.0}$	$^{-0.1}_{+0.2}$	$^{+0.0}_{+0.0}$	$^{+0.5}_{-0.7}$
	0.08	0.435	± 1.2	$^{+2.0}_{-2.0}$	$^{+0.3}_{+0.0}$	$^{-0.1}_{+0.2}$	$^{+1.1}_{-1.1}$	$^{+1.6}_{-1.6}$	$^{+0.0}_{+0.0}$	$^{+0.0}_{+0.1}$	$^{+0.0}_{+0.0}$	$^{+0.7}_{-0.7}$
	0.18	0.314	± 1.3	$^{+6.4}_{-6.3}$	$^{+0.4}_{+0.0}$	$^{-0.0}_{+0.2}$	$^{+5.7}_{-5.7}$	$^{+2.6}_{-2.6}$	$^{-0.1}_{+1.2}$	$^{+0.1}_{+0.2}$	$^{+0.0}_{+0.0}$	$^{+0.7}_{-0.6}$
450	0.008	0.993	± 1.5	$^{+2.4}_{-2.1}$	$^{+0.7}_{-0.3}$	$^{-1.4}_{+1.6}$	$^{+1.3}_{-1.3}$	$^{-0.5}_{+0.5}$	$^{+0.0}_{+0.0}$	$^{-0.2}_{+0.3}$	$^{+0.6}_{-0.6}$	$^{+0.5}_{-0.4}$
	0.013	0.857	± 1.5	$^{+1.1}_{-1.1}$	$^{+0.1}_{-0.1}$	$^{-0.5}_{+0.6}$	$^{-0.4}_{+0.4}$	$^{+0.2}_{-0.2}$	$^{+0.0}_{+0.0}$	$^{-0.6}_{+0.6}$	$^{+0.1}_{-0.1}$	$^{+0.5}_{-0.6}$
	0.021	0.685	± 1.7	$^{+1.8}_{-1.7}$	$^{+0.2}_{-0.1}$	$^{-0.4}_{+0.5}$	$^{-0.1}_{+0.1}$	$^{+1.3}_{-1.3}$	$^{+0.0}_{+0.0}$	$^{-0.7}_{+0.9}$	$^{+0.0}_{-0.0}$	$^{+0.8}_{-0.8}$
	0.032	0.591	± 1.6	$^{+1.9}_{-1.7}$	$^{+0.8}_{-0.1}$	$^{-0.2}_{+0.4}$	$^{+0.0}_{-0.0}$	$^{+1.4}_{-1.4}$	$^{+0.0}_{+0.0}$	$^{-0.5}_{+0.4}$	$^{+0.0}_{+0.0}$	$^{+1.0}_{-0.9}$
	0.05	0.519	± 1.4	$^{+2.5}_{-2.4}$	$^{+0.7}_{-0.0}$	$^{+0.0}_{+0.2}$	$^{-1.6}_{+1.6}$	$^{+1.6}_{-1.6}$	$^{+0.0}_{+0.0}$	$^{-0.4}_{+0.6}$	$^{+0.0}_{+0.0}$	$^{+0.7}_{-0.7}$
	0.08	0.432	± 1.6	$^{+2.1}_{-1.9}$	$^{+0.3}_{+0.0}$	$^{+0.1}_{+0.2}$	$^{-0.7}_{+0.7}$	$^{+1.7}_{-1.7}$	$^{+0.0}_{+0.0}$	$^{+0.1}_{+0.6}$	$^{+0.0}_{+0.0}$	$^{+0.7}_{-0.5}$
	0.13	0.359	± 1.7	$^{+4.9}_{-4.9}$	$^{+0.6}_{+0.0}$	$^{+0.1}_{+0.1}$	$^{+4.4}_{-4.4}$	$^{+1.9}_{-1.9}$	$^{+0.0}_{+0.0}$	$^{-0.4}_{+0.4}$	$^{+0.0}_{+0.0}$	$^{+0.5}_{-0.6}$
	0.25	0.262	± 2.0	$^{+5.6}_{-5.5}$	$^{+1.1}_{+0.0}$	$^{+0.2}_{+0.1}$	$^{+5.2}_{-5.2}$	$^{+1.1}_{-1.1}$	$^{-0.9}_{+0.8}$	$^{-0.1}_{+0.6}$	$^{+0.0}_{+0.0}$	$^{+0.8}_{-0.8}$

Table 8: *Systematic uncertainties with bin-to-bin correlations for the reduced cross section $\tilde{\sigma}$ for the reaction $e^- p \to e^- X$ ($\mathcal{L} = 169.9\, pb^{-1}, P_e = 0$). The left five columns of the table contain the bin centres, Q_c^2 and x_c, the measured cross section, the statistical uncertainty and the total systematic uncertainty. The right eight columns of the table list the bin-to-bin correlated systematic uncertainties for $\delta_1 - \delta_7$, and the systematic uncertainties summed in quadrature for $\delta_8 - \delta_{13}$, as defined in the section 8. The upper and lower correlated uncertainties correspond to a positive or negative variation of a cut value for example. However, if this is not possible for a particular systematic, the uncertainty is symmetrised. This table has two continuations.*

Q_c^2 (GeV^2)	x_c	$\tilde{\sigma}$	stat. (%)	sys. (%)	δ_1 (%)	δ_2 (%)	δ_3 (%)	δ_4 (%)	δ_5 (%)	δ_6 (%)	δ_7 (%)	$\delta_8 - \delta_{13}$ (%)
650	0.013	0.878	± 1.4	$^{+1.5}_{-0.8}$	$^{+1.2}_{-0.2}$	$^{-0.5}_{+0.6}$	$^{-0.0}_{+0.0}$	$^{-0.1}_{+0.1}$	$^{+0.0}_{+0.0}$	$^{-0.2}_{+0.3}$	$^{+0.5}_{-0.5}$	$^{+0.4}_{-0.3}$
	0.021	0.755	± 1.7	$^{+1.1}_{-1.1}$	$^{+0.0}_{-0.1}$	$^{-0.4}_{+0.5}$	$^{-0.3}_{+0.3}$	$^{-0.9}_{+0.9}$	$^{+0.0}_{+0.0}$	$^{-0.2}_{+0.0}$	$^{+0.1}_{-0.1}$	$^{+0.2}_{-0.2}$
	0.032	0.597	± 2.0	$^{+1.2}_{-1.0}$	$^{+0.5}_{-0.2}$	$^{-0.4}_{+0.5}$	$^{-0.5}_{+0.5}$	$^{+0.7}_{-0.7}$	$^{+0.0}_{+0.0}$	$^{+0.5}_{+0.5}$	$^{+0.0}_{-0.0}$	$^{+0.2}_{-0.2}$
	0.05	0.512	± 1.9	$^{+1.0}_{-0.9}$	$^{+0.1}_{-0.0}$	$^{-0.3}_{+0.4}$	$^{-0.4}_{+0.4}$	$^{+0.7}_{-0.7}$	$^{+0.0}_{+0.0}$	$^{+0.1}_{+0.0}$	$^{+0.0}_{+0.0}$	$^{+0.5}_{-0.4}$
	0.08	0.424	± 2.1	$^{+2.4}_{-2.3}$	$^{+0.7}_{-0.0}$	$^{-0.1}_{+0.3}$	$^{-1.8}_{+1.8}$	$^{+1.0}_{-1.0}$	$^{+0.0}_{+0.0}$	$^{+0.1}_{-0.0}$	$^{+0.0}_{+0.0}$	$^{+0.9}_{-1.1}$
	0.13	0.361	± 2.2	$^{+2.7}_{-2.4}$	$^{+0.9}_{-0.0}$	$^{-0.1}_{+0.2}$	$^{+2.1}_{-2.1}$	$^{-0.8}_{+0.8}$	$^{+0.0}_{+0.0}$	$^{+0.1}_{+0.4}$	$^{+0.0}_{+0.0}$	$^{+1.0}_{-0.9}$
	0.25	0.253	± 2.4	$^{+6.6}_{-6.5}$	$^{+1.0}_{-0.0}$	$^{-0.1}_{+0.3}$	$^{+6.3}_{-6.3}$	$^{+1.0}_{-1.0}$	$^{-0.8}_{+0.2}$	$^{-0.1}_{+0.5}$	$^{+0.0}_{+0.0}$	$^{+1.0}_{-1.1}$
800	0.013	0.860	± 1.8	$^{+1.7}_{-1.9}$	$^{+0.4}_{-1.0}$	$^{-0.8}_{+1.0}$	$^{+0.4}_{-0.4}$	$^{-1.0}_{+1.0}$	$^{+0.0}_{+0.0}$	$^{-0.1}_{+0.0}$	$^{+0.6}_{-0.6}$	$^{+0.3}_{-0.4}$
	0.021	0.733	± 2.1	$^{+1.1}_{-0.9}$	$^{+0.5}_{-0.1}$	$^{-0.4}_{+0.5}$	$^{+0.6}_{-0.6}$	$^{-0.2}_{+0.2}$	$^{+0.0}_{+0.0}$	$^{+0.0}_{+0.5}$	$^{+0.1}_{-0.1}$	$^{+0.4}_{-0.4}$
	0.032	0.634	± 2.1	$^{+1.4}_{-1.4}$	$^{+0.0}_{-0.4}$	$^{-0.4}_{+0.5}$	$^{-0.8}_{+0.8}$	$^{-0.9}_{+0.9}$	$^{+0.0}_{+0.0}$	$^{+0.3}_{+0.0}$	$^{+0.1}_{-0.1}$	$^{+0.2}_{-0.4}$
	0.05	0.522	± 2.0	$^{+2.2}_{-2.2}$	$^{+0.3}_{+0.0}$	$^{-0.3}_{+0.4}$	$^{+0.7}_{-0.7}$	$^{+2.0}_{-2.0}$	$^{+0.0}_{+0.0}$	$^{-0.4}_{+0.1}$	$^{+0.0}_{+0.0}$	$^{+0.3}_{-0.4}$
	0.08	0.448	± 2.1	$^{+2.6}_{-2.6}$	$^{+0.5}_{-0.0}$	$^{-0.2}_{+0.3}$	$^{-2.5}_{+2.5}$	$^{+0.1}_{-0.1}$	$^{+0.0}_{+0.0}$	$^{+0.5}_{-0.7}$	$^{+0.0}_{+0.0}$	$^{+0.3}_{-0.4}$
	0.13	0.377	± 2.4	$^{+1.1}_{-1.0}$	$^{+0.5}_{-0.0}$	$^{-0.2}_{+0.3}$	$^{+0.7}_{-0.7}$	$^{+0.6}_{-0.6}$	$^{+0.0}_{+0.0}$	$^{+0.1}_{-0.4}$	$^{+0.0}_{+0.0}$	$^{+0.2}_{-0.2}$
	0.25	0.257	± 2.8	$^{+3.7}_{-3.4}$	$^{+0.3}_{+0.0}$	$^{-0.2}_{+0.2}$	$^{+3.3}_{-3.3}$	$^{+0.8}_{-0.8}$	$^{+1.2}_{-0.1}$	$^{+0.7}_{-0.5}$	$^{+0.0}_{+0.0}$	$^{+0.2}_{-0.3}$
1200	0.014	0.892	± 2.3	$^{+2.4}_{-3.2}$	$^{+0.6}_{-2.2}$	$^{-0.8}_{+1.0}$	$^{-0.7}_{+0.7}$	$^{-1.4}_{+1.4}$	$^{+0.0}_{+0.0}$	$^{-0.3}_{-0.8}$	$^{+1.4}_{-1.4}$	$^{+0.5}_{-0.2}$
	0.021	0.791	± 2.1	$^{+1.9}_{-1.6}$	$^{+0.9}_{-0.1}$	$^{-0.5}_{+0.5}$	$^{+1.5}_{-1.5}$	$^{+0.0}_{-0.0}$	$^{+0.0}_{+0.0}$	$^{+0.1}_{+0.4}$	$^{+0.4}_{-0.4}$	$^{+0.3}_{-0.4}$
	0.032	0.608	± 2.1	$^{+1.2}_{-1.1}$	$^{+0.0}_{-0.1}$	$^{-0.4}_{+0.5}$	$^{-0.5}_{+0.5}$	$^{-0.7}_{+0.7}$	$^{+0.0}_{+0.0}$	$^{+0.1}_{+0.1}$	$^{+0.2}_{-0.2}$	$^{+0.6}_{-0.6}$
	0.05	0.551	± 1.8	$^{+1.3}_{-1.4}$	$^{+0.1}_{-0.0}$	$^{-0.3}_{+0.3}$	$^{-0.1}_{+0.1}$	$^{+1.2}_{-1.2}$	$^{+0.0}_{+0.0}$	$^{-0.3}_{-0.4}$	$^{+0.0}_{-0.0}$	$^{+0.4}_{-0.4}$
	0.08	0.456	± 1.9	$^{+1.4}_{-1.3}$	$^{+0.3}_{-0.0}$	$^{-0.2}_{+0.4}$	$^{-0.3}_{+0.3}$	$^{+1.2}_{-1.2}$	$^{+0.0}_{+0.0}$	$^{+0.3}_{-0.3}$	$^{+0.0}_{+0.0}$	$^{+0.4}_{-0.3}$
	0.13	0.375	± 2.1	$^{+1.1}_{-1.2}$	$^{+0.1}_{-0.0}$	$^{-0.1}_{+0.2}$	$^{-0.9}_{+0.9}$	$^{+0.4}_{-0.4}$	$^{+0.0}_{+0.0}$	$^{+0.1}_{-0.5}$	$^{+0.0}_{+0.0}$	$^{+0.3}_{-0.4}$
	0.25	0.247	± 2.4	$^{+2.4}_{-2.3}$	$^{+0.3}_{+0.0}$	$^{-0.2}_{+0.3}$	$^{+2.0}_{-2.0}$	$^{+1.0}_{-1.0}$	$^{+0.0}_{+0.0}$	$^{-0.3}_{-0.1}$	$^{+0.0}_{+0.0}$	$^{+0.5}_{-0.4}$
	0.4	0.125	± 4.1	$^{+8.1}_{-5.7}$	$^{+0.0}_{-0.1}$	$^{-0.4}_{+0.4}$	$^{+5.6}_{-5.6}$	$^{+0.6}_{-0.6}$	$^{+5.8}_{+3.4}$	$^{+0.5}_{-1.0}$	$^{+0.0}_{+0.0}$	$^{+0.5}_{-0.5}$
1500	0.021	0.765	± 3.0	$^{+2.6}_{-2.3}$	$^{+0.9}_{-0.2}$	$^{-0.6}_{+0.4}$	$^{-0.4}_{+0.4}$	$^{-0.1}_{+0.1}$	$^{+0.0}_{+0.0}$	$^{-1.0}_{+0.1}$	$^{+2.3}_{-1.9}$	$^{+0.4}_{-0.4}$
	0.032	0.629	± 2.7	$^{+0.7}_{-0.6}$	$^{+0.3}_{-0.1}$	$^{-0.3}_{+0.3}$	$^{-0.1}_{+0.1}$	$^{-0.3}_{+0.3}$	$^{+0.0}_{+0.0}$	$^{-0.1}_{-0.1}$	$^{+0.2}_{-0.2}$	$^{+0.4}_{-0.3}$
	0.05	0.522	± 2.4	$^{+0.9}_{-0.8}$	$^{+0.2}_{-0.0}$	$^{-0.3}_{+0.4}$	$^{+0.2}_{-0.2}$	$^{+0.4}_{-0.4}$	$^{+0.0}_{+0.0}$	$^{-0.4}_{+0.5}$	$^{+0.0}_{-0.0}$	$^{+0.3}_{-0.4}$
	0.08	0.477	± 2.3	$^{+1.0}_{-1.1}$	$^{+0.2}_{-0.0}$	$^{-0.3}_{+0.4}$	$^{-0.9}_{+0.9}$	$^{-0.2}_{+0.2}$	$^{+0.0}_{+0.0}$	$^{-0.4}_{+0.1}$	$^{+0.0}_{+0.0}$	$^{+0.3}_{-0.5}$
	0.13	0.376	± 2.9	$^{+2.1}_{-1.8}$	$^{+0.8}_{-0.0}$	$^{-0.1}_{+0.3}$	$^{-1.3}_{+1.3}$	$^{-1.1}_{+1.1}$	$^{+0.0}_{+0.0}$	$^{+0.8}_{-0.2}$	$^{+0.0}_{+0.0}$	$^{+0.3}_{-0.4}$
	0.18	0.312	± 3.2	$^{+1.8}_{-1.7}$	$^{+0.6}_{-0.1}$	$^{-0.3}_{+0.2}$	$^{+0.0}_{-0.0}$	$^{-1.6}_{+1.6}$	$^{+0.0}_{+0.0}$	$^{-0.3}_{-0.2}$	$^{+0.0}_{+0.0}$	$^{+0.4}_{-0.4}$
	0.25	0.264	± 3.8	$^{+1.9}_{-1.9}$	$^{+0.0}_{-0.3}$	$^{-0.3}_{+0.3}$	$^{+1.7}_{-1.7}$	$^{+0.6}_{-0.6}$	$^{+0.1}_{+0.0}$	$^{-0.1}_{-0.3}$	$^{+0.0}_{+0.0}$	$^{+0.3}_{-0.3}$
	0.4	0.128	± 5.7	$^{+8.8}_{-4.3}$	$^{+0.6}_{+0.0}$	$^{-0.5}_{+0.3}$	$^{+2.0}_{-2.0}$	$^{-0.9}_{+0.9}$	$^{+8.4}_{-3.6}$	$^{+0.3}_{-0.4}$	$^{+0.0}_{+0.0}$	$^{+0.6}_{-0.5}$
2000	0.032	0.636	± 3.3	$^{+2.5}_{-1.4}$	$^{+1.8}_{+0.0}$	$^{-0.2}_{+0.2}$	$^{+0.3}_{-0.3}$	$^{+1.0}_{-1.0}$	$^{+0.0}_{+0.0}$	$^{+0.4}_{+0.7}$	$^{+1.1}_{-0.8}$	$^{+0.3}_{-0.4}$
	0.05	0.571	± 2.9	$^{+1.0}_{-0.8}$	$^{+0.5}_{-0.0}$	$^{-0.3}_{+0.4}$	$^{-0.3}_{+0.3}$	$^{-0.6}_{+0.6}$	$^{+0.0}_{+0.0}$	$^{+0.1}_{+0.1}$	$^{+0.0}_{+0.0}$	$^{+0.3}_{-0.3}$
	0.08	0.459	± 2.9	$^{+2.0}_{-2.0}$	$^{+0.1}_{-0.1}$	$^{-0.3}_{+0.4}$	$^{-0.1}_{+0.1}$	$^{+1.9}_{-1.9}$	$^{+0.0}_{+0.0}$	$^{+0.2}_{+0.0}$	$^{+0.0}_{-0.0}$	$^{+0.3}_{-0.3}$
	0.13	0.374	± 3.4	$^{+0.8}_{-1.2}$	$^{+0.1}_{-0.6}$	$^{-0.2}_{+0.3}$	$^{-0.5}_{+0.5}$	$^{+0.5}_{-0.5}$	$^{+0.0}_{+0.0}$	$^{+0.1}_{-0.6}$	$^{+0.0}_{+0.0}$	$^{+0.3}_{-0.4}$
	0.18	0.309	± 3.8	$^{+0.6}_{-1.9}$	$^{+0.0}_{-0.7}$	$^{-0.2}_{+0.2}$	$^{-0.3}_{+0.3}$	$^{+0.1}_{-0.1}$	$^{+0.0}_{+0.0}$	$^{-0.4}_{-1.6}$	$^{+0.0}_{+0.0}$	$^{+0.4}_{-0.6}$
	0.25	0.247	± 4.5	$^{+1.7}_{-1.6}$	$^{+0.3}_{-0.0}$	$^{-0.2}_{+0.3}$	$^{+1.5}_{-1.5}$	$^{+0.5}_{-0.5}$	$^{+0.0}_{+0.0}$	$^{+0.4}_{+0.5}$	$^{+0.0}_{+0.0}$	$^{+0.5}_{-0.5}$
	0.4	0.120	± 6.5	$^{+3.7}_{-3.9}$	$^{+0.0}_{-0.2}$	$^{-0.3}_{+0.4}$	$^{+3.1}_{-3.1}$	$^{+1.1}_{-1.1}$	$^{-0.5}_{+1.0}$	$^{+0.1}_{-1.3}$	$^{+0.0}_{+0.0}$	$^{+1.2}_{-1.4}$

Table 8: *Continuation 1.*

Q_c^2 (GeV^2)	x_c	$\tilde{\sigma}$	stat. (%)	sys. (%)	δ_1 (%)	δ_2 (%)	δ_3 (%)	δ_4 (%)	δ_5 (%)	δ_6 (%)	δ_7 (%)	$\delta_8 - \delta_{13}$ (%)
3000	0.05	0.581	$\pm$ 3.7	$^{+2.0}_{-1.1}$	$^{+1.6}_{-0.1}$	$^{-0.3}_{+0.4}$	$^{+0.9}_{-0.9}$	$^{-0.0}_{+0.0}$	$^{+0.0}_{+0.0}$	$^{+0.4}_{+0.2}$	$^{+0.5}_{-0.5}$	$^{+0.4}_{-0.3}$
	0.08	0.507	$\pm$ 3.4	$^{+1.1}_{-1.1}$	$^{+0.2}_{-0.4}$	$^{-0.2}_{+0.3}$	$^{-0.4}_{+0.4}$	$^{+0.8}_{-0.8}$	$^{+0.0}_{+0.0}$	$^{+0.5}_{-0.1}$	$^{+0.1}_{-0.1}$	$^{+0.3}_{-0.5}$
	0.13	0.378	$\pm$ 4.0	$^{+0.9}_{-0.7}$	$^{+0.1}_{-0.1}$	$^{-0.2}_{+0.3}$	$^{+0.6}_{-0.6}$	$^{-0.1}_{+0.1}$	$^{+0.0}_{+0.0}$	$^{-0.3}_{-0.3}$	$^{+0.0}_{+0.0}$	$^{+0.7}_{-0.1}$
	0.18	0.320	$\pm$ 4.4	$^{+1.2}_{-1.3}$	$^{+0.0}_{-0.3}$	$^{-0.2}_{+0.2}$	$^{-0.9}_{+0.9}$	$^{-0.6}_{+0.6}$	$^{+0.0}_{+0.0}$	$^{-0.5}_{+0.2}$	$^{+0.0}_{+0.0}$	$^{+0.4}_{-0.3}$
	0.25	0.286	$\pm$ 4.9	$^{+7.4}_{-7.3}$	$^{+0.6}_{-0.0}$	$^{-0.2}_{+0.2}$	$^{+7.3}_{-7.3}$	$^{+0.2}_{-0.2}$	$^{+0.0}_{+0.0}$	$^{+1.1}_{+0.3}$	$^{+0.0}_{+0.0}$	$^{+0.8}_{-0.6}$
	0.4	0.135	$\pm$ 7.4	$^{+3.8}_{-3.5}$	$^{+1.3}_{-0.0}$	$^{-0.2}_{+0.4}$	$^{-3.4}_{+3.4}$	$^{+0.5}_{-0.5}$	$^{+0.4}_{-0.0}$	$^{+0.8}_{-0.3}$	$^{+0.0}_{+0.0}$	$^{+0.6}_{-0.6}$
	0.65	0.017	$^{+14.4}_{-12.7}$	$^{+10.2}_{-10.4}$	$^{+0.0}_{-0.6}$	$^{-0.8}_{+1.0}$	$^{-8.7}_{+8.7}$	$^{+4.6}_{-4.6}$	$^{+1.8}_{+0.7}$	$^{-2.7}_{+0.9}$	$^{+0.0}_{+0.0}$	$^{+1.7}_{-2.0}$
5000	0.08	0.527	$\pm$ 3.2	$^{+1.8}_{-0.9}$	$^{+1.6}_{-0.3}$	$^{-0.2}_{+0.2}$	$^{-0.3}_{+0.3}$	$^{+0.2}_{-0.2}$	$^{+0.0}_{+0.0}$	$^{-0.6}_{-0.4}$	$^{+0.3}_{-0.3}$	$^{+0.5}_{-0.3}$
	0.13	0.463	$\pm$ 4.1	$^{+1.0}_{-0.8}$	$^{+0.8}_{+0.0}$	$^{-0.2}_{+0.2}$	$^{-0.4}_{+0.4}$	$^{+0.3}_{-0.3}$	$^{+0.0}_{+0.0}$	$^{+0.1}_{-0.3}$	$^{+0.1}_{-0.1}$	$^{+0.2}_{-0.5}$
	0.18	0.340	$\pm$ 4.5	$^{+1.0}_{-0.5}$	$^{+0.2}_{-0.1}$	$^{-0.3}_{+0.2}$	$^{+0.2}_{-0.2}$	$^{+0.3}_{-0.3}$	$^{+0.0}_{+0.0}$	$^{-0.1}_{+0.7}$	$^{+0.0}_{+0.0}$	$^{+0.5}_{-0.3}$
	0.25	0.243	$\pm$ 5.6	$^{+1.8}_{-1.2}$	$^{+0.7}_{-0.0}$	$^{-0.2}_{+0.3}$	$^{+0.7}_{-0.7}$	$^{-0.7}_{+0.7}$	$^{+0.0}_{+0.0}$	$^{+1.2}_{-0.6}$	$^{+0.0}_{+0.0}$	$^{+0.4}_{-0.3}$
	0.4	0.140	$\pm$ 7.6	$^{+6.5}_{-6.4}$	$^{+0.0}_{-0.3}$	$^{-0.2}_{+0.3}$	$^{+6.0}_{-6.0}$	$^{-2.1}_{+2.1}$	$^{+0.0}_{+0.0}$	$^{+0.4}_{+1.3}$	$^{+0.0}_{+0.0}$	$^{+1.1}_{-1.1}$
8000	0.13	0.560	$\pm$ 4.2	$^{+1.0}_{-1.9}$	$^{+0.0}_{-1.0}$	$^{-0.3}_{+0.3}$	$^{-0.5}_{+0.5}$	$^{-0.1}_{+0.1}$	$^{+0.0}_{+0.0}$	$^{-1.3}_{+0.3}$	$^{+0.5}_{-0.3}$	$^{+0.5}_{-0.5}$
	0.18	0.433	$\pm$ 5.4	$^{+2.6}_{-2.9}$	$^{+0.1}_{-0.3}$	$^{-0.2}_{+0.2}$	$^{-2.4}_{+2.4}$	$^{+0.6}_{-0.6}$	$^{+0.0}_{+0.0}$	$^{+0.5}_{-0.3}$	$^{+0.0}_{+0.0}$	$^{+0.6}_{-1.3}$
	0.25	0.309	$\pm$ 6.6	$^{+3.8}_{-3.9}$	$^{+0.7}_{-0.1}$	$^{-0.3}_{+0.2}$	$^{-3.6}_{+3.6}$	$^{+0.4}_{-0.4}$	$^{+0.0}_{+0.0}$	$^{-1.1}_{-0.6}$	$^{+0.0}_{+0.0}$	$^{+0.4}_{-0.4}$
	0.4	0.114	$^{+11.9}_{-10.7}$	$^{+7.1}_{-7.3}$	$^{+0.1}_{-0.0}$	$^{-0.3}_{+0.4}$	$^{+7.0}_{-7.0}$	$^{-0.6}_{+0.6}$	$^{+0.0}_{+0.0}$	$^{-0.3}_{+0.5}$	$^{+0.0}_{+0.0}$	$^{+0.6}_{-2.0}$
	0.65	0.019	$^{+19.9}_{-16.9}$	$^{+4.1}_{-4.2}$	$^{+0.2}_{-1.4}$	$^{-0.9}_{+0.9}$	$^{+1.5}_{-1.5}$	$^{+2.3}_{-2.3}$	$^{+0.0}_{+0.0}$	$^{-2.6}_{+2.8}$	$^{+0.0}_{+0.0}$	$^{+0.8}_{-0.6}$
12000	0.18	0.464	$\pm$ 6.1	$^{+1.3}_{-3.8}$	$^{+1.0}_{-3.6}$	$^{-0.3}_{+0.4}$	$^{-0.4}_{+0.4}$	$^{-0.2}_{+0.2}$	$^{+0.0}_{+0.0}$	$^{-0.3}_{-0.8}$	$^{+0.2}_{-0.3}$	$^{+0.5}_{-0.6}$
	0.25	0.353	$\pm$ 8.2	$^{+2.8}_{-2.3}$	$^{+2.4}_{-0.6}$	$^{-0.2}_{+0.2}$	$^{+0.3}_{-0.3}$	$^{+0.8}_{-0.8}$	$^{+0.0}_{+0.0}$	$^{+0.3}_{-1.6}$	$^{+0.0}_{+0.0}$	$^{+1.0}_{-1.2}$
	0.4	0.156	$^{+13.4}_{-11.8}$	$^{+4.6}_{-3.8}$	$^{+2.7}_{-0.2}$	$^{-0.3}_{+0.4}$	$^{+3.2}_{-3.2}$	$^{-0.8}_{+0.8}$	$^{+0.0}_{+0.0}$	$^{-1.2}_{+1.5}$	$^{+0.0}_{+0.0}$	$^{+0.6}_{-1.3}$
20000	0.25	0.461	$\pm$ 9.2	$^{+6.1}_{-3.6}$	$^{+4.9}_{-1.8}$	$^{-1.5}_{+0.2}$	$^{-2.2}_{+2.2}$	$^{+0.1}_{-0.1}$	$^{+0.0}_{+0.0}$	$^{-0.7}_{-0.2}$	$^{+2.7}_{-1.4}$	$^{+0.6}_{-0.5}$
	0.4	0.183	$^{+16.6}_{-14.4}$	$^{+4.9}_{-3.8}$	$^{+3.6}_{+0.0}$	$^{-0.4}_{+0.4}$	$^{+0.9}_{-0.9}$	$^{+3.0}_{-3.0}$	$^{+0.0}_{+0.0}$	$^{-1.8}_{-0.3}$	$^{+0.0}_{+0.0}$	$^{+1.1}_{-1.2}$
30000	0.4	0.237	$^{+17.9}_{-15.4}$	$^{+6.9}_{-5.9}$	$^{+6.7}_{+0.0}$	$^{-0.2}_{+0.3}$	$^{-0.8}_{+0.8}$	$^{+0.7}_{-0.7}$	$^{+0.0}_{+0.0}$	$^{+0.1}_{-4.9}$	$^{+0.0}_{-2.9}$	$^{+1.3}_{-1.3}$

Table 8: *Continuation 2.*

Q^2 range (GeV^2)	Q_c^2 (GeV^2)	x range	x_c	$x\tilde{F}_3 \times 10$
2500 – 3500	3000	0.037 – 0.06	0.05	$0.26 \pm 0.28\ ^{+0.10}_{-0.08}$
		0.06 – 0.1	0.08	$1.10 \pm 0.35\ ^{+0.10}_{-0.11}$
		0.1 – 0.15	0.13	$0.56 \pm 0.56\ ^{+0.30}_{-0.10}$
		0.15 – 0.23	0.18	$0.08 \pm 0.72\ ^{+0.17}_{-0.32}$
		0.23 – 0.35	0.25	$2.25 \pm 0.95\ ^{+0.85}_{-0.93}$
		0.35 – 0.53	0.4	$-0.03 \pm 1.18\ ^{+0.51}_{-0.47}$
		0.53 – 0.75	0.65	$-0.36\ ^{+0.46}_{-0.44}\ ^{+0.31}_{-0.23}$
3500 – 5600	5000	0.04 – 0.1	0.08	$0.74 \pm 0.20\ ^{+0.09}_{-0.06}$
		0.1 – 0.15	0.13	$1.16 \pm 0.36\ ^{+0.07}_{-0.07}$
		0.15 – 0.23	0.18	$1.13 \pm 0.42\ ^{+0.09}_{-0.13}$
		0.23 – 0.35	0.25	$0.60 \pm 0.54\ ^{+0.17}_{-0.16}$
		0.35 – 0.53	0.4	$1.05 \pm 0.67\ ^{+0.38}_{-0.35}$
5600 – 9000	8000	0.07 – 0.15	0.13	$1.74 \pm 0.25\ ^{+0.07}_{-0.09}$
		0.15 – 0.23	0.18	$1.54 \pm 0.35\ ^{+0.11}_{-0.14}$
		0.23 – 0.35	0.25	$1.49 \pm 0.43\ ^{+0.19}_{-0.18}$
		0.35 – 0.53	0.4	$0.40\ ^{+0.50}_{-0.48}\ ^{+0.22}_{-0.21}$
		0.53 – 0.75	0.65	$0.23\ ^{+0.25}_{-0.19}\ ^{+0.04}_{-0.05}$
9000 – 15000	12000	0.09 – 0.23	0.18	$0.91 \pm 0.31\ ^{+0.07}_{-0.17}$
		0.23 – 0.35	0.25	$1.37 \pm 0.43\ ^{+0.09}_{-0.14}$
		0.35 – 0.53	0.4	$0.97\ ^{+0.46}_{-0.43}\ ^{+0.14}_{-0.15}$
15000 – 25000	20000	0.15 – 0.35	0.25	$2.04 \pm 0.27\ ^{+0.16}_{-0.09}$
		0.35 – 0.75	0.4	$1.02\ ^{+0.41}_{-0.31}\ ^{+0.12}_{-0.11}$
25000 – 50000	30000	0.25 – 0.75	0.4	$1.05\ ^{+0.32}_{-0.25}\ ^{+0.10}_{-0.15}$

Table 9: *The structure function $x\tilde{F}_3$ extracted using the e^-p data set ($\mathcal{L} = 169.9\,pb^{-1}, P_e = 0$) and previously published NC e^+p DIS results ($\mathcal{L} = 63.2\,pb^{-1}, P_e = 0$). The bin range and bin centre for Q^2 and x, and measured $x\tilde{F}_3$ are shown. The first (second) error on the measurement refers to the statistical (systematic) uncertainties.*

Q^2 (GeV^2)	x_c	$xF_3^{\gamma Z} \times 10$		
5000	0.032	1.53	$\pm$ 1.41	$\pm$ 0.80
	0.05	1.01	$\pm$ 1.19	$\pm$ 0.38
	0.08	3.26	$\pm$ 0.66	$\pm$ 0.24
	0.13	4.62	$\pm$ 0.62	$\pm$ 0.16
	0.18	3.01	$\pm$ 0.54	$\pm$ 0.19
	0.25	3.93	$\pm$ 0.44	$\pm$ 0.17
	0.4	2.08	$\pm$ 0.39	$\pm$ 0.15
	0.65	0.55	$\pm$ 0.63	$\pm$ 0.13

Table 10: *The interference structure function $xF_3^{\gamma Z}$ evaluated at $Q^2 = 5\,000\ GeV^2$ for x bins centred on x_c. The first (second) error on the measurement refers to the statistical (systematic) uncertainties.*

Q^2 range (GeV^2)	Q_c^2 (GeV^2)	x range	x_c	$\tilde{\sigma}$	N_{data}	$N_{\mathrm{bg}}^{\mathrm{MC}}$
185 – 240	200	0.0037 – 0.006	0.005	$1.094 \pm 0.015\ ^{+0.014}_{-0.011}$	5913	36.8
		0.006 – 0.01	0.008	$0.928 \pm 0.012\ ^{+0.018}_{-0.018}$	6914	9.8
		0.01 – 0.017	0.013	$0.785 \pm 0.009\ ^{+0.013}_{-0.013}$	7406	1.2
		0.017 – 0.025	0.021	$0.669 \pm 0.009\ ^{+0.014}_{-0.014}$	5337	0.0
		0.025 – 0.037	0.032	$0.558 \pm 0.008\ ^{+0.023}_{-0.022}$	4970	0.0
		0.037 – 0.06	0.05	$0.500 \pm 0.008\ ^{+0.012}_{-0.012}$	4615	0.0
		0.06 – 0.12	0.08	$0.435 \pm 0.006\ ^{+0.024}_{-0.024}$	5891	0.0
		0.12 – 0.25	0.18	$0.325 \pm 0.006\ ^{+0.017}_{-0.017}$	3003	0.0
240 – 310	250	0.006 – 0.01	0.008	$0.920 \pm 0.014\ ^{+0.014}_{-0.012}$	4675	10.9
		0.01 – 0.017	0.013	$0.787 \pm 0.011\ ^{+0.013}_{-0.012}$	5247	2.5
		0.017 – 0.025	0.021	$0.649 \pm 0.011\ ^{+0.010}_{-0.009}$	3703	0.6
		0.025 – 0.037	0.032	$0.564 \pm 0.010\ ^{+0.019}_{-0.018}$	3657	0.0
		0.037 – 0.06	0.05	$0.481 \pm 0.008\ ^{+0.016}_{-0.016}$	3465	0.0
		0.06 – 0.12	0.08	$0.431 \pm 0.007\ ^{+0.022}_{-0.022}$	4353	0.0
		0.12 – 0.25	0.18	$0.324 \pm 0.006\ ^{+0.016}_{-0.015}$	2864	0.0
310 – 410	350	0.006 – 0.01	0.008	$0.973 \pm 0.019\ ^{+0.021}_{-0.015}$	2902	30.0
		0.01 – 0.017	0.013	$0.826 \pm 0.014\ ^{+0.016}_{-0.010}$	4010	3.7
		0.017 – 0.025	0.021	$0.692 \pm 0.013\ ^{+0.006}_{-0.004}$	3044	0.0
		0.025 – 0.037	0.032	$0.603 \pm 0.011\ ^{+0.012}_{-0.011}$	2953	0.0
		0.037 – 0.06	0.05	$0.503 \pm 0.009\ ^{+0.013}_{-0.013}$	3112	0.0
		0.06 – 0.12	0.08	$0.432 \pm 0.008\ ^{+0.009}_{-0.009}$	3501	0.0
		0.12 – 0.25	0.18	$0.306 \pm 0.006\ ^{+0.020}_{-0.019}$	2689	0.0
410 – 530	450	0.006 – 0.01	0.008	$1.004 \pm 0.022\ ^{+0.024}_{-0.021}$	2262	35.3
		0.01 – 0.017	0.013	$0.843 \pm 0.019\ ^{+0.010}_{-0.009}$	1948	6.8
		0.017 – 0.025	0.021	$0.681 \pm 0.018\ ^{+0.012}_{-0.012}$	1523	0.5
		0.025 – 0.037	0.032	$0.567 \pm 0.014\ ^{+0.011}_{-0.010}$	1676	0.0
		0.037 – 0.06	0.05	$0.504 \pm 0.011\ ^{+0.013}_{-0.012}$	2125	0.0
		0.06 – 0.1	0.08	$0.409 \pm 0.010\ ^{+0.008}_{-0.008}$	1687	0.0
		0.1 – 0.17	0.13	$0.355 \pm 0.009\ ^{+0.017}_{-0.017}$	1545	0.0
		0.17 – 0.3	0.25	$0.252 \pm 0.008\ ^{+0.014}_{-0.014}$	1135	0.0

Table 11: *The reduced cross section $\tilde{\sigma}$ for the reaction $e^- p \to e^- X$ ($\mathcal{L} = 71.2\,pb^{-1}, P_e = +0.29$). The bin range, bin centre (Q_c^2 and x_c) and measured cross section corrected to the electroweak Born level are shown. The first (second) error on the cross section corresponds to the statistical (systematic) uncertainties. The number of observed data events (N_{data}) and simulated background events (N_{bg}^{MC}) are also shown. This table has two continuations.*

Q^2 range (GeV^2)	Q_c^2 (GeV^2)	x range	x_c	$\tilde{\sigma}$	N_{data}	$N_{\mathrm{bg}}^{\mathrm{MC}}$
530 – 710	650	0.01 – 0.017	0.013	$0.874 \pm 0.019\ ^{+0.013}_{-0.007}$	2231	25.1
		0.017 – 0.025	0.021	$0.761 \pm 0.020\ ^{+0.009}_{-0.008}$	1511	2.4
		0.025 – 0.037	0.032	$0.597 \pm 0.018\ ^{+0.007}_{-0.006}$	1151	0.6
		0.037 – 0.06	0.05	$0.499 \pm 0.015\ ^{+0.005}_{-0.005}$	1186	0.0
		0.06 – 0.1	0.08	$0.415 \pm 0.013\ ^{+0.010}_{-0.010}$	988	0.0
		0.1 – 0.17	0.13	$0.349 \pm 0.012\ ^{+0.009}_{-0.008}$	891	0.0
		0.17 – 0.3	0.25	$0.250 \pm 0.009\ ^{+0.016}_{-0.016}$	780	0.0
710 – 900	800	0.009 – 0.017	0.013	$0.828 \pm 0.023\ ^{+0.014}_{-0.016}$	1347	20.7
		0.017 – 0.025	0.021	$0.685 \pm 0.023\ ^{+0.008}_{-0.006}$	924	1.3
		0.025 – 0.037	0.032	$0.617 \pm 0.020\ ^{+0.008}_{-0.009}$	1000	3.1
		0.037 – 0.06	0.05	$0.495 \pm 0.015\ ^{+0.011}_{-0.011}$	1082	0.0
		0.06 – 0.1	0.08	$0.446 \pm 0.014\ ^{+0.012}_{-0.012}$	974	0.0
		0.1 – 0.17	0.13	$0.375 \pm 0.013\ ^{+0.004}_{-0.004}$	797	0.0
		0.17 – 0.3	0.25	$0.239 \pm 0.010\ ^{+0.009}_{-0.008}$	552	0.0
900 – 1300	1200	0.01 – 0.017	0.014	$0.875 \pm 0.030\ ^{+0.021}_{-0.028}$	911	31.9
		0.017 – 0.025	0.021	$0.744 \pm 0.024\ ^{+0.014}_{-0.012}$	1005	9.8
		0.025 – 0.037	0.032	$0.594 \pm 0.019\ ^{+0.007}_{-0.007}$	1013	4.9
		0.037 – 0.06	0.05	$0.557 \pm 0.015\ ^{+0.007}_{-0.008}$	1352	0.5
		0.06 – 0.1	0.08	$0.436 \pm 0.013\ ^{+0.006}_{-0.006}$	1215	0.0
		0.1 – 0.17	0.13	$0.364 \pm 0.012\ ^{+0.004}_{-0.004}$	995	0.0
		0.17 – 0.3	0.25	$0.225 \pm 0.009\ ^{+0.005}_{-0.005}$	716	0.0
		0.3 – 0.53	0.4	$0.120 \pm 0.008\ ^{+0.010}_{-0.007}$	257	0.0
1300 – 1800	1500	0.017 – 0.025	0.021	$0.761 \pm 0.034\ ^{+0.019}_{-0.018}$	530	24.5
		0.025 – 0.037	0.032	$0.617 \pm 0.026\ ^{+0.004}_{-0.004}$	575	3.0
		0.037 – 0.06	0.05	$0.538 \pm 0.020\ ^{+0.005}_{-0.004}$	756	0.6
		0.06 – 0.1	0.08	$0.454 \pm 0.017\ ^{+0.005}_{-0.005}$	751	0.0
		0.1 – 0.15	0.13	$0.365 \pm 0.017\ ^{+0.008}_{-0.006}$	487	0.0
		0.15 – 0.23	0.18	$0.293 \pm 0.015\ ^{+0.005}_{-0.005}$	403	0.0
		0.23 – 0.35	0.25	$0.263 \pm 0.015\ ^{+0.005}_{-0.005}$	304	0.0
		0.35 – 0.53	0.4	$0.122 \pm 0.011\ ^{+0.011}_{-0.005}$	126	0.0
1800 – 2500	2000	0.023 – 0.037	0.032	$0.631 \pm 0.032\ ^{+0.016}_{-0.009}$	405	8.0
		0.037 – 0.06	0.05	$0.529 \pm 0.024\ ^{+0.005}_{-0.004}$	476	0.0
		0.06 – 0.1	0.08	$0.438 \pm 0.020\ ^{+0.009}_{-0.009}$	497	0.5
		0.1 – 0.15	0.13	$0.417 \pm 0.021\ ^{+0.003}_{-0.005}$	412	0.0
		0.15 – 0.23	0.18	$0.295 \pm 0.017\ ^{+0.002}_{-0.006}$	288	0.0
		0.23 – 0.35	0.25	$0.232 \pm 0.017\ ^{+0.004}_{-0.004}$	197	0.0
		0.35 – 0.53	0.4	$0.118\ ^{+0.013}_{-0.012}\ ^{+0.004}_{-0.005}$	98	0.0

Table 11: *Continuation 1.*

Q^2 range (GeV^2)	Q_c^2 (GeV^2)	x range	x_c	$\tilde{\sigma}$	N_{data}	$N_{\mathrm{bg}}^{\mathrm{MC}}$
2500 – 3500	3000	0.037 – 0.06	0.05	$0.557 \pm 0.032\ ^{+0.011}_{-0.006}$	311	3.8
		0.06 – 0.1	0.08	$0.508 \pm 0.026\ ^{+0.006}_{-0.006}$	377	0.6
		0.1 – 0.15	0.13	$0.378 \pm 0.024\ ^{+0.004}_{-0.003}$	260	0.0
		0.15 – 0.23	0.18	$0.292 \pm 0.021\ ^{+0.003}_{-0.004}$	201	0.0
		0.23 – 0.35	0.25	$0.304 \pm 0.022\ ^{+0.023}_{-0.022}$	190	0.0
		0.35 – 0.53	0.4	$0.106\ ^{+0.015}_{-0.014}\ ^{+0.004}_{-0.004}$	61	0.0
		0.53 – 0.75	0.65	$0.015\ ^{+0.004}_{-0.003}\ ^{+0.002}_{-0.002}$	23	0.0
3500 – 5600	5000	0.04 – 0.1	0.08	$0.480 \pm 0.025\ ^{+0.009}_{-0.004}$	380	3.1
		0.1 – 0.15	0.13	$0.430 \pm 0.028\ ^{+0.004}_{-0.003}$	236	0.6
		0.15 – 0.23	0.18	$0.325 \pm 0.023\ ^{+0.003}_{-0.002}$	199	0.0
		0.23 – 0.35	0.25	$0.260 \pm 0.022\ ^{+0.005}_{-0.003}$	142	0.0
		0.35 – 0.53	0.4	$0.152\ ^{+0.019}_{-0.017}\ ^{+0.010}_{-0.010}$	80	0.0
5600 – 9000	8000	0.07 – 0.15	0.13	$0.534 \pm 0.035\ ^{+0.005}_{-0.010}$	231	1.9
		0.15 – 0.23	0.18	$0.430 \pm 0.036\ ^{+0.011}_{-0.012}$	143	0.0
		0.23 – 0.35	0.25	$0.294\ ^{+0.034}_{-0.031}\ ^{+0.011}_{-0.011}$	92	0.0
		0.35 – 0.53	0.4	$0.113\ ^{+0.022}_{-0.019}\ ^{+0.008}_{-0.008}$	36	0.0
		0.53 – 0.75	0.65	$0.018\ ^{+0.006}_{-0.005}\ ^{+0.001}_{-0.001}$	14	0.0
9000 – 15000	12000	0.09 – 0.23	0.18	$0.401\ ^{+0.045}_{-0.040}\ ^{+0.005}_{-0.015}$	99	0.6
		0.23 – 0.35	0.25	$0.359\ ^{+0.051}_{-0.045}\ ^{+0.010}_{-0.008}$	63	0.0
		0.35 – 0.53	0.4	$0.172\ ^{+0.035}_{-0.030}\ ^{+0.008}_{-0.007}$	33	0.0
15000 – 25000	20000	0.15 – 0.35	0.25	$0.456\ ^{+0.073}_{-0.064}\ ^{+0.028}_{-0.016}$	53	1.8
		0.35 – 0.75	0.4	$0.175\ ^{+0.050}_{-0.040}\ ^{+0.009}_{-0.007}$	19	0.0
25000 – 50000	30000	0.25 – 0.75	0.4	$0.190\ ^{+0.066}_{-0.050}\ ^{+0.013}_{-0.011}$	14	0.0

Table 11: *Continuation 2.*

Q_c^2 (GeV^2)	x_c	$\tilde{\sigma}$	stat. (%)	sys. (%)	δ_1 (%)	δ_2 (%)	δ_3 (%)	δ_4 (%)	δ_5 (%)	δ_6 (%)	δ_7 (%)	$\delta_8 - \delta_{13}$ (%)
200	0.005	1.094	± 1.4	$^{+1.3}_{-1.0}$	$^{+0.7}_{-0.0}$	$^{-0.4}_{+0.6}$	$^{+0.4}_{-0.4}$	$^{-0.4}_{+0.4}$	$^{+0.0}_{+0.0}$	$^{+0.1}_{-0.1}$	$^{+0.3}_{-0.3}$	$^{+0.7}_{-0.7}$
	0.008	0.928	± 1.2	$^{+1.9}_{-1.9}$	$^{+0.3}_{-0.0}$	$^{-0.4}_{+0.5}$	$^{+0.2}_{-0.2}$	$^{-1.6}_{+1.6}$	$^{+0.0}_{+0.0}$	$^{+0.1}_{+0.4}$	$^{+0.1}_{-0.1}$	$^{+0.8}_{-1.0}$
	0.013	0.785	± 1.2	$^{+1.7}_{-1.6}$	$^{+0.2}_{+0.0}$	$^{-0.5}_{+0.5}$	$^{-0.2}_{+0.2}$	$^{-1.3}_{+1.3}$	$^{+0.0}_{+0.0}$	$^{+0.0}_{+0.4}$	$^{+0.0}_{-0.0}$	$^{+0.8}_{-0.9}$
	0.021	0.669	± 1.4	$^{+2.1}_{-2.1}$	$^{+0.4}_{+0.0}$	$^{-0.3}_{+0.5}$	$^{-1.6}_{+1.6}$	$^{+0.9}_{-0.9}$	$^{+0.0}_{+0.0}$	$^{-0.1}_{+0.1}$	$^{+0.0}_{+0.0}$	$^{+0.8}_{-0.9}$
	0.032	0.558	± 1.5	$^{+4.0}_{-4.0}$	$^{+0.1}_{-0.0}$	$^{-0.3}_{+0.4}$	$^{-1.5}_{+1.5}$	$^{+3.6}_{-3.6}$	$^{+0.0}_{+0.0}$	$^{+0.2}_{+0.4}$	$^{+0.0}_{+0.0}$	$^{+0.8}_{-0.8}$
	0.05	0.500	± 1.5	$^{+2.5}_{-2.4}$	$^{+0.0}_{-0.3}$	$^{-0.2}_{+0.3}$	$^{-0.5}_{+0.5}$	$^{+2.2}_{-2.2}$	$^{+0.0}_{+0.0}$	$^{+0.0}_{+0.3}$	$^{+0.0}_{+0.0}$	$^{+1.0}_{-0.9}$
	0.08	0.435	± 1.3	$^{+5.5}_{-5.5}$	$^{+0.0}_{-0.1}$	$^{-0.2}_{+0.2}$	$^{+5.0}_{-5.0}$	$^{+2.0}_{-2.0}$	$^{-0.0}_{+0.0}$	$^{-0.0}_{+0.1}$	$^{+0.0}_{+0.0}$	$^{+0.8}_{-1.0}$
	0.18	0.325	± 1.9	$^{+5.4}_{-5.4}$	$^{+0.1}_{+0.0}$	$^{-0.1}_{+0.2}$	$^{+5.3}_{-5.3}$	$^{+0.5}_{-0.5}$	$^{+0.7}_{+0.2}$	$^{-0.1}_{+0.1}$	$^{+0.0}_{+0.0}$	$^{+0.7}_{-0.9}$
250	0.008	0.920	± 1.5	$^{+1.5}_{-1.3}$	$^{+0.6}_{-0.0}$	$^{-0.3}_{+0.4}$	$^{+0.5}_{-0.5}$	$^{-0.9}_{+0.9}$	$^{+0.0}_{+0.0}$	$^{-0.2}_{+0.3}$	$^{+0.1}_{-0.1}$	$^{+0.7}_{-0.7}$
	0.013	0.787	± 1.4	$^{+1.7}_{-1.5}$	$^{+0.7}_{+0.0}$	$^{-0.5}_{+0.6}$	$^{+0.0}_{-0.0}$	$^{-1.3}_{+1.3}$	$^{+0.0}_{+0.0}$	$^{-0.1}_{+0.2}$	$^{+0.0}_{-0.0}$	$^{+0.5}_{-0.7}$
	0.021	0.649	± 1.7	$^{+1.6}_{-1.4}$	$^{+0.7}_{-0.0}$	$^{-0.3}_{+0.5}$	$^{-0.1}_{+0.1}$	$^{+1.1}_{-1.1}$	$^{+0.0}_{+0.0}$	$^{-0.2}_{+0.2}$	$^{+0.0}_{-0.0}$	$^{+0.8}_{-0.7}$
	0.032	0.564	± 1.7	$^{+3.3}_{-3.3}$	$^{+0.6}_{-0.0}$	$^{-0.3}_{+0.4}$	$^{-0.8}_{+0.8}$	$^{+3.0}_{-3.0}$	$^{+0.0}_{+0.0}$	$^{+0.0}_{+0.1}$	$^{+0.0}_{+0.0}$	$^{+0.7}_{-0.9}$
	0.05	0.481	± 1.8	$^{+3.4}_{-3.3}$	$^{+0.4}_{+0.0}$	$^{-0.1}_{+0.3}$	$^{-2.4}_{+2.4}$	$^{+2.2}_{-2.2}$	$^{+0.0}_{+0.0}$	$^{-0.0}_{-0.1}$	$^{+0.0}_{+0.0}$	$^{+0.7}_{-0.6}$
	0.08	0.431	± 1.6	$^{+5.2}_{-5.1}$	$^{+0.7}_{-0.0}$	$^{-0.1}_{+0.3}$	$^{+4.6}_{-4.6}$	$^{+2.2}_{-2.2}$	$^{+0.0}_{+0.0}$	$^{-0.0}_{+0.1}$	$^{+0.0}_{+0.0}$	$^{+0.7}_{-0.7}$
	0.18	0.324	± 1.9	$^{+4.8}_{-4.7}$	$^{+0.2}_{+0.0}$	$^{+0.0}_{+0.2}$	$^{+4.1}_{-4.1}$	$^{+2.0}_{-2.0}$	$^{+0.3}_{+1.0}$	$^{+0.0}_{+0.2}$	$^{+0.0}_{+0.0}$	$^{+0.8}_{-0.8}$
350	0.008	0.973	± 1.9	$^{+2.1}_{-1.5}$	$^{+1.6}_{-0.1}$	$^{-0.5}_{+0.6}$	$^{+0.9}_{-0.9}$	$^{-0.4}_{+0.4}$	$^{+0.0}_{+0.0}$	$^{-0.6}_{+0.4}$	$^{+0.4}_{-0.4}$	$^{+0.6}_{-0.8}$
	0.013	0.826	± 1.6	$^{+1.9}_{-1.2}$	$^{+1.4}_{-0.0}$	$^{-0.2}_{+0.5}$	$^{-0.2}_{+0.2}$	$^{-1.0}_{+1.0}$	$^{+0.0}_{+0.0}$	$^{-0.2}_{+0.5}$	$^{+0.0}_{-0.0}$	$^{+0.7}_{-0.6}$
	0.021	0.692	± 1.9	$^{+0.9}_{-0.6}$	$^{+0.4}_{-0.1}$	$^{-0.3}_{+0.4}$	$^{+0.3}_{-0.3}$	$^{+0.0}_{-0.0}$	$^{+0.0}_{+0.0}$	$^{-0.2}_{-0.0}$	$^{+0.0}_{+0.0}$	$^{+0.6}_{-0.5}$
	0.032	0.603	± 1.9	$^{+1.9}_{-1.8}$	$^{+0.8}_{-0.0}$	$^{-0.2}_{+0.4}$	$^{-1.6}_{+1.6}$	$^{+0.2}_{-0.2}$	$^{+0.0}_{+0.0}$	$^{-0.3}_{+0.1}$	$^{+0.0}_{+0.0}$	$^{+0.6}_{-0.7}$
	0.05	0.503	± 1.9	$^{+2.7}_{-2.6}$	$^{+0.6}_{-0.0}$	$^{-0.1}_{+0.2}$	$^{-1.9}_{+1.9}$	$^{+1.6}_{-1.6}$	$^{+0.0}_{+0.0}$	$^{-0.1}_{+0.2}$	$^{+0.0}_{+0.0}$	$^{+0.5}_{-0.7}$
	0.08	0.432	± 1.7	$^{+2.0}_{-2.0}$	$^{+0.3}_{+0.0}$	$^{-0.1}_{+0.2}$	$^{+1.1}_{-1.1}$	$^{+1.6}_{-1.6}$	$^{+0.0}_{+0.0}$	$^{+0.0}_{+0.1}$	$^{+0.0}_{+0.0}$	$^{+0.7}_{-0.7}$
	0.18	0.306	± 2.0	$^{+6.4}_{-6.3}$	$^{+0.4}_{+0.0}$	$^{-0.0}_{+0.2}$	$^{+5.7}_{-5.7}$	$^{+2.6}_{-2.6}$	$^{-0.1}_{+1.2}$	$^{+0.1}_{+0.2}$	$^{+0.0}_{+0.0}$	$^{+0.7}_{-0.6}$
450	0.008	1.004	± 2.2	$^{+2.4}_{-2.1}$	$^{+0.7}_{-0.3}$	$^{-1.4}_{+1.6}$	$^{+1.3}_{-1.3}$	$^{-0.5}_{+0.5}$	$^{+0.0}_{+0.0}$	$^{-0.2}_{+0.3}$	$^{+0.6}_{-0.6}$	$^{+0.5}_{-0.4}$
	0.013	0.843	± 2.3	$^{+1.1}_{-1.1}$	$^{+0.1}_{-0.1}$	$^{-0.5}_{+0.6}$	$^{-0.4}_{+0.4}$	$^{+0.2}_{-0.2}$	$^{+0.0}_{+0.0}$	$^{-0.6}_{+0.6}$	$^{+0.1}_{-0.1}$	$^{+0.5}_{-0.6}$
	0.021	0.681	± 2.6	$^{+1.8}_{-1.7}$	$^{+0.2}_{-0.1}$	$^{-0.4}_{+0.5}$	$^{-0.1}_{+0.1}$	$^{+1.3}_{-1.3}$	$^{+0.0}_{+0.0}$	$^{-0.7}_{+0.9}$	$^{+0.0}_{-0.0}$	$^{+0.8}_{-0.8}$
	0.032	0.567	± 2.5	$^{+1.9}_{-1.7}$	$^{+0.8}_{-0.1}$	$^{-0.2}_{+0.4}$	$^{+0.0}_{-0.0}$	$^{+1.4}_{-1.4}$	$^{+0.0}_{+0.0}$	$^{-0.5}_{+0.4}$	$^{+0.0}_{+0.0}$	$^{+1.0}_{-0.9}$
	0.05	0.504	± 2.2	$^{+2.5}_{-2.4}$	$^{+0.7}_{-0.0}$	$^{+0.0}_{+0.2}$	$^{-1.6}_{+1.6}$	$^{+1.6}_{-1.6}$	$^{+0.0}_{+0.0}$	$^{-0.4}_{+0.6}$	$^{+0.0}_{+0.0}$	$^{+0.7}_{-0.7}$
	0.08	0.409	± 2.5	$^{+2.1}_{-1.9}$	$^{+0.3}_{+0.0}$	$^{+0.1}_{+0.2}$	$^{-0.7}_{+0.7}$	$^{+1.7}_{-1.7}$	$^{+0.0}_{+0.0}$	$^{+0.1}_{+0.6}$	$^{+0.0}_{+0.0}$	$^{+0.7}_{-0.5}$
	0.13	0.355	± 2.6	$^{+4.9}_{-4.9}$	$^{+0.6}_{+0.0}$	$^{+0.1}_{+0.1}$	$^{+4.4}_{-4.4}$	$^{+1.9}_{-1.9}$	$^{+0.0}_{+0.0}$	$^{-0.4}_{+0.4}$	$^{+0.0}_{+0.0}$	$^{+0.5}_{-0.6}$
	0.25	0.252	± 3.0	$^{+5.6}_{-5.5}$	$^{+1.1}_{+0.0}$	$^{+0.2}_{+0.1}$	$^{+5.2}_{-5.2}$	$^{+1.1}_{-1.1}$	$^{-0.9}_{+0.8}$	$^{-0.1}_{+0.6}$	$^{+0.0}_{+0.0}$	$^{+0.8}_{-0.8}$

Table 12: *Systematic uncertainties with bin-to-bin correlations for the reduced cross section $\tilde{\sigma}$ for the reaction $e^- p \to e^- X$ ($\mathcal{L} = 71.2\, pb^{-1}, P_e = +0.29$). The left five columns of the table contain the bin centres, Q_c^2 and x_c, the measured cross section, the statistical uncertainty and the total systematic uncertainty. The right eight columns of the table list the bin-to-bin correlated systematic uncertainties for $\delta_1 - \delta_7$, and the systematic uncertainties summed in quadrature for $\delta_8 - \delta_{13}$, as defined in the section 8. The upper and lower correlated uncertainties correspond to a positive or negative variation of a cut value for example. However, if this is not possible for a particular systematic, the uncertainty is symmetrised. This table has two continuations.*

Q_c^2 (GeV^2)	x_c	$\tilde{\sigma}$	stat. (%)	sys. (%)	δ_1 (%)	δ_2 (%)	δ_3 (%)	δ_4 (%)	δ_5 (%)	δ_6 (%)	δ_7 (%)	$\delta_8 - \delta_{13}$ (%)
650	0.013	0.874	± 2.2	$^{+1.5}_{-0.8}$	$^{+1.2}_{-0.2}$	$^{-0.5}_{+0.6}$	$^{-0.0}_{+0.0}$	$^{-0.1}_{+0.1}$	$^{+0.0}_{+0.0}$	$^{-0.2}_{+0.3}$	$^{+0.5}_{-0.5}$	$^{+0.4}_{-0.3}$
	0.021	0.761	± 2.6	$^{+1.1}_{-1.1}$	$^{+0.0}_{-0.1}$	$^{-0.4}_{+0.5}$	$^{-0.3}_{+0.3}$	$^{-0.9}_{+0.9}$	$^{+0.0}_{+0.0}$	$^{-0.2}_{+0.0}$	$^{+0.1}_{-0.1}$	$^{+0.2}_{-0.2}$
	0.032	0.597	± 3.0	$^{+1.2}_{-1.0}$	$^{+0.5}_{-0.2}$	$^{-0.4}_{+0.5}$	$^{-0.5}_{+0.5}$	$^{+0.7}_{-0.7}$	$^{+0.0}_{+0.0}$	$^{+0.5}_{+0.5}$	$^{+0.0}_{-0.0}$	$^{+0.2}_{-0.2}$
	0.05	0.499	± 2.9	$^{+1.0}_{-0.9}$	$^{+0.1}_{-0.0}$	$^{-0.3}_{+0.4}$	$^{-0.4}_{+0.4}$	$^{+0.7}_{-0.7}$	$^{+0.0}_{+0.0}$	$^{+0.1}_{+0.0}$	$^{+0.0}_{+0.0}$	$^{+0.5}_{-0.4}$
	0.08	0.415	± 3.2	$^{+2.4}_{-2.3}$	$^{+0.7}_{-0.0}$	$^{-0.1}_{+0.3}$	$^{-1.8}_{+1.8}$	$^{+1.0}_{-1.0}$	$^{+0.0}_{+0.0}$	$^{+0.1}_{-0.0}$	$^{+0.0}_{+0.0}$	$^{+0.9}_{-1.1}$
	0.13	0.349	± 3.4	$^{+2.7}_{-2.4}$	$^{+0.9}_{-0.0}$	$^{-0.1}_{+0.2}$	$^{+2.1}_{-2.1}$	$^{-0.8}_{+0.8}$	$^{+0.0}_{+0.0}$	$^{+0.1}_{+0.4}$	$^{+0.0}_{+0.0}$	$^{+1.0}_{-0.9}$
	0.25	0.250	± 3.6	$^{+6.6}_{-6.5}$	$^{+1.0}_{-0.0}$	$^{-0.1}_{+0.3}$	$^{+6.3}_{-6.3}$	$^{+1.0}_{-1.0}$	$^{-0.8}_{+0.2}$	$^{-0.1}_{+0.5}$	$^{+0.0}_{+0.0}$	$^{+1.0}_{-1.1}$
800	0.013	0.828	± 2.8	$^{+1.7}_{-1.9}$	$^{+0.4}_{-1.0}$	$^{-0.8}_{+1.0}$	$^{+0.4}_{-0.4}$	$^{-1.0}_{+1.0}$	$^{+0.0}_{+0.0}$	$^{-0.1}_{+0.0}$	$^{+0.6}_{-0.6}$	$^{+0.3}_{-0.4}$
	0.021	0.685	± 3.3	$^{+1.1}_{-0.9}$	$^{+0.5}_{-0.1}$	$^{-0.4}_{+0.5}$	$^{+0.6}_{-0.6}$	$^{-0.2}_{+0.2}$	$^{+0.0}_{+0.0}$	$^{+0.0}_{+0.5}$	$^{+0.1}_{-0.1}$	$^{+0.4}_{-0.4}$
	0.032	0.617	± 3.2	$^{+1.4}_{-1.4}$	$^{+0.0}_{-0.4}$	$^{-0.4}_{+0.5}$	$^{-0.8}_{+0.8}$	$^{-0.9}_{+0.9}$	$^{+0.0}_{+0.0}$	$^{+0.3}_{+0.0}$	$^{+0.1}_{-0.1}$	$^{+0.2}_{-0.4}$
	0.05	0.495	± 3.1	$^{+2.2}_{-2.2}$	$^{+0.3}_{+0.0}$	$^{-0.3}_{+0.4}$	$^{+0.7}_{-0.7}$	$^{+2.0}_{-2.0}$	$^{+0.0}_{+0.0}$	$^{-0.4}_{+0.1}$	$^{+0.0}_{+0.0}$	$^{+0.3}_{-0.4}$
	0.08	0.446	± 3.2	$^{+2.6}_{-2.6}$	$^{+0.5}_{-0.0}$	$^{-0.2}_{+0.3}$	$^{-2.5}_{+2.5}$	$^{+0.1}_{-0.1}$	$^{+0.0}_{+0.0}$	$^{+0.5}_{-0.7}$	$^{+0.0}_{+0.0}$	$^{+0.3}_{-0.4}$
	0.13	0.375	± 3.6	$^{+1.1}_{-1.0}$	$^{+0.5}_{-0.0}$	$^{-0.2}_{+0.3}$	$^{+0.7}_{-0.7}$	$^{+0.6}_{-0.6}$	$^{+0.0}_{+0.0}$	$^{+0.1}_{-0.4}$	$^{+0.0}_{+0.0}$	$^{+0.2}_{-0.2}$
	0.25	0.239	± 4.3	$^{+3.7}_{-3.4}$	$^{+0.3}_{+0.0}$	$^{-0.2}_{+0.2}$	$^{+3.3}_{-3.3}$	$^{+0.8}_{-0.8}$	$^{+1.2}_{-0.1}$	$^{+0.7}_{-0.5}$	$^{+0.0}_{+0.0}$	$^{+0.2}_{-0.3}$
1200	0.014	0.875	± 3.4	$^{+2.4}_{-3.2}$	$^{+0.6}_{-2.2}$	$^{-0.8}_{+1.0}$	$^{-0.7}_{+0.7}$	$^{-1.4}_{+1.4}$	$^{+0.0}_{+0.0}$	$^{-0.3}_{-0.8}$	$^{+1.4}_{-1.4}$	$^{+0.5}_{-0.2}$
	0.021	0.744	± 3.2	$^{+1.9}_{-1.6}$	$^{+0.9}_{-0.1}$	$^{-0.5}_{+0.5}$	$^{+1.5}_{-1.5}$	$^{+0.0}_{-0.0}$	$^{+0.0}_{+0.0}$	$^{+0.1}_{+0.4}$	$^{+0.4}_{-0.4}$	$^{+0.3}_{-0.4}$
	0.032	0.594	± 3.2	$^{+1.2}_{-1.1}$	$^{+0.0}_{-0.1}$	$^{-0.4}_{+0.5}$	$^{-0.5}_{+0.5}$	$^{-0.7}_{+0.7}$	$^{+0.0}_{+0.0}$	$^{+0.1}_{+0.1}$	$^{+0.2}_{-0.2}$	$^{+0.6}_{-0.6}$
	0.05	0.557	± 2.8	$^{+1.3}_{-1.4}$	$^{+0.1}_{-0.0}$	$^{-0.3}_{+0.3}$	$^{-0.1}_{+0.1}$	$^{+1.2}_{-1.2}$	$^{+0.0}_{+0.0}$	$^{-0.3}_{-0.4}$	$^{+0.0}_{-0.0}$	$^{+0.4}_{-0.4}$
	0.08	0.436	± 2.9	$^{+1.4}_{-1.3}$	$^{+0.3}_{-0.0}$	$^{-0.2}_{+0.4}$	$^{-0.3}_{+0.3}$	$^{+1.2}_{-1.2}$	$^{+0.0}_{+0.0}$	$^{+0.3}_{-0.3}$	$^{+0.0}_{+0.0}$	$^{+0.4}_{-0.3}$
	0.13	0.364	± 3.2	$^{+1.1}_{-1.2}$	$^{+0.1}_{-0.0}$	$^{-0.1}_{+0.2}$	$^{-0.9}_{+0.9}$	$^{+0.4}_{-0.4}$	$^{+0.0}_{+0.0}$	$^{+0.1}_{-0.5}$	$^{+0.0}_{+0.0}$	$^{+0.3}_{-0.4}$
	0.25	0.225	± 3.8	$^{+2.4}_{-2.3}$	$^{+0.3}_{+0.0}$	$^{-0.2}_{+0.3}$	$^{+2.0}_{-2.0}$	$^{+1.0}_{-1.0}$	$^{+0.0}_{+0.0}$	$^{-0.3}_{-0.1}$	$^{+0.0}_{+0.0}$	$^{+0.5}_{-0.4}$
	0.4	0.120	± 6.3	$^{+8.1}_{-5.7}$	$^{+0.0}_{-0.1}$	$^{-0.4}_{+0.4}$	$^{+5.6}_{-5.6}$	$^{+0.6}_{-0.6}$	$^{+5.8}_{+3.4}$	$^{+0.5}_{-1.0}$	$^{+0.0}_{+0.0}$	$^{+0.5}_{-0.5}$
1500	0.021	0.761	± 4.5	$^{+2.6}_{-2.3}$	$^{+0.9}_{-0.2}$	$^{-0.6}_{+0.4}$	$^{-0.4}_{+0.4}$	$^{-0.1}_{+0.1}$	$^{+0.0}_{+0.0}$	$^{-1.0}_{+0.1}$	$^{+2.3}_{-1.9}$	$^{+0.4}_{-0.4}$
	0.032	0.617	± 4.2	$^{+0.7}_{-0.6}$	$^{+0.3}_{-0.1}$	$^{-0.3}_{+0.3}$	$^{-0.1}_{+0.1}$	$^{-0.3}_{+0.3}$	$^{+0.0}_{+0.0}$	$^{-0.1}_{-0.1}$	$^{+0.2}_{-0.2}$	$^{+0.4}_{-0.3}$
	0.05	0.538	± 3.7	$^{+0.9}_{-0.8}$	$^{+0.2}_{-0.0}$	$^{-0.3}_{+0.4}$	$^{+0.2}_{-0.2}$	$^{+0.4}_{-0.4}$	$^{+0.0}_{+0.0}$	$^{-0.4}_{+0.5}$	$^{+0.0}_{-0.0}$	$^{+0.3}_{-0.4}$
	0.08	0.454	± 3.7	$^{+1.0}_{-1.1}$	$^{+0.2}_{-0.0}$	$^{-0.3}_{+0.4}$	$^{-0.9}_{+0.9}$	$^{-0.2}_{+0.2}$	$^{+0.0}_{+0.0}$	$^{-0.4}_{+0.1}$	$^{+0.0}_{+0.0}$	$^{+0.3}_{-0.5}$
	0.13	0.365	± 4.6	$^{+2.1}_{-1.8}$	$^{+0.8}_{-0.0}$	$^{-0.1}_{+0.3}$	$^{-1.3}_{+1.3}$	$^{-1.1}_{+1.1}$	$^{+0.0}_{+0.0}$	$^{+0.8}_{-0.2}$	$^{+0.0}_{+0.0}$	$^{+0.3}_{-0.4}$
	0.18	0.293	± 5.0	$^{+1.8}_{-1.7}$	$^{+0.6}_{-0.1}$	$^{-0.3}_{+0.2}$	$^{+0.0}_{-0.0}$	$^{-1.6}_{+1.6}$	$^{+0.0}_{+0.0}$	$^{-0.3}_{-0.2}$	$^{+0.0}_{+0.0}$	$^{+0.4}_{-0.4}$
	0.25	0.263	± 5.8	$^{+1.9}_{-1.9}$	$^{+0.0}_{-0.3}$	$^{-0.3}_{+0.3}$	$^{+1.7}_{-1.7}$	$^{+0.6}_{-0.6}$	$^{+0.1}_{+0.0}$	$^{-0.1}_{-0.3}$	$^{+0.0}_{+0.0}$	$^{+0.3}_{-0.3}$
	0.4	0.122	± 9.0	$^{+8.8}_{-4.3}$	$^{+0.6}_{+0.0}$	$^{-0.5}_{+0.3}$	$^{+2.0}_{-2.0}$	$^{-0.9}_{+0.9}$	$^{+8.4}_{-3.6}$	$^{+0.3}_{-0.4}$	$^{+0.0}_{+0.0}$	$^{+0.6}_{-0.5}$
2000	0.032	0.631	± 5.1	$^{+2.5}_{-1.4}$	$^{+1.8}_{+0.0}$	$^{-0.2}_{+0.2}$	$^{+0.3}_{-0.3}$	$^{+1.0}_{-1.0}$	$^{+0.0}_{+0.0}$	$^{+0.4}_{+0.7}$	$^{+1.1}_{-0.8}$	$^{+0.3}_{-0.4}$
	0.05	0.529	± 4.6	$^{+1.0}_{-0.8}$	$^{+0.5}_{-0.0}$	$^{-0.3}_{+0.4}$	$^{-0.3}_{+0.3}$	$^{-0.6}_{+0.6}$	$^{+0.0}_{+0.0}$	$^{+0.1}_{+0.1}$	$^{+0.0}_{+0.0}$	$^{+0.3}_{-0.3}$
	0.08	0.438	± 4.5	$^{+2.0}_{-2.0}$	$^{+0.1}_{-0.1}$	$^{-0.3}_{+0.4}$	$^{-0.1}_{+0.1}$	$^{+1.9}_{-1.9}$	$^{+0.0}_{+0.0}$	$^{+0.2}_{+0.0}$	$^{+0.0}_{-0.0}$	$^{+0.3}_{-0.3}$
	0.13	0.417	± 5.0	$^{+0.8}_{-1.2}$	$^{+0.1}_{-0.6}$	$^{-0.2}_{+0.3}$	$^{-0.5}_{+0.5}$	$^{+0.5}_{-0.5}$	$^{+0.0}_{+0.0}$	$^{+0.1}_{-0.6}$	$^{+0.0}_{+0.0}$	$^{+0.3}_{-0.4}$
	0.18	0.295	± 5.9	$^{+0.6}_{-1.9}$	$^{+0.0}_{-0.7}$	$^{-0.2}_{+0.2}$	$^{-0.3}_{+0.3}$	$^{+0.1}_{-0.1}$	$^{+0.0}_{+0.0}$	$^{-0.4}_{-1.6}$	$^{+0.0}_{+0.0}$	$^{+0.4}_{-0.6}$
	0.25	0.232	± 7.2	$^{+1.7}_{-1.6}$	$^{+0.3}_{-0.0}$	$^{-0.2}_{+0.3}$	$^{+1.5}_{-1.5}$	$^{+0.5}_{-0.5}$	$^{+0.0}_{+0.0}$	$^{+0.4}_{+0.5}$	$^{+0.0}_{+0.0}$	$^{+0.5}_{-0.5}$
	0.4	0.118	$^{+11.2}_{-10.1}$	$^{+3.7}_{-3.9}$	$^{+0.0}_{-0.2}$	$^{-0.3}_{+0.4}$	$^{+3.1}_{-3.1}$	$^{+1.1}_{-1.1}$	$^{-0.5}_{+1.0}$	$^{+0.1}_{-1.3}$	$^{+0.0}_{+0.0}$	$^{+1.2}_{-1.4}$

Table 12: *Continuation 1.*

Q_c^2 (GeV^2)	x_c	$\tilde{\sigma}$	stat. (%)	sys. (%)	δ_1 (%)	δ_2 (%)	δ_3 (%)	δ_4 (%)	δ_5 (%)	δ_6 (%)	δ_7 (%)	$\delta_8 - \delta_{13}$ (%)
3000	0.05	0.557	$\pm$ 5.7	$^{+2.0}_{-1.1}$	$^{+1.6}_{-0.1}$	$^{-0.3}_{+0.4}$	$^{+0.9}_{-0.9}$	$^{-0.0}_{+0.0}$	$^{+0.0}_{+0.0}$	$^{+0.4}_{+0.2}$	$^{+0.5}_{-0.5}$	$^{+0.4}_{-0.3}$
	0.08	0.508	$\pm$ 5.2	$^{+1.1}_{-1.1}$	$^{+0.2}_{-0.4}$	$^{-0.2}_{+0.3}$	$^{-0.4}_{+0.4}$	$^{+0.8}_{-0.8}$	$^{+0.0}_{+0.0}$	$^{+0.5}_{-0.1}$	$^{+0.1}_{-0.1}$	$^{+0.3}_{-0.5}$
	0.13	0.378	$\pm$ 6.2	$^{+0.9}_{-0.7}$	$^{+0.1}_{-0.1}$	$^{-0.2}_{+0.3}$	$^{+0.6}_{-0.6}$	$^{-0.1}_{+0.1}$	$^{+0.0}_{+0.0}$	$^{-0.3}_{-0.3}$	$^{+0.0}_{+0.0}$	$^{+0.7}_{-0.1}$
	0.18	0.292	$\pm$ 7.1	$^{+1.2}_{-1.3}$	$^{+0.0}_{-0.3}$	$^{-0.2}_{+0.2}$	$^{-0.9}_{+0.9}$	$^{-0.6}_{+0.6}$	$^{+0.0}_{+0.0}$	$^{-0.5}_{+0.2}$	$^{+0.0}_{+0.0}$	$^{+0.4}_{-0.3}$
	0.25	0.304	$\pm$ 7.3	$^{+7.4}_{-7.3}$	$^{+0.6}_{-0.0}$	$^{-0.2}_{+0.2}$	$^{+7.3}_{-7.3}$	$^{+0.2}_{-0.2}$	$^{+0.0}_{+0.0}$	$^{+1.1}_{+0.3}$	$^{+0.0}_{+0.0}$	$^{+0.8}_{-0.6}$
	0.4	0.106	$^{+14.5}_{-12.8}$	$^{+3.8}_{-3.5}$	$^{+1.3}_{-0.0}$	$^{-0.2}_{+0.4}$	$^{-3.4}_{+3.4}$	$^{+0.5}_{-0.5}$	$^{+0.4}_{-0.0}$	$^{+0.8}_{-0.3}$	$^{+0.0}_{+0.0}$	$^{+0.6}_{-0.6}$
	0.65	0.015	$^{+25.5}_{-20.7}$	$^{+10.2}_{-10.4}$	$^{+0.0}_{-0.6}$	$^{-0.8}_{+1.0}$	$^{-8.7}_{+8.7}$	$^{+4.6}_{-4.6}$	$^{+1.8}_{+0.7}$	$^{-2.7}_{+0.9}$	$^{+0.0}_{+0.0}$	$^{+1.7}_{-2.0}$
5000	0.08	0.480	$\pm$ 5.2	$^{+1.8}_{-0.9}$	$^{+1.6}_{-0.3}$	$^{-0.2}_{+0.2}$	$^{-0.3}_{+0.3}$	$^{+0.2}_{-0.2}$	$^{+0.0}_{+0.0}$	$^{-0.6}_{-0.4}$	$^{+0.3}_{-0.3}$	$^{+0.5}_{-0.3}$
	0.13	0.430	$\pm$ 6.5	$^{+1.0}_{-0.8}$	$^{+0.8}_{+0.0}$	$^{-0.2}_{+0.2}$	$^{-0.4}_{+0.4}$	$^{+0.3}_{-0.3}$	$^{+0.0}_{+0.0}$	$^{+0.1}_{-0.3}$	$^{+0.1}_{-0.1}$	$^{+0.2}_{-0.5}$
	0.18	0.325	$\pm$ 7.1	$^{+1.0}_{-0.5}$	$^{+0.2}_{-0.1}$	$^{-0.3}_{+0.2}$	$^{+0.2}_{-0.2}$	$^{+0.3}_{-0.3}$	$^{+0.0}_{+0.0}$	$^{-0.1}_{+0.7}$	$^{+0.0}_{+0.0}$	$^{+0.5}_{-0.3}$
	0.25	0.260	$\pm$ 8.4	$^{+1.8}_{-1.2}$	$^{+0.7}_{-0.0}$	$^{-0.2}_{+0.3}$	$^{+0.7}_{-0.7}$	$^{-0.7}_{+0.7}$	$^{+0.0}_{+0.0}$	$^{+1.2}_{-0.6}$	$^{+0.0}_{+0.0}$	$^{+0.4}_{-0.3}$
	0.4	0.152	$^{+12.5}_{-11.2}$	$^{+6.5}_{-6.4}$	$^{+0.0}_{-0.3}$	$^{-0.2}_{+0.3}$	$^{+6.0}_{-6.0}$	$^{-2.1}_{+2.1}$	$^{+0.0}_{+0.0}$	$^{+0.4}_{+1.3}$	$^{+0.0}_{+0.0}$	$^{+1.1}_{-1.1}$
8000	0.13	0.534	$\pm$ 6.6	$^{+1.0}_{-1.9}$	$^{+0.0}_{-1.0}$	$^{-0.3}_{+0.3}$	$^{-0.5}_{+0.5}$	$^{-0.1}_{+0.1}$	$^{+0.0}_{+0.0}$	$^{-1.3}_{+0.3}$	$^{+0.5}_{-0.3}$	$^{+0.5}_{-0.5}$
	0.18	0.430	$\pm$ 8.4	$^{+2.6}_{-2.9}$	$^{+0.1}_{-0.3}$	$^{-0.2}_{+0.2}$	$^{-2.4}_{+2.4}$	$^{+0.6}_{-0.6}$	$^{+0.0}_{+0.0}$	$^{+0.5}_{-0.3}$	$^{+0.0}_{+0.0}$	$^{+0.6}_{-1.3}$
	0.25	0.294	$^{+11.6}_{-10.4}$	$^{+3.8}_{-3.9}$	$^{+0.7}_{-0.1}$	$^{-0.3}_{+0.2}$	$^{-3.6}_{+3.6}$	$^{+0.4}_{-0.4}$	$^{+0.0}_{+0.0}$	$^{-1.1}_{-0.6}$	$^{+0.0}_{+0.0}$	$^{+0.4}_{-0.4}$
	0.4	0.113	$^{+19.6}_{-16.6}$	$^{+7.1}_{-7.3}$	$^{+0.1}_{-0.0}$	$^{-0.3}_{+0.4}$	$^{+7.0}_{-7.0}$	$^{-0.6}_{+0.6}$	$^{+0.0}_{+0.0}$	$^{-0.3}_{+0.5}$	$^{+0.0}_{+0.0}$	$^{+0.6}_{-2.0}$
	0.65	0.018	$^{+34.5}_{-26.5}$	$^{+4.1}_{-4.2}$	$^{+0.2}_{-1.4}$	$^{-0.9}_{+0.9}$	$^{+1.5}_{-1.5}$	$^{+2.3}_{-2.3}$	$^{+0.0}_{+0.0}$	$^{-2.6}_{+2.8}$	$^{+0.0}_{+0.0}$	$^{+0.8}_{-0.6}$
12000	0.18	0.401	$^{+11.1}_{-10.1}$	$^{+1.3}_{-3.8}$	$^{+1.0}_{-3.6}$	$^{-0.3}_{+0.4}$	$^{-0.4}_{+0.4}$	$^{-0.2}_{+0.2}$	$^{+0.0}_{+0.0}$	$^{-0.3}_{-0.8}$	$^{+0.2}_{-0.3}$	$^{+0.5}_{-0.6}$
	0.25	0.359	$^{+14.3}_{-12.6}$	$^{+2.8}_{-2.3}$	$^{+2.4}_{-0.6}$	$^{-0.2}_{+0.2}$	$^{+0.3}_{-0.3}$	$^{+0.8}_{-0.8}$	$^{+0.0}_{+0.0}$	$^{+0.3}_{-1.6}$	$^{+0.0}_{+0.0}$	$^{+1.0}_{-1.2}$
	0.4	0.172	$^{+20.6}_{-17.3}$	$^{+4.6}_{-3.8}$	$^{+2.7}_{-0.2}$	$^{-0.3}_{+0.4}$	$^{+3.2}_{-3.2}$	$^{-0.8}_{+0.8}$	$^{+0.0}_{+0.0}$	$^{-1.2}_{+1.5}$	$^{+0.0}_{+0.0}$	$^{+0.6}_{-1.3}$
20000	0.25	0.456	$^{+16.0}_{-14.0}$	$^{+6.1}_{-3.6}$	$^{+4.9}_{-1.8}$	$^{-1.5}_{+0.2}$	$^{-2.2}_{+2.2}$	$^{+0.1}_{-0.1}$	$^{+0.0}_{+0.0}$	$^{-0.7}_{-0.2}$	$^{+2.7}_{-1.4}$	$^{+0.6}_{-0.5}$
	0.4	0.175	$^{+28.6}_{-22.7}$	$^{+4.9}_{-3.8}$	$^{+3.6}_{+0.0}$	$^{-0.4}_{+0.4}$	$^{+0.9}_{-0.9}$	$^{+3.0}_{-3.0}$	$^{+0.0}_{+0.0}$	$^{-1.8}_{-0.3}$	$^{+0.0}_{+0.0}$	$^{+1.1}_{-1.2}$
30000	0.4	0.190	$^{+34.5}_{-26.4}$	$^{+6.9}_{-5.9}$	$^{+6.7}_{+0.0}$	$^{-0.2}_{+0.3}$	$^{-0.8}_{+0.8}$	$^{+0.7}_{-0.7}$	$^{+0.0}_{+0.0}$	$^{+0.1}_{-4.9}$	$^{+0.0}_{-2.9}$	$^{+1.3}_{-1.3}$

Table 12: *Continuation 2.*

Q^2 range (GeV^2)	Q_c^2 (GeV^2)	x range	x_c	$\tilde{\sigma}$	N_{data}	$N_{\mathrm{bg}}^{\mathrm{MC}}$
185 – 240	200	0.0037 – 0.006	0.005	$1.091 \pm 0.013\ ^{+0.014}_{-0.011}$	8166	51.2
		0.006 – 0.01	0.008	$0.919 \pm 0.010\ ^{+0.018}_{-0.018}$	9475	13.6
		0.01 – 0.017	0.013	$0.782 \pm 0.008\ ^{+0.013}_{-0.013}$	10222	1.7
		0.017 – 0.025	0.021	$0.657 \pm 0.008\ ^{+0.014}_{-0.014}$	7261	0.0
		0.025 – 0.037	0.032	$0.562 \pm 0.007\ ^{+0.023}_{-0.022}$	6934	0.0
		0.037 – 0.06	0.05	$0.500 \pm 0.007\ ^{+0.012}_{-0.012}$	6387	0.0
		0.06 – 0.12	0.08	$0.445 \pm 0.005\ ^{+0.024}_{-0.024}$	8344	0.0
		0.12 – 0.25	0.18	$0.341 \pm 0.005\ ^{+0.018}_{-0.018}$	4369	0.0
240 – 310	250	0.006 – 0.01	0.008	$0.948 \pm 0.012\ ^{+0.014}_{-0.012}$	6666	15.2
		0.01 – 0.017	0.013	$0.797 \pm 0.010\ ^{+0.013}_{-0.012}$	7355	3.5
		0.017 – 0.025	0.021	$0.662 \pm 0.010\ ^{+0.011}_{-0.009}$	5232	0.8
		0.025 – 0.037	0.032	$0.566 \pm 0.008\ ^{+0.019}_{-0.019}$	5088	0.0
		0.037 – 0.06	0.05	$0.504 \pm 0.007\ ^{+0.017}_{-0.017}$	5029	0.0
		0.06 – 0.12	0.08	$0.429 \pm 0.006\ ^{+0.022}_{-0.022}$	5997	0.0
		0.12 – 0.25	0.18	$0.336 \pm 0.006\ ^{+0.016}_{-0.016}$	4121	0.0
310 – 410	350	0.006 – 0.01	0.008	$0.968 \pm 0.016\ ^{+0.021}_{-0.015}$	4001	41.5
		0.01 – 0.017	0.013	$0.818 \pm 0.012\ ^{+0.016}_{-0.010}$	5495	5.2
		0.017 – 0.025	0.021	$0.694 \pm 0.011\ ^{+0.006}_{-0.004}$	4230	0.0
		0.025 – 0.037	0.032	$0.607 \pm 0.010\ ^{+0.012}_{-0.011}$	4118	0.0
		0.037 – 0.06	0.05	$0.513 \pm 0.008\ ^{+0.014}_{-0.013}$	4397	0.0
		0.06 – 0.12	0.08	$0.438 \pm 0.007\ ^{+0.009}_{-0.009}$	4916	0.0
		0.12 – 0.25	0.18	$0.319 \pm 0.005\ ^{+0.020}_{-0.020}$	3882	0.0
410 – 530	450	0.006 – 0.01	0.008	$0.987 \pm 0.018\ ^{+0.023}_{-0.021}$	3072	48.9
		0.01 – 0.017	0.013	$0.868 \pm 0.017\ ^{+0.010}_{-0.010}$	2771	9.3
		0.017 – 0.025	0.021	$0.690 \pm 0.015\ ^{+0.013}_{-0.012}$	2145	0.8
		0.025 – 0.037	0.032	$0.609 \pm 0.012\ ^{+0.012}_{-0.011}$	2497	0.0
		0.037 – 0.06	0.05	$0.531 \pm 0.010\ ^{+0.013}_{-0.013}$	3100	0.0
		0.06 – 0.1	0.08	$0.448 \pm 0.009\ ^{+0.009}_{-0.008}$	2562	0.0
		0.1 – 0.17	0.13	$0.362 \pm 0.008\ ^{+0.018}_{-0.018}$	2182	0.0
		0.17 – 0.3	0.25	$0.270 \pm 0.007\ ^{+0.015}_{-0.015}$	1684	0.0

Table 13: *The reduced cross section $\tilde{\sigma}$ for the reaction $e^- p \to e^- X$ ($\mathcal{L} = 98.7\,pb^{-1}, P_e = -0.27$). The bin range, bin centre (Q_c^2 and x_c) and measured cross section corrected to the electroweak Born level are shown. The first (second) error on the cross section corresponds to the statistical (systematic) uncertainties. The number of observed data events (N_{data}) and simulated background events (N_{bg}^{MC}) are also shown. This table has two continuations.*

Q^2 range (GeV^2)	Q_c^2 (GeV^2)	x range	x_c	$\tilde{\sigma}$	N_{data}	$N_{\mathrm{bg}}^{\mathrm{MC}}$
530 – 710	650	0.01 – 0.017	0.013	$0.884 \pm 0.016\ ^{+0.013}_{-0.007}$	3116	34.4
		0.017 – 0.025	0.021	$0.753 \pm 0.017\ ^{+0.009}_{-0.008}$	2057	3.3
		0.025 – 0.037	0.032	$0.598 \pm 0.015\ ^{+0.007}_{-0.006}$	1589	0.8
		0.037 – 0.06	0.05	$0.523 \pm 0.013\ ^{+0.005}_{-0.005}$	1722	0.0
		0.06 – 0.1	0.08	$0.432 \pm 0.012\ ^{+0.010}_{-0.010}$	1430	0.0
		0.1 – 0.17	0.13	$0.369 \pm 0.010\ ^{+0.010}_{-0.009}$	1310	0.0
		0.17 – 0.3	0.25	$0.255 \pm 0.008\ ^{+0.017}_{-0.017}$	1107	0.0
710 – 900	800	0.009 – 0.017	0.013	$0.885 \pm 0.020\ ^{+0.015}_{-0.017}$	1992	28.8
		0.017 – 0.025	0.021	$0.769 \pm 0.021\ ^{+0.009}_{-0.007}$	1436	1.8
		0.025 – 0.037	0.032	$0.648 \pm 0.017\ ^{+0.009}_{-0.009}$	1453	4.3
		0.037 – 0.06	0.05	$0.543 \pm 0.014\ ^{+0.012}_{-0.012}$	1637	0.0
		0.06 – 0.1	0.08	$0.452 \pm 0.012\ ^{+0.012}_{-0.012}$	1358	0.0
		0.1 – 0.17	0.13	$0.379 \pm 0.012\ ^{+0.004}_{-0.004}$	1106	0.0
		0.17 – 0.3	0.25	$0.270 \pm 0.009\ ^{+0.010}_{-0.009}$	853	0.0
900 – 1300	1200	0.01 – 0.017	0.014	$0.908 \pm 0.026\ ^{+0.022}_{-0.029}$	1306	43.8
		0.017 – 0.025	0.021	$0.828 \pm 0.022\ ^{+0.015}_{-0.014}$	1548	13.4
		0.025 – 0.037	0.032	$0.620 \pm 0.017\ ^{+0.007}_{-0.007}$	1465	6.8
		0.037 – 0.06	0.05	$0.550 \pm 0.013\ ^{+0.007}_{-0.008}$	1845	0.8
		0.06 – 0.1	0.08	$0.473 \pm 0.011\ ^{+0.007}_{-0.006}$	1824	0.0
		0.1 – 0.17	0.13	$0.385 \pm 0.010\ ^{+0.004}_{-0.005}$	1456	0.0
		0.17 – 0.3	0.25	$0.263 \pm 0.008\ ^{+0.006}_{-0.006}$	1156	0.0
		0.3 – 0.53	0.4	$0.129 \pm 0.007\ ^{+0.010}_{-0.007}$	384	0.0
1300 – 1800	1500	0.017 – 0.025	0.021	$0.771 \pm 0.030\ ^{+0.020}_{-0.018}$	743	33.8
		0.025 – 0.037	0.032	$0.641 \pm 0.023\ ^{+0.005}_{-0.004}$	827	4.1
		0.037 – 0.06	0.05	$0.514 \pm 0.016\ ^{+0.004}_{-0.004}$	1000	0.8
		0.06 – 0.1	0.08	$0.496 \pm 0.015\ ^{+0.005}_{-0.005}$	1136	0.0
		0.1 – 0.15	0.13	$0.386 \pm 0.015\ ^{+0.008}_{-0.007}$	714	0.0
		0.15 – 0.23	0.18	$0.328 \pm 0.013\ ^{+0.006}_{-0.006}$	625	0.0
		0.23 – 0.35	0.25	$0.265 \pm 0.013\ ^{+0.005}_{-0.005}$	425	0.0
		0.35 – 0.53	0.4	$0.134 \pm 0.010\ ^{+0.012}_{-0.006}$	192	0.0
1800 – 2500	2000	0.023 – 0.037	0.032	$0.644 \pm 0.028\ ^{+0.016}_{-0.009}$	572	11.1
		0.037 – 0.06	0.05	$0.605 \pm 0.022\ ^{+0.006}_{-0.005}$	753	0.0
		0.06 – 0.1	0.08	$0.477 \pm 0.018\ ^{+0.010}_{-0.009}$	749	0.8
		0.1 – 0.15	0.13	$0.345 \pm 0.016\ ^{+0.003}_{-0.004}$	471	0.0
		0.15 – 0.23	0.18	$0.322 \pm 0.016\ ^{+0.002}_{-0.006}$	435	0.0
		0.23 – 0.35	0.25	$0.259 \pm 0.015\ ^{+0.005}_{-0.004}$	305	0.0
		0.35 – 0.53	0.4	$0.122 \pm 0.010\ ^{+0.004}_{-0.005}$	141	0.0

Table 13: *Continuation 1.*

Q^2 range (GeV^2)	Q_c^2 (GeV^2)	x range	x_c	$\tilde{\sigma}$	N_{data}	$N_{\mathrm{bg}}^{\mathrm{MC}}$
2500 – 3500	3000	0.037 – 0.06	0.05	$0.603 \pm 0.028\ ^{+0.012}_{-0.007}$	466	5.2
		0.06 – 0.1	0.08	$0.511 \pm 0.022\ ^{+0.006}_{-0.006}$	525	0.9
		0.1 – 0.15	0.13	$0.381 \pm 0.020\ ^{+0.004}_{-0.003}$	363	0.0
		0.15 – 0.23	0.18	$0.343 \pm 0.019\ ^{+0.004}_{-0.004}$	327	0.0
		0.23 – 0.35	0.25	$0.274 \pm 0.018\ ^{+0.020}_{-0.020}$	237	0.0
		0.35 – 0.53	0.4	$0.156 \pm 0.014\ ^{+0.006}_{-0.005}$	124	0.0
		0.53 – 0.75	0.65	$0.018\ ^{+0.003}_{-0.003}\ ^{+0.002}_{-0.002}$	39	0.0
3500 – 5600	5000	0.04 – 0.1	0.08	$0.567 \pm 0.023\ ^{+0.010}_{-0.005}$	621	4.2
		0.1 – 0.15	0.13	$0.492 \pm 0.026\ ^{+0.005}_{-0.004}$	374	0.8
		0.15 – 0.23	0.18	$0.354 \pm 0.021\ ^{+0.003}_{-0.002}$	300	0.0
		0.23 – 0.35	0.25	$0.233 \pm 0.018\ ^{+0.004}_{-0.003}$	176	0.0
		0.35 – 0.53	0.4	$0.132\ ^{+0.015}_{-0.013}\ ^{+0.009}_{-0.008}$	96	0.0
5600 – 9000	8000	0.07 – 0.15	0.13	$0.586 \pm 0.032\ ^{+0.006}_{-0.011}$	351	2.6
		0.15 – 0.23	0.18	$0.441 \pm 0.031\ ^{+0.012}_{-0.013}$	203	0.0
		0.23 – 0.35	0.25	$0.323 \pm 0.027\ ^{+0.012}_{-0.012}$	140	0.0
		0.35 – 0.53	0.4	$0.116\ ^{+0.019}_{-0.016}\ ^{+0.008}_{-0.008}$	51	0.0
		0.53 – 0.75	0.65	$0.020\ ^{+0.005}_{-0.004}\ ^{+0.001}_{-0.001}$	21	0.0
9000 – 15000	12000	0.09 – 0.23	0.18	$0.516 \pm 0.039\ ^{+0.007}_{-0.019}$	176	0.8
		0.23 – 0.35	0.25	$0.354\ ^{+0.042}_{-0.038}\ ^{+0.010}_{-0.008}$	86	0.0
		0.35 – 0.53	0.4	$0.146\ ^{+0.027}_{-0.023}\ ^{+0.007}_{-0.006}$	39	0.0
15000 – 25000	20000	0.15 – 0.35	0.25	$0.473\ ^{+0.062}_{-0.056}\ ^{+0.029}_{-0.017}$	76	2.6
		0.35 – 0.75	0.4	$0.193\ ^{+0.043}_{-0.036}\ ^{+0.009}_{-0.007}$	29	0.0
25000 – 50000	30000	0.25 – 0.75	0.4	$0.275\ ^{+0.062}_{-0.052}\ ^{+0.019}_{-0.016}$	28	0.0

Table 13: *Continuation 2.*

Q_c^2 (GeV^2)	x_c	$\tilde{\sigma}$	stat. (%)	sys. (%)	δ_1 (%)	δ_2 (%)	δ_3 (%)	δ_4 (%)	δ_5 (%)	δ_6 (%)	δ_7 (%)	$\delta_8 - \delta_{13}$ (%)
200	0.005	1.091	± 1.2	$^{+1.3}_{-1.0}$	$^{+0.7}_{-0.0}$	$^{-0.4}_{+0.6}$	$^{+0.4}_{-0.4}$	$^{-0.4}_{+0.4}$	$^{+0.0}_{+0.0}$	$^{+0.1}_{-0.1}$	$^{+0.3}_{-0.3}$	$^{+0.7}_{-0.7}$
	0.008	0.919	± 1.1	$^{+1.9}_{-1.9}$	$^{+0.3}_{-0.0}$	$^{-0.4}_{+0.5}$	$^{+0.2}_{-0.2}$	$^{-1.6}_{+1.6}$	$^{+0.0}_{+0.0}$	$^{+0.1}_{+0.4}$	$^{+0.1}_{-0.1}$	$^{+0.8}_{-1.0}$
	0.013	0.782	± 1.0	$^{+1.7}_{-1.6}$	$^{+0.2}_{+0.0}$	$^{-0.5}_{+0.5}$	$^{-0.2}_{+0.2}$	$^{-1.3}_{+1.3}$	$^{+0.0}_{+0.0}$	$^{+0.0}_{+0.4}$	$^{+0.0}_{-0.0}$	$^{+0.8}_{-0.9}$
	0.021	0.657	± 1.2	$^{+2.1}_{-2.1}$	$^{+0.4}_{+0.0}$	$^{-0.3}_{+0.5}$	$^{-1.6}_{+1.6}$	$^{+0.9}_{-0.9}$	$^{+0.0}_{+0.0}$	$^{-0.1}_{+0.1}$	$^{+0.0}_{+0.0}$	$^{+0.8}_{-0.9}$
	0.032	0.562	± 1.3	$^{+4.0}_{-4.0}$	$^{+0.1}_{-0.0}$	$^{-0.3}_{+0.4}$	$^{-1.5}_{+1.5}$	$^{+3.6}_{-3.6}$	$^{+0.0}_{+0.0}$	$^{+0.2}_{+0.4}$	$^{+0.0}_{+0.0}$	$^{+0.8}_{-0.8}$
	0.05	0.500	± 1.3	$^{+2.5}_{-2.4}$	$^{+0.0}_{-0.3}$	$^{-0.2}_{+0.3}$	$^{-0.5}_{+0.5}$	$^{+2.2}_{-2.2}$	$^{+0.0}_{+0.0}$	$^{+0.0}_{+0.3}$	$^{+0.0}_{+0.0}$	$^{+1.0}_{-0.9}$
	0.08	0.445	± 1.1	$^{+5.5}_{-5.5}$	$^{+0.0}_{-0.1}$	$^{-0.2}_{+0.2}$	$^{+5.0}_{-5.0}$	$^{+2.0}_{-2.0}$	$^{-0.0}_{+0.0}$	$^{-0.0}_{+0.1}$	$^{+0.0}_{+0.0}$	$^{+0.8}_{-1.0}$
	0.18	0.341	± 1.6	$^{+5.4}_{-5.4}$	$^{+0.1}_{+0.0}$	$^{-0.1}_{+0.2}$	$^{+5.3}_{-5.3}$	$^{+0.5}_{-0.5}$	$^{+0.7}_{+0.2}$	$^{-0.1}_{+0.1}$	$^{+0.0}_{+0.0}$	$^{+0.7}_{-0.9}$
250	0.008	0.948	± 1.3	$^{+1.5}_{-1.3}$	$^{+0.6}_{-0.0}$	$^{-0.3}_{+0.4}$	$^{+0.5}_{-0.5}$	$^{-0.9}_{+0.9}$	$^{+0.0}_{+0.0}$	$^{-0.2}_{+0.3}$	$^{+0.1}_{-0.1}$	$^{+0.7}_{-0.7}$
	0.013	0.797	± 1.2	$^{+1.7}_{-1.5}$	$^{+0.7}_{+0.0}$	$^{-0.5}_{+0.6}$	$^{+0.0}_{-0.0}$	$^{-1.3}_{+1.3}$	$^{+0.0}_{+0.0}$	$^{-0.1}_{+0.2}$	$^{+0.0}_{-0.0}$	$^{+0.5}_{-0.7}$
	0.021	0.662	± 1.4	$^{+1.6}_{-1.4}$	$^{+0.7}_{-0.0}$	$^{-0.3}_{+0.5}$	$^{-0.1}_{+0.1}$	$^{+1.1}_{-1.1}$	$^{+0.0}_{+0.0}$	$^{-0.2}_{+0.2}$	$^{+0.0}_{-0.0}$	$^{+0.8}_{-0.7}$
	0.032	0.566	± 1.5	$^{+3.3}_{-3.3}$	$^{+0.6}_{-0.0}$	$^{-0.3}_{+0.4}$	$^{-0.8}_{+0.8}$	$^{+3.0}_{-3.0}$	$^{+0.0}_{+0.0}$	$^{+0.0}_{+0.1}$	$^{+0.0}_{+0.0}$	$^{+0.7}_{-0.9}$
	0.05	0.504	± 1.5	$^{+3.4}_{-3.3}$	$^{+0.4}_{+0.0}$	$^{-0.1}_{+0.3}$	$^{-2.4}_{+2.4}$	$^{+2.2}_{-2.2}$	$^{+0.0}_{+0.0}$	$^{-0.0}_{-0.1}$	$^{+0.0}_{+0.0}$	$^{+0.7}_{-0.6}$
	0.08	0.429	± 1.4	$^{+5.2}_{-5.1}$	$^{+0.7}_{-0.0}$	$^{-0.1}_{+0.3}$	$^{+4.6}_{-4.6}$	$^{+2.2}_{-2.2}$	$^{+0.0}_{+0.0}$	$^{-0.0}_{+0.1}$	$^{+0.0}_{+0.0}$	$^{+0.7}_{-0.7}$
	0.18	0.336	± 1.6	$^{+4.8}_{-4.7}$	$^{+0.2}_{+0.0}$	$^{+0.0}_{+0.2}$	$^{+4.1}_{-4.1}$	$^{+2.0}_{-2.0}$	$^{+0.3}_{+1.0}$	$^{+0.0}_{+0.2}$	$^{+0.0}_{+0.0}$	$^{+0.8}_{-0.8}$
350	0.008	0.968	± 1.7	$^{+2.1}_{-1.5}$	$^{+1.6}_{-0.1}$	$^{-0.5}_{+0.6}$	$^{+0.9}_{-0.9}$	$^{-0.4}_{+0.4}$	$^{+0.0}_{+0.0}$	$^{-0.6}_{+0.4}$	$^{+0.4}_{-0.4}$	$^{+0.6}_{-0.8}$
	0.013	0.818	± 1.4	$^{+1.9}_{-1.2}$	$^{+1.4}_{-0.0}$	$^{-0.2}_{+0.5}$	$^{-0.2}_{+0.2}$	$^{-1.0}_{+1.0}$	$^{+0.0}_{+0.0}$	$^{-0.2}_{+0.5}$	$^{+0.0}_{-0.0}$	$^{+0.7}_{-0.6}$
	0.021	0.694	± 1.6	$^{+0.9}_{-0.6}$	$^{+0.4}_{-0.1}$	$^{-0.3}_{+0.4}$	$^{+0.3}_{-0.3}$	$^{+0.0}_{-0.0}$	$^{+0.0}_{+0.0}$	$^{-0.2}_{-0.0}$	$^{+0.0}_{+0.0}$	$^{+0.6}_{-0.5}$
	0.032	0.607	± 1.6	$^{+1.9}_{-1.8}$	$^{+0.8}_{-0.0}$	$^{-0.2}_{+0.4}$	$^{-1.6}_{+1.6}$	$^{+0.2}_{-0.2}$	$^{+0.0}_{+0.0}$	$^{-0.3}_{+0.1}$	$^{+0.0}_{+0.0}$	$^{+0.6}_{-0.7}$
	0.05	0.513	± 1.6	$^{+2.7}_{-2.6}$	$^{+0.6}_{-0.0}$	$^{-0.1}_{+0.2}$	$^{-1.9}_{+1.9}$	$^{+1.6}_{-1.6}$	$^{+0.0}_{+0.0}$	$^{-0.1}_{+0.2}$	$^{+0.0}_{+0.0}$	$^{+0.5}_{-0.7}$
	0.08	0.438	± 1.5	$^{+2.0}_{-2.0}$	$^{+0.3}_{+0.0}$	$^{-0.1}_{+0.2}$	$^{+1.1}_{-1.1}$	$^{+1.6}_{-1.6}$	$^{+0.0}_{+0.0}$	$^{+0.0}_{+0.1}$	$^{+0.0}_{+0.0}$	$^{+0.7}_{-0.7}$
	0.18	0.319	± 1.7	$^{+6.4}_{-6.3}$	$^{+0.4}_{+0.0}$	$^{-0.0}_{+0.2}$	$^{+5.7}_{-5.7}$	$^{+2.6}_{-2.6}$	$^{-0.1}_{+1.2}$	$^{+0.1}_{+0.2}$	$^{+0.0}_{+0.0}$	$^{+0.7}_{-0.6}$
450	0.008	0.987	± 1.9	$^{+2.4}_{-2.1}$	$^{+0.7}_{-0.3}$	$^{-1.4}_{+1.6}$	$^{+1.3}_{-1.3}$	$^{-0.5}_{+0.5}$	$^{+0.0}_{+0.0}$	$^{-0.2}_{+0.3}$	$^{+0.6}_{-0.6}$	$^{+0.5}_{-0.4}$
	0.013	0.868	± 2.0	$^{+1.1}_{-1.1}$	$^{+0.1}_{-0.1}$	$^{-0.5}_{+0.6}$	$^{-0.4}_{+0.4}$	$^{+0.2}_{-0.2}$	$^{+0.0}_{+0.0}$	$^{-0.6}_{+0.6}$	$^{+0.1}_{-0.1}$	$^{+0.5}_{-0.6}$
	0.021	0.690	± 2.2	$^{+1.8}_{-1.7}$	$^{+0.2}_{-0.1}$	$^{-0.4}_{+0.5}$	$^{-0.1}_{+0.1}$	$^{+1.3}_{-1.3}$	$^{+0.0}_{+0.0}$	$^{-0.7}_{+0.9}$	$^{+0.0}_{-0.0}$	$^{+0.8}_{-0.8}$
	0.032	0.609	± 2.0	$^{+1.9}_{-1.7}$	$^{+0.8}_{-0.1}$	$^{-0.2}_{+0.4}$	$^{+0.0}_{-0.0}$	$^{+1.4}_{-1.4}$	$^{+0.0}_{+0.0}$	$^{-0.5}_{+0.4}$	$^{+0.0}_{+0.0}$	$^{+1.0}_{-0.9}$
	0.05	0.531	± 1.8	$^{+2.5}_{-2.4}$	$^{+0.7}_{-0.0}$	$^{+0.0}_{+0.2}$	$^{-1.6}_{+1.6}$	$^{+1.6}_{-1.6}$	$^{+0.0}_{+0.0}$	$^{-0.4}_{+0.6}$	$^{+0.0}_{+0.0}$	$^{+0.7}_{-0.7}$
	0.08	0.448	± 2.0	$^{+2.1}_{-1.9}$	$^{+0.3}_{+0.0}$	$^{+0.1}_{+0.2}$	$^{-0.7}_{+0.7}$	$^{+1.7}_{-1.7}$	$^{+0.0}_{+0.0}$	$^{+0.1}_{+0.6}$	$^{+0.0}_{+0.0}$	$^{+0.7}_{-0.5}$
	0.13	0.362	± 2.2	$^{+4.9}_{-4.9}$	$^{+0.6}_{+0.0}$	$^{+0.1}_{+0.1}$	$^{+4.4}_{-4.4}$	$^{+1.9}_{-1.9}$	$^{+0.0}_{+0.0}$	$^{-0.4}_{+0.4}$	$^{+0.0}_{+0.0}$	$^{+0.5}_{-0.6}$
	0.25	0.270	± 2.5	$^{+5.6}_{-5.5}$	$^{+1.1}_{+0.0}$	$^{+0.2}_{+0.1}$	$^{+5.2}_{-5.2}$	$^{+1.1}_{-1.1}$	$^{-0.9}_{+0.8}$	$^{-0.1}_{+0.6}$	$^{+0.0}_{+0.0}$	$^{+0.8}_{-0.8}$

Table 14: *Systematic uncertainties with bin-to-bin correlations for the reduced cross section $\tilde{\sigma}$ for the reaction $e^- p \to e^- X$ ($\mathcal{L} = 98.7\, pb^{-1}, P_e = -0.27$). The left five columns of the table contain the bin centres, Q_c^2 and x_c, the measured cross section, the statistical uncertainty and the total systematic uncertainty. The right eight columns of the table list the bin-to-bin correlated systematic uncertainties for $\delta_1 - \delta_7$, and the systematic uncertainties summed in quadrature for $\delta_8 - \delta_{13}$, as defined in the section 8. The upper and lower correlated uncertainties correspond to a positive or negative variation of a cut value for example. However, if this is not possible for a particular systematic, the uncertainty is symmetrised. This table has two continuations.*

Q_c^2 (GeV^2)	x_c	$\tilde{\sigma}$	stat. (%)	sys. (%)	δ_1 (%)	δ_2 (%)	δ_3 (%)	δ_4 (%)	δ_5 (%)	δ_6 (%)	δ_7 (%)	$\delta_8 - \delta_{13}$ (%)
650	0.013	0.884	± 1.8	$^{+1.5}_{-0.8}$	$^{+1.2}_{-0.2}$	$^{-0.5}_{+0.6}$	$^{-0.0}_{+0.0}$	$^{-0.1}_{+0.1}$	$^{+0.0}_{+0.0}$	$^{-0.2}_{+0.3}$	$^{+0.5}_{-0.5}$	$^{+0.4}_{-0.3}$
	0.021	0.753	± 2.3	$^{+1.1}_{-1.1}$	$^{+0.0}_{-0.1}$	$^{-0.4}_{+0.5}$	$^{-0.3}_{+0.3}$	$^{-0.9}_{+0.9}$	$^{+0.0}_{+0.0}$	$^{-0.2}_{+0.0}$	$^{+0.1}_{-0.1}$	$^{+0.2}_{-0.2}$
	0.032	0.598	± 2.6	$^{+1.2}_{-1.0}$	$^{+0.5}_{-0.2}$	$^{-0.4}_{+0.5}$	$^{-0.5}_{+0.5}$	$^{+0.7}_{-0.7}$	$^{+0.0}_{+0.0}$	$^{+0.5}_{+0.5}$	$^{+0.0}_{-0.0}$	$^{+0.2}_{-0.2}$
	0.05	0.523	± 2.5	$^{+1.0}_{-0.9}$	$^{+0.1}_{-0.0}$	$^{-0.3}_{+0.4}$	$^{-0.4}_{+0.4}$	$^{+0.7}_{-0.7}$	$^{+0.0}_{+0.0}$	$^{+0.1}_{+0.0}$	$^{+0.0}_{+0.0}$	$^{+0.5}_{-0.4}$
	0.08	0.432	± 2.7	$^{+2.4}_{-2.3}$	$^{+0.7}_{-0.0}$	$^{-0.1}_{+0.3}$	$^{-1.8}_{+1.8}$	$^{+1.0}_{-1.0}$	$^{+0.0}_{+0.0}$	$^{+0.1}_{-0.0}$	$^{+0.0}_{+0.0}$	$^{+0.9}_{-1.1}$
	0.13	0.369	± 2.8	$^{+2.7}_{-2.4}$	$^{+0.9}_{-0.0}$	$^{-0.1}_{+0.2}$	$^{+2.1}_{-2.1}$	$^{-0.8}_{+0.8}$	$^{+0.0}_{+0.0}$	$^{+0.1}_{+0.4}$	$^{+0.0}_{+0.0}$	$^{+1.0}_{-0.9}$
	0.25	0.255	± 3.1	$^{+6.6}_{-6.5}$	$^{+1.0}_{-0.0}$	$^{-0.1}_{+0.3}$	$^{+6.3}_{-6.3}$	$^{+1.0}_{-1.0}$	$^{-0.8}_{+0.2}$	$^{-0.1}_{+0.5}$	$^{+0.0}_{+0.0}$	$^{+1.0}_{-1.1}$
800	0.013	0.885	± 2.3	$^{+1.7}_{-1.9}$	$^{+0.4}_{-1.0}$	$^{-0.8}_{+1.0}$	$^{+0.4}_{-0.4}$	$^{-1.0}_{+1.0}$	$^{+0.0}_{+0.0}$	$^{-0.1}_{+0.0}$	$^{+0.6}_{-0.6}$	$^{+0.3}_{-0.4}$
	0.021	0.769	± 2.7	$^{+1.1}_{-0.9}$	$^{+0.5}_{-0.1}$	$^{-0.4}_{+0.5}$	$^{+0.6}_{-0.6}$	$^{-0.2}_{+0.2}$	$^{+0.0}_{+0.0}$	$^{+0.0}_{+0.5}$	$^{+0.1}_{-0.1}$	$^{+0.4}_{-0.4}$
	0.032	0.648	± 2.7	$^{+1.4}_{-1.4}$	$^{+0.0}_{-0.4}$	$^{-0.4}_{+0.5}$	$^{-0.8}_{+0.8}$	$^{-0.9}_{+0.9}$	$^{+0.0}_{+0.0}$	$^{+0.3}_{+0.0}$	$^{+0.1}_{-0.1}$	$^{+0.2}_{-0.4}$
	0.05	0.543	± 2.5	$^{+2.2}_{-2.2}$	$^{+0.3}_{+0.0}$	$^{-0.3}_{+0.4}$	$^{+0.7}_{-0.7}$	$^{+2.0}_{-2.0}$	$^{+0.0}_{+0.0}$	$^{-0.4}_{+0.1}$	$^{+0.0}_{+0.0}$	$^{+0.3}_{-0.4}$
	0.08	0.452	± 2.8	$^{+2.6}_{-2.6}$	$^{+0.5}_{-0.0}$	$^{-0.2}_{+0.3}$	$^{-2.5}_{+2.5}$	$^{+0.1}_{-0.1}$	$^{+0.0}_{+0.0}$	$^{+0.5}_{-0.7}$	$^{+0.0}_{+0.0}$	$^{+0.3}_{-0.4}$
	0.13	0.379	± 3.1	$^{+1.1}_{-1.0}$	$^{+0.5}_{-0.0}$	$^{-0.2}_{+0.3}$	$^{+0.7}_{-0.7}$	$^{+0.6}_{-0.6}$	$^{+0.0}_{+0.0}$	$^{+0.1}_{-0.4}$	$^{+0.0}_{+0.0}$	$^{+0.2}_{-0.2}$
	0.25	0.270	± 3.5	$^{+3.7}_{-3.4}$	$^{+0.3}_{+0.0}$	$^{-0.2}_{+0.2}$	$^{+3.3}_{-3.3}$	$^{+0.8}_{-0.8}$	$^{+1.2}_{-0.1}$	$^{+0.7}_{-0.5}$	$^{+0.0}_{+0.0}$	$^{+0.2}_{-0.3}$
1200	0.014	0.908	± 2.9	$^{+2.4}_{-3.2}$	$^{+0.6}_{-2.2}$	$^{-0.8}_{+1.0}$	$^{-0.7}_{+0.7}$	$^{-1.4}_{+1.4}$	$^{+0.0}_{+0.0}$	$^{-0.3}_{-0.8}$	$^{+1.4}_{-1.4}$	$^{+0.5}_{-0.2}$
	0.021	0.828	± 2.6	$^{+1.9}_{-1.6}$	$^{+0.9}_{-0.1}$	$^{-0.5}_{+0.5}$	$^{+1.5}_{-1.5}$	$^{+0.0}_{-0.0}$	$^{+0.0}_{+0.0}$	$^{+0.1}_{+0.4}$	$^{+0.4}_{-0.4}$	$^{+0.3}_{-0.4}$
	0.032	0.620	± 2.7	$^{+1.2}_{-1.1}$	$^{+0.0}_{-0.1}$	$^{-0.4}_{+0.5}$	$^{-0.5}_{+0.5}$	$^{-0.7}_{+0.7}$	$^{+0.0}_{+0.0}$	$^{+0.1}_{+0.1}$	$^{+0.2}_{-0.2}$	$^{+0.6}_{-0.6}$
	0.05	0.550	± 2.4	$^{+1.3}_{-1.4}$	$^{+0.1}_{-0.0}$	$^{-0.3}_{+0.3}$	$^{-0.1}_{+0.1}$	$^{+1.2}_{-1.2}$	$^{+0.0}_{+0.0}$	$^{-0.3}_{-0.4}$	$^{+0.0}_{-0.0}$	$^{+0.4}_{-0.4}$
	0.08	0.473	± 2.4	$^{+1.4}_{-1.3}$	$^{+0.3}_{-0.0}$	$^{-0.2}_{+0.4}$	$^{-0.3}_{+0.3}$	$^{+1.2}_{-1.2}$	$^{+0.0}_{+0.0}$	$^{+0.3}_{-0.3}$	$^{+0.0}_{+0.0}$	$^{+0.4}_{-0.3}$
	0.13	0.385	± 2.7	$^{+1.1}_{-1.2}$	$^{+0.1}_{-0.0}$	$^{-0.1}_{+0.2}$	$^{-0.9}_{+0.9}$	$^{+0.4}_{-0.4}$	$^{+0.0}_{+0.0}$	$^{+0.1}_{-0.5}$	$^{+0.0}_{+0.0}$	$^{+0.3}_{-0.4}$
	0.25	0.263	± 3.0	$^{+2.4}_{-2.3}$	$^{+0.3}_{+0.0}$	$^{-0.2}_{+0.3}$	$^{+2.0}_{-2.0}$	$^{+1.0}_{-1.0}$	$^{+0.0}_{+0.0}$	$^{-0.3}_{-0.1}$	$^{+0.0}_{+0.0}$	$^{+0.5}_{-0.4}$
	0.4	0.129	± 5.2	$^{+8.1}_{-5.7}$	$^{+0.0}_{-0.1}$	$^{-0.4}_{+0.4}$	$^{+5.6}_{-5.6}$	$^{+0.6}_{-0.6}$	$^{+5.8}_{+3.4}$	$^{+0.5}_{-1.0}$	$^{+0.0}_{+0.0}$	$^{+0.5}_{-0.5}$
1500	0.021	0.771	± 3.8	$^{+2.6}_{-2.3}$	$^{+0.9}_{-0.2}$	$^{-0.6}_{+0.4}$	$^{-0.4}_{+0.4}$	$^{-0.1}_{+0.1}$	$^{+0.0}_{+0.0}$	$^{-1.0}_{+0.1}$	$^{+2.3}_{-1.9}$	$^{+0.4}_{-0.4}$
	0.032	0.641	± 3.5	$^{+0.7}_{-0.6}$	$^{+0.3}_{-0.1}$	$^{-0.3}_{+0.3}$	$^{-0.1}_{+0.1}$	$^{-0.3}_{+0.3}$	$^{+0.0}_{+0.0}$	$^{-0.1}_{-0.1}$	$^{+0.2}_{-0.2}$	$^{+0.4}_{-0.3}$
	0.05	0.514	± 3.2	$^{+0.9}_{-0.8}$	$^{+0.2}_{-0.0}$	$^{-0.3}_{+0.4}$	$^{+0.2}_{-0.2}$	$^{+0.4}_{-0.4}$	$^{+0.0}_{+0.0}$	$^{-0.4}_{+0.5}$	$^{+0.0}_{-0.0}$	$^{+0.3}_{-0.4}$
	0.08	0.496	± 3.0	$^{+1.0}_{-1.1}$	$^{+0.2}_{-0.0}$	$^{-0.3}_{+0.4}$	$^{-0.9}_{+0.9}$	$^{-0.2}_{+0.2}$	$^{+0.0}_{+0.0}$	$^{-0.4}_{+0.1}$	$^{+0.0}_{+0.0}$	$^{+0.3}_{-0.5}$
	0.13	0.386	± 3.8	$^{+2.1}_{-1.8}$	$^{+0.8}_{-0.0}$	$^{-0.1}_{+0.3}$	$^{-1.3}_{+1.3}$	$^{-1.1}_{+1.1}$	$^{+0.0}_{+0.0}$	$^{+0.8}_{-0.2}$	$^{+0.0}_{+0.0}$	$^{+0.3}_{-0.4}$
	0.18	0.328	± 4.0	$^{+1.8}_{-1.7}$	$^{+0.6}_{-0.1}$	$^{-0.3}_{+0.2}$	$^{+0.0}_{-0.0}$	$^{-1.6}_{+1.6}$	$^{+0.0}_{+0.0}$	$^{-0.3}_{-0.2}$	$^{+0.0}_{+0.0}$	$^{+0.4}_{-0.4}$
	0.25	0.265	± 4.9	$^{+1.9}_{-1.9}$	$^{+0.0}_{-0.3}$	$^{-0.3}_{+0.3}$	$^{+1.7}_{-1.7}$	$^{+0.6}_{-0.6}$	$^{+0.1}_{+0.0}$	$^{-0.1}_{-0.3}$	$^{+0.0}_{+0.0}$	$^{+0.3}_{-0.3}$
	0.4	0.134	± 7.3	$^{+8.8}_{-4.3}$	$^{+0.6}_{+0.0}$	$^{-0.5}_{+0.3}$	$^{+2.0}_{-2.0}$	$^{-0.9}_{+0.9}$	$^{+8.4}_{-3.6}$	$^{+0.3}_{-0.4}$	$^{+0.0}_{+0.0}$	$^{+0.6}_{-0.5}$
2000	0.032	0.644	± 4.3	$^{+2.5}_{-1.4}$	$^{+1.8}_{+0.0}$	$^{-0.2}_{+0.2}$	$^{+0.3}_{-0.3}$	$^{+1.0}_{-1.0}$	$^{+0.0}_{+0.0}$	$^{+0.4}_{+0.7}$	$^{+1.1}_{-0.8}$	$^{+0.3}_{-0.4}$
	0.05	0.605	± 3.7	$^{+1.0}_{-0.8}$	$^{+0.5}_{-0.0}$	$^{-0.3}_{+0.4}$	$^{-0.3}_{+0.3}$	$^{-0.6}_{+0.6}$	$^{+0.0}_{+0.0}$	$^{+0.1}_{+0.1}$	$^{+0.0}_{+0.0}$	$^{+0.3}_{-0.3}$
	0.08	0.477	± 3.7	$^{+2.0}_{-2.0}$	$^{+0.1}_{-0.1}$	$^{-0.3}_{+0.4}$	$^{-0.1}_{+0.1}$	$^{+1.9}_{-1.9}$	$^{+0.0}_{+0.0}$	$^{+0.2}_{+0.0}$	$^{+0.0}_{-0.0}$	$^{+0.3}_{-0.3}$
	0.13	0.345	± 4.6	$^{+0.8}_{-1.2}$	$^{+0.1}_{-0.6}$	$^{-0.2}_{+0.3}$	$^{-0.5}_{+0.5}$	$^{+0.5}_{-0.5}$	$^{+0.0}_{+0.0}$	$^{+0.1}_{-0.6}$	$^{+0.0}_{+0.0}$	$^{+0.3}_{-0.4}$
	0.18	0.322	± 4.8	$^{+0.6}_{-1.9}$	$^{+0.0}_{-0.7}$	$^{-0.2}_{+0.2}$	$^{-0.3}_{+0.3}$	$^{+0.1}_{-0.1}$	$^{+0.0}_{+0.0}$	$^{-0.4}_{-1.6}$	$^{+0.0}_{+0.0}$	$^{+0.4}_{-0.6}$
	0.25	0.259	± 5.8	$^{+1.7}_{-1.6}$	$^{+0.3}_{-0.0}$	$^{-0.2}_{+0.3}$	$^{+1.5}_{-1.5}$	$^{+0.5}_{-0.5}$	$^{+0.0}_{+0.0}$	$^{+0.4}_{+0.5}$	$^{+0.0}_{+0.0}$	$^{+0.5}_{-0.5}$
	0.4	0.122	± 8.5	$^{+3.7}_{-3.9}$	$^{+0.0}_{-0.2}$	$^{-0.3}_{+0.4}$	$^{+3.1}_{-3.1}$	$^{+1.1}_{-1.1}$	$^{-0.5}_{+1.0}$	$^{+0.1}_{-1.3}$	$^{+0.0}_{+0.0}$	$^{+1.2}_{-1.4}$

Table 14: *Continuation 1.*

Q_c^2 (GeV^2)	x_c	$\tilde{\sigma}$	stat. (%)	sys. (%)	δ_1 (%)	δ_2 (%)	δ_3 (%)	δ_4 (%)	δ_5 (%)	δ_6 (%)	δ_7 (%)	$\delta_8 - \delta_{13}$ (%)
3000	0.05	0.603	$\pm$ 4.7	$^{+2.0}_{-1.1}$	$^{+1.6}_{-0.1}$	$^{-0.3}_{+0.4}$	$^{+0.9}_{-0.9}$	$^{-0.0}_{+0.0}$	$^{+0.0}_{+0.0}$	$^{+0.4}_{+0.2}$	$^{+0.5}_{-0.5}$	$^{+0.4}_{-0.3}$
	0.08	0.511	$\pm$ 4.4	$^{+1.1}_{-1.1}$	$^{+0.2}_{-0.4}$	$^{-0.2}_{+0.3}$	$^{-0.4}_{+0.4}$	$^{+0.8}_{-0.8}$	$^{+0.0}_{+0.0}$	$^{+0.5}_{-0.1}$	$^{+0.1}_{-0.1}$	$^{+0.3}_{-0.5}$
	0.13	0.381	$\pm$ 5.3	$^{+0.9}_{-0.7}$	$^{+0.1}_{-0.1}$	$^{-0.2}_{+0.3}$	$^{+0.6}_{-0.6}$	$^{-0.1}_{+0.1}$	$^{+0.0}_{+0.0}$	$^{-0.3}_{-0.3}$	$^{+0.0}_{+0.0}$	$^{+0.7}_{-0.1}$
	0.18	0.343	$\pm$ 5.6	$^{+1.2}_{-1.3}$	$^{+0.0}_{-0.3}$	$^{-0.2}_{+0.2}$	$^{-0.9}_{+0.9}$	$^{-0.6}_{+0.6}$	$^{+0.0}_{+0.0}$	$^{-0.5}_{+0.2}$	$^{+0.0}_{+0.0}$	$^{+0.4}_{-0.3}$
	0.25	0.274	$\pm$ 6.5	$^{+7.4}_{-7.3}$	$^{+0.6}_{-0.0}$	$^{-0.2}_{+0.2}$	$^{+7.3}_{-7.3}$	$^{+0.2}_{-0.2}$	$^{+0.0}_{+0.0}$	$^{+1.1}_{+0.3}$	$^{+0.0}_{+0.0}$	$^{+0.8}_{-0.6}$
	0.4	0.156	$\pm$ 9.0	$^{+3.8}_{-3.5}$	$^{+1.3}_{-0.0}$	$^{-0.2}_{+0.4}$	$^{-3.4}_{+3.4}$	$^{+0.5}_{-0.5}$	$^{+0.4}_{-0.0}$	$^{+0.8}_{-0.3}$	$^{+0.0}_{+0.0}$	$^{+0.6}_{-0.6}$
	0.65	0.018	$^{+18.8}_{-16.0}$	$^{+10.2}_{-10.4}$	$^{+0.0}_{-0.6}$	$^{-0.8}_{+1.0}$	$^{-8.7}_{+8.7}$	$^{+4.6}_{-4.6}$	$^{+1.8}_{+0.7}$	$^{-2.7}_{+0.9}$	$^{+0.0}_{+0.0}$	$^{+1.7}_{-2.0}$
5000	0.08	0.567	$\pm$ 4.0	$^{+1.8}_{-0.9}$	$^{+1.6}_{-0.3}$	$^{-0.2}_{+0.2}$	$^{-0.3}_{+0.3}$	$^{+0.2}_{-0.2}$	$^{+0.0}_{+0.0}$	$^{-0.6}_{-0.4}$	$^{+0.3}_{-0.3}$	$^{+0.5}_{-0.3}$
	0.13	0.492	$\pm$ 5.2	$^{+1.0}_{-0.8}$	$^{+0.8}_{+0.0}$	$^{-0.2}_{+0.2}$	$^{-0.4}_{+0.4}$	$^{+0.3}_{-0.3}$	$^{+0.0}_{+0.0}$	$^{+0.1}_{-0.3}$	$^{+0.1}_{-0.1}$	$^{+0.2}_{-0.5}$
	0.18	0.354	$\pm$ 5.8	$^{+1.0}_{-0.5}$	$^{+0.2}_{-0.1}$	$^{-0.3}_{+0.2}$	$^{+0.2}_{-0.2}$	$^{+0.3}_{-0.3}$	$^{+0.0}_{+0.0}$	$^{-0.1}_{+0.7}$	$^{+0.0}_{+0.0}$	$^{+0.5}_{-0.3}$
	0.25	0.233	$\pm$ 7.6	$^{+1.8}_{-1.2}$	$^{+0.7}_{-0.0}$	$^{-0.2}_{+0.3}$	$^{+0.7}_{-0.7}$	$^{-0.7}_{+0.7}$	$^{+0.0}_{+0.0}$	$^{+1.2}_{-0.6}$	$^{+0.0}_{+0.0}$	$^{+0.4}_{-0.3}$
	0.4	0.132	$^{+11.3}_{-10.2}$	$^{+6.5}_{-6.4}$	$^{+0.0}_{-0.3}$	$^{-0.2}_{+0.3}$	$^{+6.0}_{-6.0}$	$^{-2.1}_{+2.1}$	$^{+0.0}_{+0.0}$	$^{+0.4}_{+1.3}$	$^{+0.0}_{+0.0}$	$^{+1.1}_{-1.1}$
8000	0.13	0.586	$\pm$ 5.4	$^{+1.0}_{-1.9}$	$^{+0.0}_{-1.0}$	$^{-0.3}_{+0.3}$	$^{-0.5}_{+0.5}$	$^{-0.1}_{+0.1}$	$^{+0.0}_{+0.0}$	$^{-1.3}_{+0.3}$	$^{+0.5}_{-0.3}$	$^{+0.5}_{-0.5}$
	0.18	0.441	$\pm$ 7.0	$^{+2.6}_{-2.9}$	$^{+0.1}_{-0.3}$	$^{-0.2}_{+0.2}$	$^{-2.4}_{+2.4}$	$^{+0.6}_{-0.6}$	$^{+0.0}_{+0.0}$	$^{+0.5}_{-0.3}$	$^{+0.0}_{+0.0}$	$^{+0.6}_{-1.3}$
	0.25	0.323	$\pm$ 8.5	$^{+3.8}_{-3.9}$	$^{+0.7}_{-0.1}$	$^{-0.3}_{+0.2}$	$^{-3.6}_{+3.6}$	$^{+0.4}_{-0.4}$	$^{+0.0}_{+0.0}$	$^{-1.1}_{-0.6}$	$^{+0.0}_{+0.0}$	$^{+0.4}_{-0.4}$
	0.4	0.116	$^{+16.1}_{-14.0}$	$^{+7.1}_{-7.3}$	$^{+0.1}_{-0.0}$	$^{-0.3}_{+0.4}$	$^{+7.0}_{-7.0}$	$^{-0.6}_{+0.6}$	$^{+0.0}_{+0.0}$	$^{-0.3}_{+0.5}$	$^{+0.0}_{+0.0}$	$^{+0.6}_{-2.0}$
	0.65	0.020	$^{+26.9}_{-21.6}$	$^{+4.1}_{-4.2}$	$^{+0.2}_{-1.4}$	$^{-0.9}_{+0.9}$	$^{+1.5}_{-1.5}$	$^{+2.3}_{-2.3}$	$^{+0.0}_{+0.0}$	$^{-2.6}_{+2.8}$	$^{+0.0}_{+0.0}$	$^{+0.8}_{-0.6}$
12000	0.18	0.516	$\pm$ 7.6	$^{+1.3}_{-3.8}$	$^{+1.0}_{-3.6}$	$^{-0.3}_{+0.4}$	$^{-0.4}_{+0.4}$	$^{-0.2}_{+0.2}$	$^{+0.0}_{+0.0}$	$^{-0.3}_{-0.8}$	$^{+0.2}_{-0.3}$	$^{+0.5}_{-0.6}$
	0.25	0.354	$^{+12.0}_{-10.8}$	$^{+2.8}_{-2.3}$	$^{+2.4}_{-0.6}$	$^{-0.2}_{+0.2}$	$^{+0.3}_{-0.3}$	$^{+0.8}_{-0.8}$	$^{+0.0}_{+0.0}$	$^{+0.3}_{-1.6}$	$^{+0.0}_{+0.0}$	$^{+1.0}_{-1.2}$
	0.4	0.146	$^{+18.7}_{-16.0}$	$^{+4.6}_{-3.8}$	$^{+2.7}_{-0.2}$	$^{-0.3}_{+0.4}$	$^{+3.2}_{-3.2}$	$^{-0.8}_{+0.8}$	$^{+0.0}_{+0.0}$	$^{-1.2}_{+1.5}$	$^{+0.0}_{+0.0}$	$^{+0.6}_{-1.3}$
20000	0.25	0.473	$^{+13.1}_{-11.8}$	$^{+6.1}_{-3.6}$	$^{+4.9}_{-1.8}$	$^{-1.5}_{+0.2}$	$^{-2.2}_{+2.2}$	$^{+0.1}_{-0.1}$	$^{+0.0}_{+0.0}$	$^{-0.7}_{-0.2}$	$^{+2.7}_{-1.4}$	$^{+0.6}_{-0.5}$
	0.4	0.193	$^{+22.2}_{-18.5}$	$^{+4.9}_{-3.8}$	$^{+3.6}_{+0.0}$	$^{-0.4}_{+0.4}$	$^{+0.9}_{-0.9}$	$^{+3.0}_{-3.0}$	$^{+0.0}_{+0.0}$	$^{-1.8}_{-0.3}$	$^{+0.0}_{+0.0}$	$^{+1.1}_{-1.2}$
30000	0.4	0.275	$^{+22.7}_{-18.8}$	$^{+6.9}_{-5.9}$	$^{+6.7}_{+0.0}$	$^{-0.2}_{+0.3}$	$^{-0.8}_{+0.8}$	$^{+0.7}_{-0.7}$	$^{+0.0}_{+0.0}$	$^{+0.1}_{-4.9}$	$^{+0.0}_{-2.9}$	$^{+1.3}_{-1.3}$

Table 14: *Continuation 2.*

Q^2 range (GeV^2)			Q_c^2 (GeV^2)	$d\sigma/dQ^2$ (pb/ GeV^2)	$N_{\rm data}$	$N_{\rm bg}^{\rm MC}$
185.0	–	300.0	250	$(1.08 \pm 0.00\ ^{+0.01}_{-0.01})\cdot 10^{1}$	74098	105.5
300.0	–	400.0	350	$4.77 \pm 0.03\ ^{+0.07}_{-0.05}$	25380	57.6
400.0	–	475.7	440	$2.73 \pm 0.03\ ^{+0.05}_{-0.05}$	10769	34.0
475.7	–	565.7	520	$1.78 \pm 0.02\ ^{+0.02}_{-0.02}$	7685	30.7
565.7	–	672.7	620	$1.19 \pm 0.02\ ^{+0.02}_{-0.01}$	5715	32.6
672.7	–	800.0	730	$(7.77 \pm 0.11\ ^{+0.06}_{-0.06})\cdot 10^{-1}$	5242	17.8
800.0	–	1050.0	900	$(4.60 \pm 0.06\ ^{+0.04}_{-0.04})\cdot 10^{-1}$	6873	36.8
1050.0	–	1460.0	1230	$(2.13 \pm 0.03\ ^{+0.01}_{-0.02})\cdot 10^{-1}$	5558	38.9
1460.0	–	2080.0	1730	$(8.81 \pm 0.15\ ^{+0.05}_{-0.05})\cdot 10^{-2}$	3551	23.7
2080.0	–	3120.0	2500	$(3.42 \pm 0.07\ ^{+0.03}_{-0.02})\cdot 10^{-2}$	2269	14.2
3120.0	–	5220.0	3900	$(1.06 \pm 0.03\ ^{+0.01}_{-0.01})\cdot 10^{-2}$	1363	4.4
5220.0	–	12500.0	7000	$(2.34 \pm 0.08\ ^{+0.05}_{-0.01})\cdot 10^{-3}$	778	3.7
12500.0	–	51200.0	22400	$(6.24 \pm 0.52\ ^{+0.23}_{-0.14})\cdot 10^{-5}$	144	1.8

Table 15: *The single differential cross section $d\sigma/dQ^2$ ($y < 0.9$) for the reaction $e^-p \to e^-X$ ($\mathcal{L} = 71.2\,pb^{-1}, P_e = +0.29$). The bin range, bin centre (Q_c^2) and measured cross section corrected to the electroweak Born level are shown. The first (second) error on the cross section corresponds to the statistical (systematic) uncertainties. The number of observed data events (N_{data}) and simulated background events (N_{bg}^{MC}) are also shown.*

Q_c^2 (GeV^2)	$d\sigma/dQ^2$ (pb/ GeV^2)	stat. (%)	sys. (%)	δ_1 (%)	δ_2 (%)	δ_3 (%)	δ_4 (%)	δ_5 (%)	δ_6 (%)	δ_7 (%)	$\delta_8 - \delta_{13}$ (%)
250	$1.08 \cdot 10^{1}$	$\pm$ 0.4	$^{+1.2}_{-1.1}$	$^{+0.3}_{-0.0}$	$^{-0.5}_{+0.6}$	$^{+0.5}_{-0.5}$	$^{+0.4}_{-0.4}$	$^{-0.1}_{+0.2}$	$^{-0.0}_{+0.2}$	$^{+0.1}_{-0.1}$	$^{+0.7}_{-0.8}$
350	4.77	$\pm$ 0.6	$^{+1.5}_{-1.1}$	$^{+0.8}_{-0.0}$	$^{-0.5}_{+0.7}$	$^{+0.5}_{-0.5}$	$^{+0.6}_{-0.6}$	$^{-0.0}_{+0.2}$	$^{-0.2}_{+0.2}$	$^{+0.1}_{-0.1}$	$^{+0.6}_{-0.6}$
440	2.73	$\pm$ 1.0	$^{+1.8}_{-1.7}$	$^{+0.3}_{-0.0}$	$^{-0.5}_{+0.6}$	$^{+0.5}_{-0.5}$	$^{+1.3}_{-1.3}$	$^{-0.2}_{+0.2}$	$^{-0.4}_{+0.7}$	$^{+0.1}_{-0.1}$	$^{+0.6}_{-0.6}$
520	1.78	$\pm$ 1.2	$^{+1.3}_{-0.9}$	$^{+0.7}_{-0.1}$	$^{-0.5}_{+0.7}$	$^{+0.0}_{-0.0}$	$^{+0.1}_{-0.1}$	$^{-0.1}_{+0.2}$	$^{-0.2}_{+0.3}$	$^{+0.2}_{-0.2}$	$^{+0.7}_{-0.7}$
620	1.19	$\pm$ 1.3	$^{+1.4}_{-1.0}$	$^{+0.9}_{-0.1}$	$^{-0.6}_{+0.7}$	$^{+0.2}_{-0.2}$	$^{-0.6}_{+0.6}$	$^{-0.1}_{-0.0}$	$^{+0.1}_{+0.2}$	$^{+0.2}_{-0.2}$	$^{+0.4}_{-0.5}$
730	$7.77 \cdot 10^{-1}$	$\pm$ 1.4	$^{+0.8}_{-0.7}$	$^{+0.0}_{-0.2}$	$^{-0.5}_{+0.6}$	$^{+0.3}_{-0.3}$	$^{+0.1}_{-0.1}$	$^{+0.2}_{+0.1}$	$^{+0.1}_{-0.1}$	$^{+0.1}_{-0.1}$	$^{+0.2}_{-0.3}$
900	$4.60 \cdot 10^{-1}$	$\pm$ 1.2	$^{+0.9}_{-0.8}$	$^{+0.1}_{-0.0}$	$^{-0.4}_{+0.5}$	$^{-0.2}_{+0.2}$	$^{+0.6}_{-0.6}$	$^{+0.1}_{-0.1}$	$^{-0.0}_{-0.0}$	$^{+0.2}_{-0.2}$	$^{+0.3}_{-0.3}$
1230	$2.13 \cdot 10^{-1}$	$\pm$ 1.4	$^{+0.7}_{-0.7}$	$^{+0.1}_{-0.0}$	$^{-0.3}_{+0.4}$	$^{+0.3}_{-0.3}$	$^{-0.1}_{+0.1}$	$^{+0.0}_{+0.1}$	$^{-0.0}_{-0.3}$	$^{+0.3}_{-0.3}$	$^{+0.3}_{-0.4}$
1730	$8.81 \cdot 10^{-2}$	$\pm$ 1.7	$^{+0.6}_{-0.5}$	$^{+0.2}_{-0.0}$	$^{-0.3}_{+0.3}$	$^{+0.1}_{-0.1}$	$^{+0.0}_{-0.0}$	$^{+0.2}_{-0.0}$	$^{-0.2}_{-0.1}$	$^{+0.3}_{-0.3}$	$^{+0.3}_{-0.3}$
2500	$3.42 \cdot 10^{-2}$	$\pm$ 2.1	$^{+0.9}_{-0.6}$	$^{+0.4}_{-0.0}$	$^{-0.2}_{+0.3}$	$^{+0.3}_{-0.3}$	$^{+0.2}_{-0.2}$	$^{-0.1}_{-0.0}$	$^{+0.3}_{+0.1}$	$^{+0.3}_{-0.2}$	$^{+0.3}_{-0.3}$
3900	$1.06 \cdot 10^{-2}$	$\pm$ 2.7	$^{+1.3}_{-0.6}$	$^{+1.2}_{-0.1}$	$^{-0.2}_{+0.3}$	$^{-0.4}_{+0.4}$	$^{-0.1}_{+0.1}$	$^{-0.0}_{-0.0}$	$^{-0.2}_{-0.1}$	$^{+0.1}_{-0.1}$	$^{+0.3}_{-0.3}$
7000	$2.34 \cdot 10^{-3}$	$\pm$ 3.6	$^{+2.3}_{-0.6}$	$^{+2.2}_{-0.0}$	$^{-0.3}_{+0.3}$	$^{-0.0}_{+0.0}$	$^{+0.1}_{-0.1}$	$^{+0.0}_{+0.0}$	$^{-0.3}_{+0.1}$	$^{+0.5}_{-0.2}$	$^{+0.3}_{-0.4}$
22400	$6.24 \cdot 10^{-5}$	$\pm$ 8.4	$^{+3.7}_{-2.3}$	$^{+3.4}_{-0.4}$	$^{-0.7}_{+0.3}$	$^{-1.0}_{+1.0}$	$^{+0.7}_{-0.7}$	$^{+0.0}_{+0.0}$	$^{-1.0}_{-1.6}$	$^{+0.5}_{-0.5}$	$^{+0.6}_{-0.6}$

Table 16: *Systematic uncertainties with bin-to-bin correlations for $d\sigma/dQ^2$ ($y < 0.9$) for the reaction $e^-p \to e^-X$ ($\mathcal{L} = 71.2\,pb^{-1}, P_e = +0.29$). The left four columns of the table contain the bin centre (Q_c^2), the measured cross section, the statistical uncertainty and the total systematic uncertainty. The right eight columns of the table list the bin-to-bin correlated systematic uncertainties for $\delta_1 - \delta_7$, and the total systematic uncertainties summed in quadrature for $\delta_8 - \delta_{13}$, as defined in the section 8. The upper and lower correlated uncertainties correspond to a positive or negative variation of a cut value for example. However, if this is not possible for a particular systematic, the uncertainty is symmetrised.*

Q^2 range (GeV^2)	Q_c^2 (GeV^2)	$d\sigma/dQ^2$ ($\mathrm{pb}/\mathrm{GeV}^2$)	N_{data}	$N_{\mathrm{bg}}^{\mathrm{MC}}$
185.0 – 300.0	250	$(1.08 \pm 0.00\ ^{+0.01}_{-0.01})\cdot 10^{1}$	103254	146.9
300.0 – 400.0	350	$4.83 \pm 0.03\ ^{+0.07}_{-0.06}$	35547	80.0
400.0 – 475.7	440	$2.80 \pm 0.02\ ^{+0.05}_{-0.05}$	15291	47.0
475.7 – 565.7	520	$1.87 \pm 0.02\ ^{+0.02}_{-0.02}$	11190	42.4
565.7 – 672.7	620	$1.19 \pm 0.01\ ^{+0.02}_{-0.01}$	7926	45.0
672.7 – 800.0	730	$(8.30 \pm 0.10\ ^{+0.07}_{-0.06})\cdot 10^{-1}$	7719	24.7
800.0 – 1050.0	900	$(4.89 \pm 0.05\ ^{+0.05}_{-0.04})\cdot 10^{-1}$	10094	51.1
1050.0 – 1460.0	1230	$(2.25 \pm 0.03\ ^{+0.02}_{-0.02})\cdot 10^{-1}$	8111	53.7
1460.0 – 2080.0	1730	$(9.25 \pm 0.13\ ^{+0.05}_{-0.05})\cdot 10^{-2}$	5158	32.7
2080.0 – 3120.0	2500	$(3.61 \pm 0.06\ ^{+0.03}_{-0.02})\cdot 10^{-2}$	3314	19.4
3120.0 – 5220.0	3900	$(1.16 \pm 0.03\ ^{+0.02}_{-0.01})\cdot 10^{-2}$	2065	6.0
5220.0 – 12500.0	7000	$(2.48 \pm 0.07\ ^{+0.06}_{-0.02})\cdot 10^{-3}$	1143	5.0
12500.0 – 51200.0	22400	$(6.26 \pm 0.45\ ^{+0.23}_{-0.14})\cdot 10^{-5}$	200	2.6

Table 17: *The single differential cross section $d\sigma/dQ^2$ ($y < 0.9$) for the reaction $e^- p \to e^- X$ ($\mathcal{L} = 98.7\,pb^{-1}, P_e = -0.27$). The bin range, bin centre (Q_c^2) and measured cross section corrected to the electroweak Born level are shown. The first (second) error on the cross section corresponds to the statistical (systematic) uncertainties. The number of observed data events (N_{data}) and simulated background events (N_{bg}^{MC}) are also shown.*

Q_c^2 (GeV^2)	$d\sigma/dQ^2$ ($\mathrm{pb}/\mathrm{GeV}^2$)	stat. (%)	sys. (%)	δ_1 (%)	δ_2 (%)	δ_3 (%)	δ_4 (%)	δ_5 (%)	δ_6 (%)	δ_7 (%)	$\delta_8 - \delta_{13}$ (%)
250	$1.08 \cdot 10^{1}$	± 0.3	$^{+1.2}_{-1.1}$	$^{+0.3}_{-0.0}$	$^{-0.5}_{+0.6}$	$^{+0.5}_{-0.5}$	$^{+0.4}_{-0.4}$	$^{-0.1}_{+0.2}$	$^{-0.0}_{+0.2}$	$^{+0.1}_{-0.1}$	$^{+0.7}_{-0.8}$
350	4.83	± 0.6	$^{+1.5}_{-1.1}$	$^{+0.8}_{-0.0}$	$^{-0.5}_{+0.7}$	$^{+0.5}_{-0.5}$	$^{+0.6}_{-0.6}$	$^{-0.0}_{+0.2}$	$^{-0.2}_{+0.2}$	$^{+0.1}_{-0.1}$	$^{+0.6}_{-0.6}$
440	2.80	± 0.8	$^{+1.8}_{-1.7}$	$^{+0.3}_{-0.0}$	$^{-0.5}_{+0.6}$	$^{+0.5}_{-0.5}$	$^{+1.3}_{-1.3}$	$^{-0.2}_{+0.2}$	$^{-0.4}_{+0.7}$	$^{+0.1}_{-0.1}$	$^{+0.6}_{-0.6}$
520	1.87	± 1.0	$^{+1.3}_{-0.9}$	$^{+0.7}_{-0.1}$	$^{-0.5}_{+0.7}$	$^{+0.0}_{-0.0}$	$^{+0.1}_{-0.1}$	$^{-0.1}_{+0.2}$	$^{-0.2}_{+0.3}$	$^{+0.2}_{-0.2}$	$^{+0.7}_{-0.7}$
620	1.19	± 1.1	$^{+1.4}_{-1.0}$	$^{+0.9}_{-0.1}$	$^{-0.6}_{+0.7}$	$^{+0.2}_{-0.2}$	$^{-0.6}_{+0.6}$	$^{-0.1}_{-0.0}$	$^{+0.1}_{+0.2}$	$^{+0.2}_{-0.2}$	$^{+0.4}_{-0.5}$
730	$8.30 \cdot 10^{-1}$	± 1.2	$^{+0.8}_{-0.7}$	$^{+0.0}_{-0.2}$	$^{-0.5}_{+0.6}$	$^{+0.3}_{-0.3}$	$^{+0.1}_{-0.1}$	$^{+0.2}_{+0.1}$	$^{+0.1}_{-0.1}$	$^{+0.1}_{-0.1}$	$^{+0.2}_{-0.3}$
900	$4.89 \cdot 10^{-1}$	± 1.0	$^{+0.9}_{-0.8}$	$^{+0.1}_{-0.0}$	$^{-0.4}_{+0.5}$	$^{-0.2}_{+0.2}$	$^{+0.6}_{-0.6}$	$^{+0.1}_{-0.1}$	$^{-0.0}_{-0.0}$	$^{+0.2}_{-0.2}$	$^{+0.3}_{-0.3}$
1230	$2.25 \cdot 10^{-1}$	± 1.1	$^{+0.7}_{-0.7}$	$^{+0.1}_{-0.0}$	$^{-0.3}_{+0.4}$	$^{+0.3}_{-0.3}$	$^{-0.1}_{+0.1}$	$^{+0.0}_{+0.1}$	$^{-0.0}_{-0.3}$	$^{+0.3}_{-0.3}$	$^{+0.3}_{-0.4}$
1730	$9.25 \cdot 10^{-2}$	± 1.4	$^{+0.6}_{-0.5}$	$^{+0.2}_{-0.0}$	$^{-0.3}_{+0.3}$	$^{+0.1}_{-0.1}$	$^{+0.0}_{-0.0}$	$^{+0.2}_{-0.0}$	$^{-0.2}_{-0.1}$	$^{+0.3}_{-0.3}$	$^{+0.3}_{-0.3}$
2500	$3.61 \cdot 10^{-2}$	± 1.8	$^{+0.9}_{-0.6}$	$^{+0.4}_{-0.0}$	$^{-0.2}_{+0.3}$	$^{+0.3}_{-0.3}$	$^{+0.2}_{-0.2}$	$^{-0.1}_{-0.0}$	$^{+0.3}_{+0.1}$	$^{+0.3}_{-0.2}$	$^{+0.3}_{-0.3}$
3900	$1.16 \cdot 10^{-2}$	± 2.2	$^{+1.3}_{-0.6}$	$^{+1.2}_{-0.1}$	$^{-0.2}_{+0.3}$	$^{-0.4}_{+0.4}$	$^{-0.1}_{+0.1}$	$^{-0.0}_{-0.0}$	$^{-0.2}_{-0.1}$	$^{+0.1}_{-0.1}$	$^{+0.3}_{-0.3}$
7000	$2.48 \cdot 10^{-3}$	± 3.0	$^{+2.3}_{-0.6}$	$^{+2.2}_{-0.0}$	$^{-0.3}_{+0.3}$	$^{-0.0}_{+0.0}$	$^{+0.1}_{-0.1}$	$^{+0.0}_{+0.0}$	$^{-0.3}_{+0.1}$	$^{+0.5}_{-0.2}$	$^{+0.3}_{-0.4}$
22400	$6.26 \cdot 10^{-5}$	± 7.2	$^{+3.7}_{-2.3}$	$^{+3.4}_{-0.4}$	$^{-0.7}_{+0.3}$	$^{-1.0}_{+1.0}$	$^{+0.7}_{-0.7}$	$^{+0.0}_{+0.0}$	$^{-1.0}_{-1.6}$	$^{+0.5}_{-0.5}$	$^{+0.6}_{-0.6}$

Table 18: *Systematic uncertainties with bin-to-bin correlations for $d\sigma/dQ^2$ ($y < 0.9$) for the reaction $e^- p \to e^- X$ ($\mathcal{L} = 98.7\,pb^{-1}, P_e = -0.27$). The left four columns of the table contain the bin centre (Q_c^2), the measured cross section, the statistical uncertainty and the total systematic uncertainty. The right eight columns of the table list the bin-to-bin correlated systematic uncertainties for $\delta_1 - \delta_7$, and the total systematic uncertainties summed in quadrature for $\delta_8 - \delta_{13}$, as defined in the section 8. The upper and lower correlated uncertainties correspond to a positive or negative variation of a cut value for example. However, if this is not possible for a particular systematic, the uncertainty is symmetrised.*

Q^2 range (GeV^2)			Q_c^2 (GeV^2)	Asymmetry A^- $\times 10$	
185.0	–	300.0	250	-0.11	$\pm$0.09
300.0	–	400.0	350	-0.21	$\pm$0.15
400.0	–	475.7	440	-0.45	$\pm$0.23
475.7	–	565.7	520	-0.89	$\pm$0.27
565.7	–	672.7	620	-0.03	$\pm$0.32
672.7	–	800.0	730	-1.19	$\pm$0.32
800.0	–	1050.0	900	-1.09	$\pm$0.28
1050.0	–	1460.0	1230	-0.95	$\pm$0.32
1460.0	–	2080.0	1730	-0.86	$\pm$0.39
2080.0	–	3120.0	2500	-0.96	$\pm$0.49
3120.0	–	5220.0	3900	-1.61	$\pm$0.63
5220.0	–	12500.0	7000	-1.06	$\pm$0.83
12500.0	–	51200.0	22400	-0.06	$\pm$1.97

Table 19: *The polarisation asymmetry measured using positively and negatively polarised e^-p beams ($\mathcal{L} = 71.2\,pb^{-1}, P_e = +0.29$ and $\mathcal{L} = 98.7\,pb^{-1}, P_e = -0.27$, respectively). The bin range, bin centre (Q_c^2) and measured Asymmetry A^- are shown. Only the statistical uncertainties on the measurement are shown as systematic uncertainties are assumed to cancel.*